federal State Autonomous Educational Institution of Higher Education
I.M. Sechenov First Moscow State Medical University
of the Ministry of Health of the Russian Federation
(Sechenovskiy University)

Centre of Master's Programs

Bensaada Hichem
2nd year master, group 729-04

siRNA Delivery Using Single-Walled Carbon Nanotubes (SWCNTs) and Plant-Derived Exosome-Like Nanoparticles (PELNs): Design, Characterization, and In Vitro Evaluation

QUALIFICATION WORK
Specialty 19.04.01 – Biotechnology

Moscow 2025

The work was carried out at the A.P. Nelyubin Institute of Pharmacy of Sechenov University and at the National Research Center Institute of Immunology of the Federal Medical Biological Agency of Russia (NRC Institute of Immunology FMBA of Russia), and The Laboratory of NanoMaterials at Skoltech University

Director of A.P. Nelyubin Institute of Pharmacy of Sechenov University: Galina V. Ramenskaya, D.Pharm., professor

.

Supervisor of the thesis:

Professor
Doctor of Pharmaceutical Sciences *Smirnov Valery Valerievich*

Senior Research Scientist,
Doctor of Inorganic Chemistry and
Chemistry of Solid State.
Laboratory of Nanomaterials, *Goldt Anastasia Evgenievna*
Skoltech University

The thesis is available for review at the Department of Pharmaceutical and Toxicological Chemistry named after A.P. Arzamastsev of the A.P. Nelyubin Institute of Pharmacy of Sechenov University at the address: Moscow, Vernadsky Ave., 96, Bldg. 1.

1 ACKNOWLEDGEMENT

Bismillāhir-Raḥmānir-Raḥīm ***بِسْمِ اللهِ الرَّحْمٰنِ الرَّحِيْمِ***

This dissertation is a product of an incredibly enriching partnership between Skoltech and Sechenov universities. I am sincerely appreciative of Professor Valery Valerievich Smirnov, my supervisor, who initially sparked my interest in siRNA therapeutics and then provided unwavering support throughout this research endeavour. I am profoundly grateful to Professor Anastasia Evgenievna Goldt, Senior Research Scientist at Skoltech in the Nanomaterials Laboratory. She wholeheartedly accepted my proposal for this collaborative effort between institutions. Without her invaluable mentorship and direction, this project would not have realized its full potential.

I offer my heartfelt thanks to Aliya Rifovna Vildanova, a PhD candidate in Materials Science at Skoltech. Under her technical skills, insightful discussions, and relentless encouragement, I saw all aspects of my work lifted into experiences that opened up my eyes to the fascinating world of carbon nanomaterials.

At the NRC Institute of Immunology FMBA of Russia, my very special thanks to Dr. Evgeny Alexandrovich Turetsky, Senior Lecturer of Pharmaceutical and Toxicological Chemistry at Sechenov University, together with Dr. Vladislav Nikolaevich Turenko, Senior Researcher and Lecturer of the same department. Without much of their advice, training, mentorship, and cooperation, the conception of this project would have never come into existence.

I would also like to thank Professor Jhon Fredy Betancur P. and Professor Juan Carlos Carmona-Hernández, both of whom belong to the Faculty of Health Sciences at the University of Manizales, Colombia. Their insights and discussions deeply affected my decision to shift from medical practice to scientific research and to pursue this Master of Biotechnology.

I would like to take this opportunity to profoundly convey my heartfelt and sincere gratitude to the remarkable Anastasiia Druzhinina, who serves as both a distinguished Scientific Researcher and an inspiring lecturer at the prestigious ITMO University, since

it is her unwavering and steadfast support, along with her relentless motivation, that has served as an invaluable guide, leading me triumphantly through every hurdle and obstacle I have encountered throughout my enriching and transformative time here in the magnificent country of Russia.

Last but certainly not least, I thank my family. My siblings: Zakaria, Sara, and Faten; And especially my mother, whose unwavering belief in me and unconditional love have been my greatest source of strength.

All of you, thank you for the guidance, patience, and faith in this project. Your contributions made this project excel beyond measure.

2 TABLE OF CONTENTS

3 LIST OF ABBREVIATIONS:

5PL: Five-Parameter Logistic model

AGO2: Argonaute 2

AFM: Atomic Force Microscopy

ANOVA: Analysis of Variance

AuNPs: Gold Nanoparticles

BSA: Bovine Serum Albumin

CCR4–NOT: Carbon catabolite repression 4–negative on TATA-less

CoMoCAT: Cobalt-Molybdenum Catalytic Synthesis (of Carbon Nanotubes)

CNT: Carbon Nanotubes

diH_2O: Deionized Water

DLS: Dynamic Light Scattering

DMSO: Dimethyl Sulfoxide

DMEM: Dulbecco's Modified Eagle's Medium

DSPE-PEG-PEI: Polyethylenimine conjugated to 1,2-distearoyl-sn-glycero-3-phosphoethanolamine-N-[amino(polyethylene glycol)-2000]

dsRNA: Double-Stranded RNA

FDA: Food and Drug Administration

FBS: Fetal Bovine Serum

FMBA: Federal Medical Biological Agency

GalNAc: N-Acetylgalactosamine

GELNs: Ginger-Derived Exosome-Like Nanoparticles

GNRs: Gold Nanorods

HiPCO: High-Pressure Carbon Monoxide Process (for synthesizing CNTs)

Hsc70/Hsp90: Heat Shock Co-Chaperone Proteins

iNaD: Inorganic Nanoparticle Device

IRF: Interferon Regulatory Factor

KK46: Peptide used for CNT functionalization

KRAS: Kirsten Rat Sarcoma Viral Oncogene Homolog

LNPs: Lipid Nanoparticles

MAPK: Mitogen-Activated Protein Kinase

MID: Middle Domain (of Argonaute protein)

mRNA: Messenger RNA

MSC: Mesenchymal Stem Cell

MSNs: Mesoporous Silica Nanoparticles

MTT: 3-(4,5-dimethylthiazol-2-yl)-2,5-diphenyltetrazolium bromide (cytotoxicity assay)

MW: Molecular Weight

ND / NDs: Nanodiamonds

NF-κB: Nuclear Factor kappa-light-chain-enhancer of activated B cells

NIR: Near-Infrared

NRC: National Research Center

NTL: KK46-CNT formulation without siRNA

PAZ: PAZ Domain (binds the 3′ end of the guide strand in RNAi)

PEI: Polyethyleneimine

PELNs: Plant-Derived Exosome-Like Nanoparticles

PDI: Polydispersity Index

PEG: Polyethylene Glycol

PF-QNM: PeakForce™ Quantitative Nanomechanical Mapping

PIWI: PIWI Domain (of Argonaute protein responsible for catalytic activity)

PL: Photoluminescence

PLGA: Poly(lactic-co-glycolic acid)

R^2: Coefficient of Determination

RISC: RNA-Induced Silencing Complex

RLC: RISC-Loading Complex

RNAi: RNA Interference

siRNA: Small Interfering RNA

siSTAT3: Small Interfering RNA targeting STAT3

SPIONs: Superparamagnetic Iron Oxide Nanoparticles

SWCNT: Single-Walled Carbon Nanotubes

SD: Standard Deviation

TAE: Tris-acetate-EDTA Buffer

TME: Tumor Microenvironment

TRBP: Transactivation Response RNA-Binding Protein

Tukey's HSD: Tukey's Honestly Significant Difference test

UV–Vis–NIR : Ultraviolet–Visible–Near Infra Red

ζ-Potential: Zeta Potential

4 INTRODUCTION

In the year 2006, Craig Mello and Andrew Fire received the prestigious Nobel Prize for their discovery concerning the RNA interference (RNAi) mechanism in 1998 [1]. Subsequently, two distinct research teams articulated that double-stranded RNA (dsRNA) comprising 21-22 nucleotides, referred to as small interfering RNA (siRNA), possesses the capability to effectively induce gene silencing in mammalian cellular contexts [2][3]. Since then, gene silencing through RNAi has surfaced as an influential approach for addressing a multitude of diseases by precisely downregulating the expression of target genes at the post-transcriptional stage [2]. siRNA therapeutics occupy a central position in this domain owing to their straightforward design process and remarkable sequence specificity [4].

After the uptake of siRNA molecules into the cytoplasm, the molecules are incorporated into the RNA-induced silencing complex (RISC). The dsRNA will be then broken into 2 separate strands, with the guide strand then guiding the complex to a complementary target messenger RNA (mRNA) molecule, ending in its cleavage and the resultant silencing of the gene [2][5][6].

The specificity of siRNA is predicated on its complementary sequence alignment with the target mRNA, enabling effective gene silencing [2]. This characteristic has established siRNA as an exceptionally potent therapeutic instrument, as it possesses the ability to target genes that are conventionally deemed "undruggable" by standard small molecule pharmaceuticals or monoclonal antibodies [7][8]. Nonetheless, the therapeutic promise of siRNA is significantly undermined by their vulnerability to rapid degradation in biological fluids, restricted cellular uptake, and potential off-target effects [9]. Therefore, the development of safe and stable delivery vectors that can provide stabilization for siRNA while facilitating efficient cellular uptake is of paramount importance.

Carbon nanotubes (CNT) gain lots of interest as nanocarriers for siRNA due to their exceptional physical characteristics, which entail a high aspect ratio, enormous surface area, and intrinsic near-infrared photoluminescence for optical imaging [10]. Yet, pristine

CNTs bear an inherent hydrophobic characteristic, which promotes their agglomeration on contact with aqueous media, thus leading to poor dispersion and potential cytotoxicity [11]. To overcome these obstacles, extensive studies have been devoted to surface functionalization with biocompatible groups. This research delves into two non-covalent functionalizations: the first involves bovine serum albumin (BSA), a well-studied protein dispersant long known to significantly enhance the stability of CNT through hydrophobic interactions and electrostatic covering; the second involves the "***KK46***" peptide, a newly introduced cationic dendrimer developed at the National Research Centre Institute of Immunology of the Federal Medical Biological Agency of Russia (NRC Institute of Immunology FMBA of Russia). The KK46 peptide has a branched structure and high densities of arginine- and histidine-residues (Appendix Figure 1), thereby promoting siRNA binding through stable electrostatic interactions and internalization within the cells [12].

Two types of single-walled carbon nanotubes (SWCNT) are explored in this study; **1. HiPCO** which is a high-pressure carbon monoxide process producing SWCNT with a broad diameter range. And **2. CoMoCAT** uses a catalytic method (cobalt-molybdenum) to synthesize SWCNT with narrower, chirality-controlled diameters. All our samples used HiPCO CNT, while we used CoMoCAT for comparison.

The main objective of our work is to conduct a side-by-side comparison of BSA- and KK46-functionalized CNTs as vectors for siRNA delivery. We compared their quality of dispersion, optical properties (through UV–Vis–NIR spectroscopy and photoluminescence mapping), surface charge (zeta potential), and siRNA binding aptitude (through agarose electrophoresis), and their in vitro cytotoxicity profiles determined through MTT assays. We hypothesize that although BSA functionalization can produce more ideal optical performance through well-controlled protein adsorption, the KK46 peptide with its high cationic and dendrimeric nature will provide a better safety profile and better siRNA retention.

Along with exploring CNTs, we continue to work on developing a simple approach to harvest plant-derived exosome-like nanoparticles (PELNs), in particular from ginger, as a natural siRNA delivery alternative. These biological vesicles recently came into the

spotlight for having low immunogenicity, intrinsic stability, and the capability to cross biological barriers, which makes them attractive candidates for RNA therapeutics [13][14][15][16][17][18]. The topic of this study remained on the isolation, purification, characterization, and loading of ginger-derived exosome-like nanoparticles (GELNs) with siRNA for in vitro evaluation. siRNA was loaded into GELNs via passive incubation, followed by a further purification step to remove any remaining free oligonucleotide. Loading efficiency was determined by fluorescence quantification. In vitro gene-silencing activity was then tested in suitable cell models. This research arm will allow us to verify the suitability of PELNs as a natural and biocompatible siRNA delivery vehicle alongside our more engineered CNT-based systems.

These data serve to establish the physicochemical bases and safety standards required to proceed with in vitro gene silencing experiments. Insights from this work will provide the rationale for further studies concerning the design and optimization of the next generation of siRNA delivery systems: synthetic, such as CNT-based carriers, and bio-inspired, such as PELNs, with each system offering different opportunities for safe and efficacious therapeutic applications.

5 OBJECTIVES AND AIMS

5.1 Aim

To systematically explore and characterize two distinct siRNA delivery platforms—synthetic single-walled carbon nanotube (SWCNT) formulations and natural ginger-derived exosome-like nanoparticles (GELNs), with the goal not to compare, but to define their physicochemical properties, siRNA-loading capacities, safety, and preliminary in vitro performance as complementary carrier systems.

5.2 Objectives

5.2.1 Preparation and physicochemical characterization of SWCNT-based carriers

5.2.1.1 Functionalization & dispersion of SWCNTs

Coat HiPCO and CoMoCAT SWCNTs with BSA or KK46 peptide, then verify nanotube individualization and siRNA binding by UV–Vis–NIR spectroscopy and photoluminescence mapping, ensuring the chosen coatings both debundle CNTs and provide an effective cargo-binding interface.

5.2.1.2 Surface charge & morphology

Measure ζ-potential (with and without generic siRNA) to assess colloidal stability and electrostatic wrapping, and acquire AFM images for visualization.

5.2.1.3 siRNA loading assessment

Load a model siRNA via bath sonication, monitor changes in fluorescence intensity (spectrofluorometer) and shifts in electrophoretic mobility on agarose gels, and verify accompanying ζ-potential changes to confirm complex formation.

5.2.1.4 Safety profiling of CNT carriers

Cytotoxicity: Determine HeLa cell viability after treatment with each CNT formulation (± generic siRNA) over 0.0005 to 0.1 mg/mL using the MTT assay. Fit dose-response data to a five-parameter logistic (5PL) model to capture asymmetric response

profiles, and validate model robustness via high R^2, residual distribution analysis, and bootstrap comparisons between peptide- and protein-coated carriers, yielding statistically sound IC_{50} values.

5.2.2 Isolation and physicochemical characterization of GELNs

5.2.2.1 Purification methods

Isolate GELNs from ginger extract by PEG 4000 precipitation, then divide into two purification workflows: dead-end filtration and membrane dialysis. Compare total yield, size distribution (DLS) and ζ-potential.

5.2.2.2 Surface charge analysis

Measure ζ-potential to assess electrostatic changes, thus stability.

5.2.2.3 siRNA loading into GELNs

Passive incubation: Incubate GELNs with siRNA, then quantify recovered siRNA by spectrofluorophotometry against the established calibration curve, establishing baseline passive loading efficiency.

5.2.2.4 Loading efficiency comparison

Compare loading percentages between dead-end filtration and membrane dialysis-purified GELNs to verify whether or not the purification method can limit passive cargo incorporation.

5.2.3 Preliminary in vitro gene-silencing efficacy

5.2.3.1 siSTAT3 delivery efficacy

Treat A549 cells with siSTAT3-loaded SWCNTs and siSTAT3-loaded GELNs, isolate total RNA, perform reverse transcription, and quantify STAT3 knockdown by real-time PCR using the $\Delta\Delta C_t$ method, demonstrating functional intracellular delivery of a therapeutically relevant siRNA.

5.2.3.2 Correlation of carrier metrics with functional outcome

Correlate each platform's siRNA-loading efficiency, surface charge, and dispersion homogeneity with the magnitude of STAT3 silencing to identify the key physicochemical drivers of effective gene knockdown.

6 LITERATURE REVIEW

6.1 Clinical Successes of siRNA Therapeutics:

The therapeutic potential of siRNA is evidenced by the approval of various siRNA-therapeutic agents by regulatory authorities, mainly the FDA. They have exhibited considerable effectiveness in the management of diseases that were hitherto difficult to treat using traditional medicines.

As of mid-2025, up to six siRNA therapeutics had gone on to be ratified by regulatory agencies, the landmark event for RNAi-based medicine. The first product to get approval was Patisiran in 2018. Commercially, it was sold under the trade name ONPATTRO® by Alnylam. The drug was approved for hereditary transthyretin amyloidosis, with TTR decreasing by about 81% in the serum and impressive improvements in polyneuropathy scores in the APOLLO Phase III trial [19]. In 2019, Givosiran (GIVLAARI®, Alnylam) was approved for acute hepatic porphyria, lowering porphyria attack rates by ~70% in the ENVISION phase 3 trial and gaining fast-track FDA designation [20][21] . Approved in 2020, Lumasiran (OXLUMO®) is a treatment for primary hyperoxaluria type 1, with random control trials affirming its significant effectiveness in reducing oxalate in urine [22]. Next came Inclisiran (LEQVIO®, Novartis/Alnylam) in 2021, when it was approved in various countries for the lowering of LDL-C in familial hypercholesterolemia patients [23]. Vutrisiran (AMVUTTRA®) gained FDA approval in 2022 for neuropathy and cardiomyopathy in ATTR amyloidosis and became the first subcutaneous siRNA drug with quarterly dosing [24]. Nedosiran (RIVFLOZA®, Dicerna Pharmaceuticals) was most recently approved in September 2023 for primary hyperoxaluria and therefore became the sixth siRNA on the market using GalXC™ (GalNAc-mediated structure) [25].

Other siRNA therapeutics under clinical consideration exceed 50, depending on the various target molecules and modes of operation. Some examples are Zilebesiran against hypertension (Phase 2: NCT06272487, NCT06423352) [26][27], Olpasiran (Phase 3: NCT05581303)[28] and Zerlasiran (SLN360) (Phase 2: NCT05537571)[29] targeting

cardiovascular risk via Lp(a) and apolipoproteins, RBD1016 for hepatitis B clearance (Phase 2: NCT05961098)[30], and STP705 (Phase 2: NCT04669808), a dual siRNA against TGF-β1 and COX-2 in peptide nanoparticles for Basal Cell Carcinoma[31].

During a Phase 2 trial reported in March 2025, Lepodisiran (LY3819469) (another GalNAc-siRNA-based lipoprotein(a) lowering drug) appeared to drop the cardiovascular risk markers by more than 94% at the highest dose tested [32]. Arrowhead Pharmaceuticals recently revealed data featuring another siRNA therapeutics, ARO-INHBE and ARO-ALK7, for metabolic diseases, as well as SRSD107, the very first Factor XI inhibitor with durable haemostatic control in Phase 1 evaluation (NCT06116617) [33].

Together these achievements attest to the shift of siRNA therapeutics, from those targeting rare genetic disorders to complex chronic and cardiovascular conditions, helped by the advent of improved delivery platforms (lipid nanoparticles, GalNAc conjugates, peptide nanoparticles) and improved molecular designs. The present wave of late-phase and seeking-approval programs in 2025 once again places siRNA therapeutics as a modality forefront within precision medicine.

6.2 Market overview:

6.2.1 Market Size:

The global market for small interfering RNA (siRNA) therapeutics is experiencing significant expansion, with estimates for the market value during the period of 2023-2024 projected to fall between approximately USD 1.2 billion and USD 2.93 billion, as reported by leading industry research organizations [34][35][36][37][38]. Revenue forecasts for the latter part of the decade and subsequent years exhibit considerable variability, with the majority of analyses suggesting that the market will achieve a total valuation ranging from USD 5.8 billion to USD 12.4 billion by the years 2030-2033, accompanied by compound annual growth rates (CAGR) between 14.3% and 18.8% [34][35][36][37][38]. Notably, there exist a few divergent projections, such as those from Maximize Market Research, which anticipates a substantial increase to USD 39.2 billion

by 2029 [39]. Furthermore, Research Nester posits an even more ambitious valuation, forecasting the market to approach nearly USD 15 billion in 2024 and predicting an escalation to over USD 117 billion by 2037 [40]. Whereas this is a matter of great importance, one must realize that these divergent estimations could be a result of broad market interpretations or alternate methodological approaches. While there are discrepancies in the absolute extent of the volume estimations, all reports concur regarding a strong double-digit CAGR which outlines the growth path of this industry. Technically, the growth is supported by the increase in regulatory approvals, advances in delivery technologies, increased demand, and widespread clinical applications of siRNA-based therapeutics, thereby emerging as an increasingly fast-paced sector for the biopharmaceutical market.

6.2.2 The Evolving Patent Landscape:

Chen et al., (2022) compiled a large dataset comprising 11,509 patent documents grouped into 3,309 patent families, all focused on technologies for delivering therapeutic siRNA. They noted that patenting activity concerning siRNA delivery has seen quite a huge spurt over the last two decades. In terms of patent filing, the U.S. takes the first place, followed by Japan and China.

The patents were technically classified into 10 classes. Two big classes of approaches have been registered from the patent database:

- **Carrier-based delivery**: This involves the transport of siRNA through viral and non-viral vectors.
- **Molecular-scale delivery**: This includes chemical modifications and ligand-siRNA conjugates.

The results show that the lipid-based carriers and polymer carriers are the two most commonly used systems, representing 20% each. The study further brings forth that some patent families simultaneously comprised more than one delivery technology, thus embracing a changing and expanding approach to siRNA delivery issues [41].

The present scenario of siRNA delivery technologies, therefore, bears witness to the instrumental role patents must play in clearing the way for future R&D. It, by itself,

raises the need for continued innovation toward overcoming hindrances yet there and extending the therapeutic horizon of siRNA.

6.3 Molecular Mechanisms of RISC-Mediated siRNA:

RNAi is an essential, conserved mechanism of cellular defence and regulatory control when dsRNA molecules are present. dsRNA molecules degrade a specific kind of mRNA and consequently sabotage the translation of mRNA into protein. RISC is an active participant in the targeted degradation of complementary mRNA sequences that are directed by siRNAs [42].

Initially, long dsRNAs undergo cleavage in the cytoplasmic environment by the RNase-III enzyme known as Dicer, resulting in the formation of approximately 21-24 nucleotide siRNAs that are distinguished by their 2-nucleotide 3′ overhangs and a 5′ phosphate moiety [43]. Synthetic siRNAs are chemically synthesized, typically 20–24 bp in length, mimicking Dicer-generated siRNAs [44].

The double-stranded siRNAs are recognized and incorporated into the RISC-loading complex (RLC). This consists of the RNase III enzyme Dicer, certain dsRNA-binding cofactors, such as TRBP in mammals (Trans-activation response RNA-binding protein), the heat shock protein (Hsc70/Hsp90) molecular chaperone system, and Argonaute (AGO) proteins [45]. Such loading of siRNAs is ATP-dependent and has to do with correctly positioning both strands of siRNA in the PAZ, MID, and PIWI domains of AGO2 so that the complex can be activated for maximum slicing efficacy and target specificity [44]. Strand selection follows the principle of thermodynamic asymmetry; the strand of the siRNA that exhibits less stable base-pairing at the 5′ terminus is considered the guide strand, whereas the complementary passenger strand is discarded and degraded through the slicer activity of Argonaute II (AGO2) enzyme [44]. The mature RISC, loaded with a guide strand, scans cytoplasmic mRNAs using a diffusion-controlled “hit-and-run” mechanism rather than sliding along transcripts [46].

Upon the identification of a target mRNA that exhibits complementarity to the respective nucleotide positions 2–8 (seed), 9–12 (cleavage), and 13–17 (supplementary) of the guide, AGO2 facilitates endonucleolytic cleavage occurring between nucleotides

10 and 11, thereby commencing the exonucleolytic degradation of the resulting mRNA fragments. The efficiency of assembly of the RISC complex, the loading of the guide strand, and the binding and subsequent cleavage of the target can be influenced by factors such as the thermodynamic stability of siRNA, the secondary structural configuration of mRNA, and the conformational adaptability of RISC [46].

Structural investigations elucidate the functions of AGO domains: the PAZ domain attaches to the 3′ terminus, MID stabilizes the 5′ phosphate group, and the PIWI domain accommodates the catalytic DDH motif that is integral for slicing [44]. Furthermore, co-chaperones Hsc70/Hsp90 prepare AGO for the loading of duplexes, while proteins such as GW182 engage deadenylase complexes (e.g., CCR4–NOT) to promote subsequent mRNA degradation [45]. Although only AGO2 in humans possesses slicer functionality, other AGO isoforms (AGO1, AGO3, and AGO4) also participate in gene silencing but through different mechanisms. They are implicated in translational repression and/or deadenylation (the removal of a poly-A tail) through their association with a protein called GW182, which is instrumental in guiding the mRNA towards translational repression or deadenylation [47]. The unique ability of AGO2 to directly cleave mRNA substrates carries profound implications. In the context of therapeutic RNAi strategies, it is mainly to ensure that the RNAi therapies used for the design are indeed compatible with AGO2 slicing capacity, so that the corresponding drug can have great efficacy [48][49].

From a therapeutic perspective, a well-thought-out sequence design and the incorporation of chemical modifications in siRNA, such as 2′-O-methyl (2′-OMe) phosphorothioate [19], alongside the strategic design of Dicer-substrate siRNAs [50], serves to augment the loading efficiency into the RISC, enhance molecular stability, and improve target specificity, all while concurrently reducing the activation of innate immune responses.

The RNAi pathway has significant implications for both basic research and therapeutic applications. siRNAs can be designed to target specific genes, making them powerful tools for studying gene function and developing treatments for diseases. However, the efficiency and specificity of siRNAs once in the cytoplasm can be

influenced by various factors, including the sequence of the siRNA, the structure of the RISC complex, and the presence of accessory proteins.

6.4 Primary Barriers to siRNA Delivery and Their Impact on Clinical Translation:

In the clinical development of siRNA-based therapeutics, the delivery constitutes the major bottleneck. The problems comprise extracellular and intracellular impediments which affect the therapeutic usefulness and clinical potential of the siRNA. Among the jamming barriers are the rapid degradation of siRNA by nuclease, poor cellular uptake, inefficient endosomal escape (99% of siRNAs are not able to access the cytosol [51]), off-target effects, and immune activation [52][53][54]. In addition, naked siRNAs are large (~12 kDa), anionic (>40 phosphodiester bonds) and hydrophilic and cannot pass through the phospholipid bilayer without aid from delivery materials, making their delivery that much more difficult [53][51]. Adding to this, the rapid renal clearance of siRNAs due to their small size and the recognition and opsonization by the reticuloendothelial system (RES), reduces their bioavailability [52].

Following intravenous administration, siRNA carriers are required to traverse the circulatory system, evade immunological detection, exit the vascular compartment, infiltrate tissue, penetrate cellular membranes, and resist degradation during their transit to the RISC located in the cytosol [55]. A seminal framework proposed by Guo et al., delineates the clinical impediments associated with siRNA as “the 3 E challenges”: Entry, Escape, and Efficacy [56].

- **Entry:** Encompasses circulation, biodistribution, and cellular uptake.
- **Escape:** Pertains to the release from endosomal compartments into the cytosol.
- **Efficacy:** Relates to the preservation of siRNA integrity, loading onto RISC, and the avoidance of off-target or immunological responses.

These barriers represent critical challenges in advancing siRNA therapeutics. Surmounting these obstacles necessitates the development of specialized nanocarrier chemistries that effectively balance stability and release kinetics, along with innovations

in functionalization, targeting methodologies, size optimization, and sequence alterations to diminish immunogenicity and off-target effects.

6.4.1 Cellular Internalization and Endosomal Escape:

Recently, innovative ways to enhance the delivery of siRNA into the cytosol have been proposed. Park et al., demonstrated that the substitution of Na^{+} by Ca^{2+} in the synthesis of siRNA-based spherical nucleic acids diminished endosomal retention by approximately 22% and stimulated gene silencing up to 20-fold in U87-MG and SK-OV-3 cancer cells [57]. Studies of Janus base nanopieces (JBNTs) loaded with siRNA discovered that these non-covalent, fabric-like arrangements encouraged macropinocytosis uptake while ensuring endosomal escape via the proton sponge mechanism with almost negligible toxicity [58]. Du Rietz et al., further studied cholesterol-conjugated siRNA escape in spheroid models by means of live-cell imaging of galectin-9 to monitor endosomal disruption; following pharmacological treatment, its escape was magnified by almost 47-fold [59].

6.4.2 Systemic Delivery & Extracellular Stability:

The design of siRNA for enhanced stability requires chemical modifications of the siRNA to resist enzymatic degradation and tailoring carriers to prevent rapid clearance and improve biodistribution [53]. siRNAs below 14 kDa undergo degradation in serum and are eliminated quite fast by filtration through kidneys unless protected by carriers such as PEGylated LNPs or polymers, who also serve to hinder clearance via RES sequestration along the lines of enhancing time of residence in circulation and biodistribution[53].

6.4.3 Immune Response and Side Effects:

Strategies formulated to facilitate the evasion of siRNA from endosomal compartments may inadvertently stimulate the immune response by rendering the siRNA accessible to intracellular detection mechanisms. Such mechanisms encompass endosomal receptors, including TLR3 and TLR7/8, in addition to cytosolic sensors such

as RIG-I and PKR. The activation of these receptors initiates signalling cascades involving NF-κB and IRF, which enhance the synthesis of pro-inflammatory cytokines (e.g., IFN-α/β, TNF-α, and IL-6), potentially culminating in a systemic inflammatory reaction [60].

The chemical alterations of the siRNA strand have been proven to reduce the immune response and, likewise, do this without having a negative effect on the gene-silencing ability of siRNAs. Modifications such as 2′-O-methyl (2′-OMe) and 2′-fluoro (2′-F) of the ribose sugars, modifications of the backbone by phosphorothioates (PS), and locked nucleic acids (LNA) were made to stabilize the siRNA duplex and reduce the immune stimulation [61]. Carefully selected modifications to the backbone and sugar components are critical**,** not only preserving silencing capability and enhancing serum stability but also attenuating the activation of innate immune receptors, thus augmenting the clinical applicability of siRNA-based therapies.

6.5 Emerging non-viral siRNA Delivery Systems:

A variety of siRNA delivery systems have been formulated, encompassing both conventional lipid-based nanoparticles and novel conjugate-based platforms.

In principle, the delivery systems must **(a)** *protect siRNA in the systemic circulation,* **(b)** *promote cellular internalization,* **(c)** *release of the endosomes,* and **(d)** *release therapeutics selectively on target sites* [62][53]. Both traditional and novel carriers have been designed to overcome such challenges, their development is driven by ongoing input from preclinical and clinical studies.

6.5.1 Lipid Nanoparticles (LNPs):

Lipid nanoparticles or solid Lipid Nanoparticles are one of the best-studied and clinically well-validated siRNA delivery methods. Originally designed to deliver siRNAs, they have been more recently used in other types of cancer gene therapies and vaccination approaches [63] such as COVID-19 vaccines [64]. These nanoparticles consist of lipid molecules that can be cationic or ionizable and are meant to encapsulate siRNA, thereby protecting it from degradation in the biological milieu and ensuring easy

uptake by the cells [65]. LNPs are put to a clinical trial successfully, exemplified by the approval by the FDA of Patisiran (Onpattro®), the first FDA-approved siRNA therapeutic to make use of a second-generation LNP delivery system in treating hereditary transthyretin-mediated amyloidosis [66][67].

LNPs have good biocompatibility, stability, and targetability to tissues. Further, they may be functionalized with targeting ligands to impart specificity [68][69].

Despite their promise, LNPs often deliver only ~2% of siRNA to the cytoplasm, with most trapped and degraded, while ionizable/cationic lipids can harm healthy cells and trigger immune responses, causing cytokine release, infusion reactions, or even anaphylaxis [70]. LNPs also have the tendency to accumulate in the liver (and sometimes spleen or kidneys) due to the rapid uptake by the liver's RES and biomolecular corona formation, limiting functionality to other organs [71]. Lastly, a few changes in particle size, surface charge, or Polyethylene glycolation (PEGylation) with slight variations during manufacturing change the efficacy and safety profile greatly and make scale-up very complicated with batch-to-batch consistency [71].

6.5.2 Liposomes:

Unlike the next generation LNPs, which are solid colloidal carriers composed of lipid materials that form solid particles at body temperature, liposomes are vesicular structures synthetically made of phospholipids organized into clear bilayers [63]. Liposomes have also been widely examined for the delivery of siRNAs [72]. Further design can be pursued to include any targeting ligand or cell-penetrating peptide to improve delivery even for the BBB [73]. Liposomes are biocompatible and can carry both hydrophilic drugs by encapsulation and hydrophobic molecules in their lipophilic membrane, making them an appealing drug delivery system [74]. Dioleoyl phosphatidylcholine (DOPC) based formulations for instance show efficacy in tumour size reduction in breast cancer settings and delivering siRNA molecules that target a gene for an oestrogen receptor [75]. However, Liposomes often form a protein corona in the bloodstream that alters their behaviour, triggers immune clearance, and, along with aggregation and complex manufacturing requirements [76][77], reduces their targeting

efficiency [63]. In contrast, LNPs' more compact, ionizable-lipid–based structure offers better protection and delivery of nucleic acids, simpler formulation, and improved bioavailability with lower toxicity [78][63].

6.5.3 GalNAc-siRNA Conjugates:

Chemical conjugation techniques such as that of siRNA with targeting ligands like N-acetylgalactosamine (GalNAc) have appeared to be one of the most attractive alternatives [79]. These naked conjugates are designed to exploit receptor-mediated internalization into hepatocytes via the the asialoglycoprotein receptor (ASGPR) and thus augment specificity [80]. Their chemical uniformity facilitates scalable and precisely defined synthesis, while simultaneously minimizing batch-to-batch variability [80]. The conjugation process frequently yields diminished immunogenic profiles in comparison to larger nanoparticle systems such as LNPs, and other advantages like easier method of administration (subcutaneous injection), as well as the dosage and frequency of administration, which has been instrumental in the success of most FDA-approved siRNA therapies and several GalNAc conjugates in various stages of clinical development [81][79]. Nonetheless, the pronounced specificity for hepatic tissues may present a limitation when siRNA therapy is directed towards pathologies extending beyond hepatocytes. Furthermore, A significant limitation is the inefficient release of siRNA from endosomes into the cytoplasm, with less than 1% achieving this transition, which can impact therapeutic efficacy [82]. Also, there is a risk of siRNA-mediated silencing of unintended genes, leading to potential hepatotoxicity [83][84]. Besides the off-target effects, the intracellular accumulation and chemical reactivity with metabolites also contribute to hepatotoxicity, thereby several chemical modifications have been proposed to mitigate these issues [84] [85][86].

6.5.4 Polymeric Nanoparticles:

Developed from biodegradable materials such as chitosan, PEG, poly(lactic-co-glycolic acid) (PLGA), or polyethyleneimine (PEI), these systems are easily modified for the control of siRNA release. Due to their flexibility, they can also be designed to attack

a specific type of cell or tissue. Polymer nanoparticles, therefore, are highly flexible, allowing them to be engineered with respect to size, charge, and surface modification. They provide protection against enzymatic degradation and, with modification, they can achieve high transfection efficiency [87] [88]. Some polymers, however, like PEI with higher molecular weight, have shown toxic effects on cells and hence possibly hinder their use in humans [72]. Researchers, in an attempt to overcome these problems, modify or conjugate the polymers with some other biocompatible material, however, these modifications increase the complexity of nanoparticle design [72].

6.5.5 Inorganic Nanoparticles

A number of Inorganic Nanoparticles (INPs) have been considered for siRNA delivery since they have specific physicochemical characteristics: high surface area to volume ratio, tuneable surface chemistry, or intrinsic properties like magnetism or photoluminescence for efficient loading, protection, and targeted delivery of siRNA [89]. These intrinsic features equip the INPs with an advantage in terms of stability, targeting, and multifunctionality [89].

In particular, magnetic, metallic, and silica-based nanoparticles have been underscored for their significant role in the delivery of siRNA aimed at cancer-associated genes, such as programmed death ligand-1 (PD-L1) and vascular endothelial growth factor (VEGF), consequently facilitating apoptosis and reducing the activity of cancerous cells [90]. Materials such as mesoporous silica nanoparticles (MSNs) provide extensive surface areas and tuneable pore dimensions, thereby permitting considerable siRNA loading and regulated release characteristics[91]. For instance, MSNs possessing pore sizes between 6 and 50 nm have demonstrated efficacy in encapsulating siRNA molecules, shielding them from enzymatic degradation and enabling a prolonged release within targeted cells [91].

Several developments have been increasingly centred around the design of stimuli-responsive inorganic nanoparticles that release siRNA responding to an external stimulus like a change in pH, magnetic field, or thermal response, thereby enhancing therapeutic efficacy and minimizing side effects [92][93]. Iron oxide nanoparticles for instance have

been encapsulated with β-cyclodextrin and PEG were utilized for the targeted delivery of 5-fluorouracil, an anti-neoplastic agent, facilitating an enhanced drug release in vitro at PH of 6.8, which may be encountered in the tumour microenvironment [94].

The development of super carbonate apatite (sCA) and its advanced form of inorganic nanoparticle device (iNaD) has shown great potential in enhancing tumour-targeted delivery while diminishing hepatic toxicity in vivo, thereby promising inorganic nanoparticles for clinical utilization [95]. Surface functionalization of inorganic nanoparticles can popularly occur through diverse functional groups for increased safety profile, greater targeting specificity, and enhanced cellular uptake. For instance, with mesoporous silica nanoparticles, being PEI coated would imply that the complex has a slight positive charge to interact electrostatically with negatively charged siRNA molecules, thereby enhancing cell uptake and the ability to escape endosomes [96]. Certain INPs, including superparamagnetic iron oxide nanoparticles (SPIONs), exhibit magnetic properties that enable external magnetic field-guided targeting, a process referred to as magnetofection [97]. By this method, prolonging siRNA-loaded nanoparticle retention from designated sites is increased, thereby improving transfection efficiency [97]. Similarly, gold nanoparticles (AuNPs) possess some special properties and can be functionalized to deliver siRNA, gene silencing efficiently with relatively less toxic consequences [98]. They have been used to deliver TGF-β1 siRNA, hence inhibiting tumour growth and improving life expectancy in mouse models [99]. Gold Nanorods (GNRs) were used to facilitate siRNA delivery to brain tissues. In a rat hippocampus model, GNR-siRNA complexes exhibited great knockdown of target genes without cytotoxic effects [100]. Thus, PEI-capped pSiNPs are applied to deliver MRP1 siRNA in glioblastoma models to obtain significant target gene silencing and reduction of tumour growth in vivo [101]. Nanodiamonds (NDs), owing to their unique surface properties, have been employed for siRNA delivery in Ewing sarcoma cells for targeted gene silencing with minimal cytotoxicity [102].

On the other hand, aspects involved with managing the size of INPs, their chemical composition, and surface charge, meanwhile enhancing intracellular transport and reducing off-target effects, are truly challenging [89]. The long-term safety profile

comprising numerous inorganic nanoparticles has yet to be completely elucidated [103]. One major aspect that need to be estimated is their long term effect under chronic exposure [103]. Escalating the dilemma is that INPs can be highly variable due to their sensitivity to minor changes in synthesis, which can result in unexpected toxic responses, making it difficult to scale up or standardize their usage for safe clinical applications [103]. In summary, while inorganic nanoparticles hold significant potential for siRNA delivery, addressing their toxicity, delivery efficiency, and manufacturing challenges is crucial for their successful clinical application.

6.6 Exosomes and the Role of PELNs in Overcoming siRNA Delivery Challenges:

Exosomes were discovered in the extracellular environment in 1983 [104]. Originally, exosomes were considered remnants shed by cells undergoing injury or simply by-products of cellular homeostasis, with no major effects on adjacent cells [105]. It is only lately that these extracellular vesicles have been considered working bodies carrying a complex mixture of proteins, lipids, and nucleic acids, transcription factors, metabolites [106], having the ability to express and deliver these molecular cargos toward certain target cells [105].

These nano-sized extracellular vesicles have come to be established as suitable vehicles for the delivery of siRNA, addressing the great hurdles of drug delivery [107]. They are inherently secreted by almost all cells [108] both by mammalian and plant cells [109]. With a phospholipid bilayer membrane that is similar to other cellular structures [108], They exhibit distinctive characteristics such as high biocompatibility, reduced immunogenicity, and the capacity to navigate biological barriers, rendering them exemplary candidates for siRNA delivery [107][110][111][112]. The endosomal origin of exosomes allows them to merge with the membrane of target cells, and deliver siRNA therapeutic inside the cytoplasm [113]. Furthermore, mammalian exosomes can be engineered to present specific targeting ligands, thereby augmenting their specificity for pathological cells [113], particularly in the context of delivering siRNA to neoplastic cells [16].

For example, mammalian exosomes derived from mesenchymal stem cells (MSCs) that are loaded with siRNA directed against connective tissue growth factor (CTGF) have demonstrated effectiveness in mitigating inflammation and fostering neural regeneration in models of spinal cord injury [114]. In a different study, MSCs exosomes -siRNA complexes were successful in targeting the STAT3 gene and significantly improved liver function in mice with established liver fibrosis [115]. Similarly, milk-derived exosomes have been used to deliver siRNA against vascular endothelial growth factor (VEGF), epidermal growth factor receptor (EGFR), AKT, mitogen-activated protein kinase (MAPK), and Kirsten rat sarcoma viral oncogene homolog (KRAS). Successful gene silencing was achieved and the inhibition of tumour progression in various cancer models [116]. Additionally, mammalian exosomes have been harnessed for the delivery of siRNA in the treatment of inflammatory conditions, such as inflammatory bowel disease (IBD) with an oral delivery [117]. Exosomes that are loaded with siRNA targeting oncogenes hold great promises in cancer therapy with several successful results, by targeting genes involved in cancer cell growth, survival, or resistance to drugs [118]. At present, a phase 1 clinical trial is being conducted at the M.D. Anderson Cancer Centre located in Houston, Texas, United States, involves participants diagnosed with pancreatic carcinoma, utilizing exosomes derived from MSCs that are loaded with siRNA [119][120]. This first therapeutic trial on human using engineered exosomes derived from MSCs shows how far exosomes advanced as a promising delivery platform for siRNA therapeutics.

While exosomes derived from mammalian sources have been the subject of extensive research, plant-derived exosome-like nanoparticles (PELNs), which are also designated as plant-derived nanovesicles (PDNVs) or plant-derived extracellular vesicles (PDEVs), have emerged as a compelling alternative in the field of nanomedicine due to their distinctive advantages [121]. They exhibit analogous morphological and structural features to their mammalian equivalents, encompassing a lipid bilayer and a varied assortment of biologically active constituents [122][16][17]. PELNs can mitigate numerous limitations associated with the nature of siRNA, attributed to their biocompatibility, minimal immunogenicity, stability, and their natural origin from

consumable plants, thereby facilitating the encapsulation and protection of siRNAs from degradation while promoting their delivery to target cells [123][124][17][125]. Their membranes protect encapsulated siRNA from degradation in harsh environments, and for this reason, they are very suitable for oral or systemic delivery [112]. One can also design them to increase stability and specificity in targeting, thereby enabling controlled release and targeted distribution into desired cells or tissues [126].

In comparison to mammalian exosomes, PELNs present potential advantages in terms of biocompatibility, reduced immunogenicity, cost-effectiveness, and the feasibility of large-scale production from edible sources, thereby establishing them as appealing candidates for therapeutic interventions and drug delivery mechanisms [13][14][15][16][17][18]. Research pertaining to plant-derived exosomes is advancing swiftly, with a growing number of in vivo investigations illustrating their therapeutic capabilities. Nevertheless, the quantity of clinical trials remains relatively sparse. Numerous preclinical investigations have assessed the therapeutic efficacy of PELNs across various disease models. For instance, grapefruit-derived extracellular vesicles have been effectively utilized to encapsulate siRNAs, with one study documenting an encapsulation efficiency of 11% alongside successful intracellular delivery and gene suppression outcomes in human keratinocytes (HaCaT cells) utilizing a microfluidic device [125]. Another study investigated intranasal administration of therapeutic miR-17 (microRNA) to brain tumour cells by means of grapefruit exosomes that, when coated with a PEI/RNA complex, greatly increased the miR-17 loading capacity and lessened PEI-associated cytotoxicity [123]. And several studies focused on ginger, for example, ginger-derived exosome-like nanoparticles (GELNs) carrying divalent metal-ion transporter 1 (Dmt1) siRNA were found to inhibit the expression of Dmt1 and alleviate iron loading in murine hereditary hemochromatosis [127]. A different study shows that oral administration of GELNs loaded with CD98-targeting siRNA can successfully reduce colonic CD98 expression in ulcerative colitis models, with an encapsulation efficiency of about 61% [128]. Nonetheless, there were clinical trials involving a variety of plant-derived exosomes for additional therapeutic applications, such as assessing

ginger-derived exosomes for inflammatory bowel disease [129] and lemon exosomes for lowering LDL cholesterol levels [130] as constituents of dietary supplements.

However, several challenges seem to be holding PELNs back. The current methodologies for their isolation lack adequate sensitivity and standardization [122][124]. Consequently, investigators continue to encounter difficulties in the reliable detection and quantification of these diminutive vesicles in a manner that facilitates uniform quality control [124]. Also, more efficient methods to load them with therapeutic molecules are needed, the efficiency of cargo loading is frequently suboptimal or detrimental: passive incubation results in inadequate siRNA incorporation, whereas active techniques such as electroporation, sonication, or freeze-thaw cycles may jeopardize vesicle integrity, induce aggregation, and ultimately yield only modest loading levels [131]. And even though their natural origin implies that they have lower toxicity and fewer side effects in the body, there are still regulatory challenges. There is a need for extensive safety testing and clinical data to prove that these PELNs do not trigger unwanted immune responses or accumulate toxins from the plants, especially if the fruits and vegetables are not from organic agriculture [124].

6.7 Role of CNT in Overcoming siRNA Delivery Challenges:

Carbon nanotubes or CNTs denote cylindrical nanostructures made of carbon atoms arranged in a hexagonal lattice. The main types of CNTs are named single-walled (SWCNT) and multi-walled (MWCNT). SWCNTs have the most fundamental geometric configuration and have been characterized as possessing diameters lying between 0.4 and 3 nm [132].

They demonstrate, undoubtedly, fascinating mechanical and optical properties that would make them candidates for highly specialized applications. Mechanically, they exhibit Young's modulus surpassing 1 TPa, with tensile strengths approaching ~63 GPa, 50 times more than steel, all while preserving a low density (~1.3 g/cm^3), which is one-sixth that of stainless steel [133]. They can undergo large bending, twisting, and elongation (reaching about 18%) without structural failure, which is attributed to the seamless cylindrical structure made of graphene and the very strong sp^2 carbon-carbon

bonds [133]. Optically, SWCNTs exhibit distinct absorption bands relative to their diameters and chiralities, with semiconducting varieties being photoluminescent, which facilitates defect detection, assessment of purity, and characterization [133]. The flexibility with which these optical properties can be tuned according to chirality and surface functionalization will greatly enhance their versatility [133].

Adding to these exceptional physical characteristics, and because of their high surface area, electrical conductivity, high aspect ratios, and potentially enhanced adsorption capabilities attributed to their cylindrical morphology, CNTs gain lots of interest as nanocarriers [4].

CNTs can be further functionalized with a variety of molecules, either by *non-covalent* or *covalent* interactions to increase siRNA loading, protect the cargo against enzymatic degradation, and enhance cellular uptake [134]. In addition, CNTs can be made to be conjugated with targeting ligands, such as peptides or antibodies, for increased specificity, targeting ability, and minimizing off-targeting effect [135]. They are also able to cross biological barriers, such as cell membranes and blood-brain barriers (BBB), hence ideal for the delivery of siRNA to target tissues that are inaccessible [135].

The rapid degradation of siRNA within the body is a major downside to their effectiveness. CNTs can offer protection and stability for the siRNA molecules. Kirkpatrick et al., showed that siRNA attached to SWCNTs remain protected on exposure to ribonucleases, with 80% of the siRNA remaining intact after 2 hours and 70% after 3 hours, whereas they were degraded almost completely within 1 hour if in the free form [136]. Pristine CNTs (pCNTs) however, bear an inherent hydrophobic characteristic, which promotes their agglomeration on contact with aqueous media, thus leading to poor dispersion and potential cytotoxicity [11]. To overcome these obstacles, extensive studies have been devoted to surface functionalization with biocompatible groups. PEGylation may be used, for instance, to further enhance the stability and increase circulation time [137]. PEGylated phospholipids are used to confer stabilization and improved loading capacities to the delivery system, which consequently contributes to increased delivery rates of siRNA [138].

6.7.1.1 Covalent functionalization:

In this covalent functionalization, the surface of the CNTs establishes a bond with functional groups such as carboxylic acids, amines, or polymeric chains. This is usually achieved through oxidative reactions [139] [140]. The covalent attachment of these groups creates a stable interface, which can be further modified to bind oligonucleotides [141], ensuring their attachment to CNTs during delivery and reducing premature release, however, covalent functionalization can damage CNTs' structure due to the harsh chemical reactions, affecting their electronic and mechanical properties [142].

Al-Jamal et al., showed that covalently grafting second-generation quaternary ammonium dendrons onto multi-walled carbon nanotubes (MWCNTs) enhances cellular uptake of siRNA and achieves gene silencing in vitro [143]. Furthermore, -CONH-$(CH_2)_6$-$NH_3^+Cl^-$ functionalized SWCNTs have been employed for the delivery of telomerase reverse transcriptase siRNA, leading to the inhibition of tumour proliferation in both murine and human cell lines [144].

6.7.1.2 Non-Covalent Functionalization:

Non-covalent functionalization involves relatively weaker forces like π-π stacking, hydrophobic interactions, and electrostatic forces to attach molecules to the surfaces of CNTs. Quite often, this process is considered simpler and gentler than covalent approaches with respect to maintaining the structural integrity of CNTs [145]. For example, non-covalently functionalized CNTs using lipopolymers or succinated polyethyleneimine are highly effective in complex formation with siRNA, providing high stability and loading capacity, facilitating uptake by cells, as well as effective delivery to various tumour cell lines with low toxicity profile [146][147]. This methodology of functionalization is notably efficacious in facilitating reversible interactions with the surfaces CNTs and the controlled release of siRNA upon exposure to external stimuli such as near-infrared (NIR) light irradiation [148]. Nevertheless, relatively weaker bonds can cause a reduction in the stability of siRNA-CNT complexes resulting in the rapid release of the therapeutic agent [149].

6.8 Summary:

In essence, the therapeutic potential of siRNA lies in overcoming its intrinsic instability, uptake, and endosomal entrapment by cells and its off-target or immunogenic effects. Nanocarriers have been investigated for the past decades to resolve these barriers, with CNTs and PELNs becoming most noteworthy due to their unique properties. CNTs combine exceptional mechanical strength, high aspect ratio and surface area, and tuneable optical and electronic features, which can be harnessed to load, protect and deliver siRNA with high efficiency, whereas non-covalent functionalization has advantages in preserving the structural integrity of CNTs. They not only can protect siRNAs from enzymatic degradation but also promote directed cellular uptake and, in some designs, stimulus-responsive release while overcoming challenging biological barriers such as BBB.

Similarly, PELNs provide a biologically derived alternative that takes advantage of the intrinsic biocompatibility, low immunogenicity, and scalability of plant materials. Isolated from fruits and vegetables like ginger or grapefruit, these vesicles encapsulate siRNA within a phospholipid bilayer similar to that of mammalian exosomes. They are protective of the cargo from passing through physiological barriers and, when appropriately engineered, can be triggered to release and target at the cellular level. Current methods for isolation and loading are not yet quite ideal, while the regulatory pathways remain to be established. Still, preclinical models of PELNs demonstrate gene silencing in vitro and in vivo and emphasize the promise of these vesicles as a cheap natural system for siRNA delivery.

Advances in CNTs and plant exosomes serve as examples in this greater transition toward multifunctional, tuneable carriers which, beyond siRNA protection, actively guide its delivery to diseased cells so that it may produce fewer off-targets and immunogenicity. The global RNA therapeutics market is expected to grow expeditiously in the next decades; hence, these novel platforms present rather tempting prospects for investment and commercialization. Perfecting functionalization chemistry, loading strategies, and ideally including up-scaled manufacturing will always constitute the basis for translating

the platform from bench to bedside and thus usher in more precise, potent, and patient-friendly RNAi-based therapeutics.

7 MATERIALS AND METHODS

7.1 Materials

7.1.1 Reagents and Biological material:

All chemicals and materials were used as received and stored at 4 °C unless otherwise specified.

- HiPCO SWCNT (Purified, Nanointegris company, Canada).
- CoMoCat SWCNTs (6,5 enriched, Sigma Aldrich).
- Bovine Serum Albumin (BSA) (≥98% purity, Helicon, Russia).
- Phosphate Buffered Saline (PBS) (Paneco company, Russia).
- Ethidium Bromide (AppliChem, Germany).
- Agarose (Paneco company, Russia).
- PEG 4000 (KhimMed company, Russia).
- Dulbecco's Modified Eagle's Medium (DMEM) (Gibco™).
- Sodium Pyruvate (Gibco™).
- Fetal Bovine Serum (FBS) (Gibco™).
- Penicillin/Streptomycin (Gibco™).
- Buffer for DNA Loading Dye (Paneco company, Russia).
- DNA Ladder (50–1,000 bp) (Sigma-Aldrich™).
- MTT Solution (4 mg/mL) (Merck™).
- DMSO (Merck™).
- Saponin (Sigma-Aldrich™).
- Guanidine-thiocyanate (Sigma-Aldrich™).
- siRk12 (siRNA Produced in-house at NRC Institute of Immunology FMBA of Russia; MW: 14 018 Da; Guide strand sequence: GAAUAGAGCUCGCACCGUAtt).

- siSTAT3 (Purchased from DNA technology, Russia; MW: 16 569 Da; Guide strand sequence: UAUACCACAGGAUUGAUGCtt).
- siRNA with fluorescent label (si-Interleukin 4 with VIC lable «siIL4-VIC», Purchased from DNA technology, Russia).
- Peptide Dendrimer KK46 (Synthesized in-house at NRC Institute of Immunology FMBA of Russia).
- HeLa Cells (From the collection of Gamaleia Institute, Russia).
- A549 Cells (From the collection of Gamaleia Institute, Russia).
- Ginger (from the local market).

7.1.2 Laboratory equipment

The following equipment was used to perform the work:

7.1.2.1 For CNT Complexes

- Branson 450 Digital Horn Sonicator.
- Ultrasonic Bath (ODA Service, Russia).
- Sigma 3K30 Centrifuge.
- UV–Vis–NIR Spectrophotometer (Perkin Elmer Lambda 1050).
- UV–Vis–NIR Cuvettes (10 × 10 mm^2) (Hellma Analytics).
- Horiba Jobin Yvon NanoLog 4 Spectrofluorometer (Equipped with a nitrogen-cooled InGaAs detector for excitation-emission mapping).
- Particule size analyzer (Zetasizer Nano ZS, Malvern Panalytical, UK)
- Bruker Multimode V8 Microscope (Utilized in PeakForce™ Quantitative Nanomechanical Mapping (PF-QNM) mode for AFM).
- Gel Doc XR+ System (Bio-Rad) (For imaging agarose gel electrophoresis results).
- Thermo Scientific Multiskan Sky Microplate Spectrophotometer.
- Virtis Advantage XL 70 W Freeze Drier.
- Cary 100 UV-Vis spectrophotometer from Agilent Technologies
- Cuvette 10×10 mm, quartz (MiniMed, Russia).

- Electrophoresis Power Supply (DNA technology, Russia; used in agarose electrophoresis).

7.1.2.2 For GELNs

- Centrifuge (Beckman Coulter, used J-20 rotor, USA).
- Centrifuge (CM-Micro SCO Tech, Germany)
- Particle Size and Zeta Potential Analyzer: Dynamic Light Scattering (Photocor Compact Z, Russia).
- Minicentrifuge-Vortex (Microspin FV-2400, Latvia)
- Incubator thermostat (DNA technology, Russia)
- Incubator (Domel, Slovenia
- Ultrasonic bath CT-408 (CT brand, China)
- Shimadzu RF 6000 Spectrofluorophotometer.
- Macro Flourescence Cuvette Type 1FL with PTFE Cover (Material: UV Quartz) (Lightpath: 10mm) (Fireflysci, USA).
- Amicon 8010 Stirred Ultrafiltration Cell 10 mL.
- Ultrafiltration membrane XM300 25mm (30 nm cutoff). (Diaflo®, Amicon, USA)
- Single-head diaphragm (oil-free) vacuum pump and compressor
- Spectra/Por 6 Dialysis Membrane Tubing (MWCO 12–14 kDa).

7.2 Methods

7.2.1 Sample Preparation for CNTs-BSA/KK46-siRNA complexes

All dispersions and their optical and physicochemical characterization were conducted at the Laboratory of NanoMaterials at Skoltech University and stored at 4 °C. The dispersion protocol was based on the work of Zaremba et al., (2019) [150] with added steps and modifications.

7.2.1.1 BSA–CNT Complexes:

BSA was dissolved in phosphate-buffered saline (PBS) at concentrations of 5, 2.5, or 1 mg/mL, followed by filtration through a 0.45 µm syringe filter. Accurately weighed HiPCO SWCNTs were then added to achieve final CNT concentrations of 1, 0.5, 0.05, or 0.01 mg/mL. The resulting mixtures were sonicated in an ice bath (maintained at 11 °C) using a Branson 450 digital horn sonicator at 60 W for 90 minutes. Subsequently, the dispersions were centrifuged at 15,000 g for 45 minutes at 4 °C (Sigma 3K30 centrifuge), and the clear supernatants were collected for further processing.

7.2.1.2 KK46–CNT Complexes

KK46 peptide solutions were prepared in PBS at 1 or 0.5 mg/mL. CNTs (either HiPCO or, for comparison studies, CoMoCat) were added to these peptide solutions to achieve final concentrations of 0.05 or 0.01 mg/mL. The dispersion protocol was identical to that for BSA-CNT complexes, involving sonication under the same parameters and centrifugation at 15,000 g for 45 minutes at 4 °C.

7.2.1.3 siRNA Loading and Lyophilization

To each CNT dispersion, siRNA was added to reach final concentrations of 20, 40, 80, or 150 µg/mL. The mixtures were gently bath-sonicated at room temperature for 10 minutes to promote siRNA complexation. After complexation, the dispersions were freeze-dried using a Virtis Advantage XL-70 W freeze-drier overnight and stored at -80 °C until subsequent characterization. The freeze-drying step was performed at the NRC Institute of Immunology FMBA of Russia.

7.3 CNTs-BSA/KK46-siRNA complexes Characterization

7.3.1 UV–Vis–NIR Spectroscopy:

Absorbance spectra (200–860 nm) were recorded on a UV–Vis–NIR spectrophotometer (Perkin-Elmer Lambda 1050) utilizing 10 × 10 mm^2 light path cuvettes (Hellma Analytics).

7.3.2 Photoluminescence (PL):

Excitation–emission maps were acquired on a fluorescence spectrometer (Horiba Jobin Yvon NanoLog-4 spectrofluorometer with a nitrogen-cooled InGaAs detector).

7.3.3 Zeta-Potential:

Samples were diluted 100× in RNase-free water to achieve conductivity < 10 mS/cm. Measurements were performed at 25 °C using a Zetasizer Nano ZS, and the mean ± SD of three runs was reported.

7.3.4 Atomic Force Microscopy (AFM):

The imagery was collected utilizing the PeakForce™ Quantitative Nanomechanical (PF-QNM) Mapping mode on a Bruker Multimode V8 microscope.

7.3.5 Agarose Electrophoresis

A 2 % agarose gel was prepared in 1× TAE buffer containing a nucleic acid stain (ethidium bromide). 10 µL of each sample were mixed with 2 µL loading dye, loaded alongside a 50–1 000 bp DNA ladder, and a free siRNA was used as a reference. Electrophoresed at 100 V for 30 min in 1× TAE (Power Supply: DNA technology, Russia) Bands were visualized using a gel imager (Gel Doc XR+ System from Bio-Rad).

7.4 MTT Cytotoxicity Assay for CNT complexes

Cell culture and MTT assays were performed at the NRC Institute of Immunology FMBA of Russia.

7.4.1 Cell Culture:

HeLa cells were maintained in Dulbecco's Modified Eagle's Medium (DMEM) supplemented with 10% FBS and 1% penicillin/streptomycin at 37 °C in a humidified atmosphere containing 5% CO_2.

Cells were seeded at 1×10^4 cells/well in 96-well plates and allowed to adhere for 24 h. Test samples were redissolved in deionized water (diH_2O). (BSA-CNTs, KK46-CNTs, with and without siRNA) and controls (PBS, diH_2O) were added in triplicate across serial dilutions (0,1/0,05/0,01/0,005/0,001 and 0,0005 mg/mL) and incubated for 24 hours.

7.4.2 MTT Protocol:

Following treatment, 25 µL of 4 mg/mL MTT solution was added to each well. Plates were then incubated for 4 hours at 37 °C in 5% CO_2 to allow formazan crystal formation. The supernatant was carefully removed, and 100 µL of DMSO was added to each well to dissolve the formazan crystals. Absorbance was measured at 570 nm (with 650 nm used for background correction) using a Thermo Scientific™ Multiskan Sky Microplate Spectrophotometer. The absorption was calculated using the formula:

$$Absorption = Absorption\ at\ 570\ nm - Absorption\ at\ 650\ nm$$

The following formulations were evaluated:

- Sample named ***"BSA"*** (BSA-CNTs without siRNA): initial sample before freeze drying was: BSA= 5 mg/mL, CNTs= 1 mg/mL
- Sample named ***"KK46"*** (KK46-CNTs with siRNA): initial sample before freeze drying was: KK46= 0.5 mg/mL, CNTs= 0.05 mg/mL, siRNA= 80 ug/mL
- Sample named ***"NTL"*** (KK46 without siRNA): CNTs were dispersed in KK46 peptide with an initial concentration of KK46 = 0.5 mg/mL and CNTs = 0.05 mg/mL.
- **BSA-CNTs with siRNA:** Two formulations were prepared:
    - Sample named *"**RNA_150**"*: The initial sample before freeze drying was BSA = 2.5 mg/mL, CNTs = 0.01 mg/mL, and siRNA = 150 µg/mL.
    - Sample named *"**RNA_80**"*: The initial sample before freeze drying was BSA = 2.5 mg/mL, CNTs = 0.01 mg/mL, and siRNA = 80 µg/mL.
- **Positive Control (diH2O):** Deionized water was used as a positive control, representing 100% cell death.

- **Negative Control (PBS):** Phosphate-buffered saline (PBS) was used as a negative control, representing untreated cells with expected high viability.

7.5 Ginger-derived exosome-like nanoparticles (GELNs) isolation and purification:

The protocol was based on a protocol shared with me by Pr. Jhon Fredy Betancur, Professor and Researcher at the University of Manizales, Colombia [151]. We modified it and used PEG precipitation + membrane dialysis/dead-end filtration instead of ultracentrifugation.

7.5.1 Processing of Ginger

Approximately 600 g of ginger was procured from the local market and washed three times with 20 % Extran to remove surface impurities. The outer skin was then peeled away, yielding about 460 g of unpeeled ginger, which was ground and processed in a blender. Afterwards, the slurry was filtered through a filter paper to obtain nearly 300 mL of ginger extract to be then kept at 4 °C.

7.5.2 Exosome Isolation and Purification:

Samples of ginger extract were diluted 1:1 in PBS, by placing 7.5 mL of extract plus 7.5 mL of PBS in 15 mL Falcon tubes before submitting to three cycles of vortex mixing for 30 seconds, with 1-minute intervals to avoid overheating. Initial centrifugation at 400 g for 20 minutes (4 °C) removed cells and large debris; the supernatant was then spun at 800 g for another 20 minutes to discard the remaining debris. A subsequent 10,000 g spin for 40 minutes yielded a microvesicle pellet, which was resuspended in 500 µL of PBS and stored at –20 °C. The final supernatant was also kept at –20 °C for exosome purification and, prior to precipitation, was passed through 0.45 µm filters to remove residual particulates.

7.5.3 PEG Precipitation (PEG 4000)

A 10 % solution of PEG 4000 in PBS was prepared and mixed 1:1 with the filtered exosome-containing supernatant in a clean tube. The entire mixture was kept overnight at 4 °C to ensure good precipitation of exosomes. Later after incubation, the sample was subjected to centrifugation at 8,000 g for 30 minutes at 4 °C. After centrifugation, the slightly translucent pellet of exosomes was carefully collected and resuspended in PBS.

7.5.4 Filtration:

For concentration and buffer exchange, the resuspended exosome preparation was processed through an Amicon 8010 Stirred Ultrafiltration Cell (10 mL, 30 nm cutoff) using a pressure pump, and the final concentrate was stored at –20 °C. In parallel, an aliquot of the pellet was loaded into Spectra/Por 6 Dialysis Membrane Tubing (MWCO 12-14 kDa). The tubing was cut to length, soaked in distilled water for 30 minutes to remove preservatives, rinsed thoroughly, filled with exosome suspension, and dialyzed overnight against PBS at 4 °C following the manufacturer's instructions.

7.6 siRNA loading to GELNs:

Here, the loading protocol was adapted from Kocholatá et al. (2024) [152]. It was considered that the exosomes were to be dosed at 10 µg siSTAT3/mL, meaning that in the case of a batch being sized for 10 mL, 100 µg siSTAT3 was going to be needed. siSTAT3 with amounts up to nearly 100 µg was placed in a sterile 1.5-mL tube and then diluted with RNase-free PBS, 1×, up to a volume of 1 mL to make a final concentration of 100 µg/mL. The tubes were closed tightly, flicked gently for mixing, and kept on ice. Samples were then centrifuged at 45,000 g for 2 h; the resulting pellet was collected and resuspended in PBS.GELNs Characterization

7.7 Dynamic Light Scattering (DLS) Analysis:

Assess size distribution and zeta potential using Particle size and zeta potential analyzer (Photocor Compact-Z, Russia). The samples were measured without preparation.

7.8 Spectrofluorophotometer analysis:

Spectrofluorophotometer analysis was performed on ginger exosome samples labelled with siRNA following a standardized lysis and measurement protocol. First, each 10 µl sample was mixed with 10 µl of freshly prepared 2 % saponin in PBS and incubated at room temperature for 10 minutes. The mixture underwent ultrasonic conditioning for 3 minutes prior to adding 250-µl guanidine-thiocyanate. Following vortexing for 2 minutes, the samples plus reagents were incubated at room temperature for about 20 minutes, after which there was again a 2-minute period of vortexing. Initially, the samples were made to stay in ice water for 2 minutes to stabilize the reaction; afterwards, the samples were treated with ultrasonic energy for one last 30 seconds. Both the standard solutions and the treated samples were used for fluorescence measurements on a Shimadzu RF-6000 spectrofluorophotometer, with a fixed excitation wavelength of 525.0 nm and an emission wavelength of 546.0 nm. These raw data were then fed forward for further analysis.

7.9 In-Vitro Assay (Waiting for the results: ongoing work)

8 RESULTS

8.1 Optical and Physicochemical Characterization of CNTs' dispersions

8.1.1 UV–Vis–NIR Absorption Spectroscopy (200–860 nm)

Absorption spectra of all the samples were taken to analyse their dispersion quality, state of aggregation, and interaction with the functionalization reagents (BSA, KK46, and siRNA).

The spectra showed a prominent peak in the UV range (~220-300 nm) primarily due to π–π* transitions of BSA and KK46 aromatic residues and intrinsic CNT absorption (Figure 1 shows only spectra starting from 300 nm).

Beyond the UV domain, the absorption gradually declined, revealing broad modulations across the visible and NIR ranges. The spectra in both BSA-CNT and KK46-CNT dispersions revealed fine modulations in the 550-860 nm range, which correspond to CNT excitonic transitions, specifically E_{22} in the visible range (~550-650 nm) and E_{11} in the near-infrared (~700-860 nm) (Figure 1. A and 1.B). The visibility of such transitions is an encouraging indication of the individualization of nanotubes because bundled CNT exhibit broader, poorly defined spectral features. These observations attest that KK46 and BSA both effectively wrap CNT with their characteristic electronic transitions.

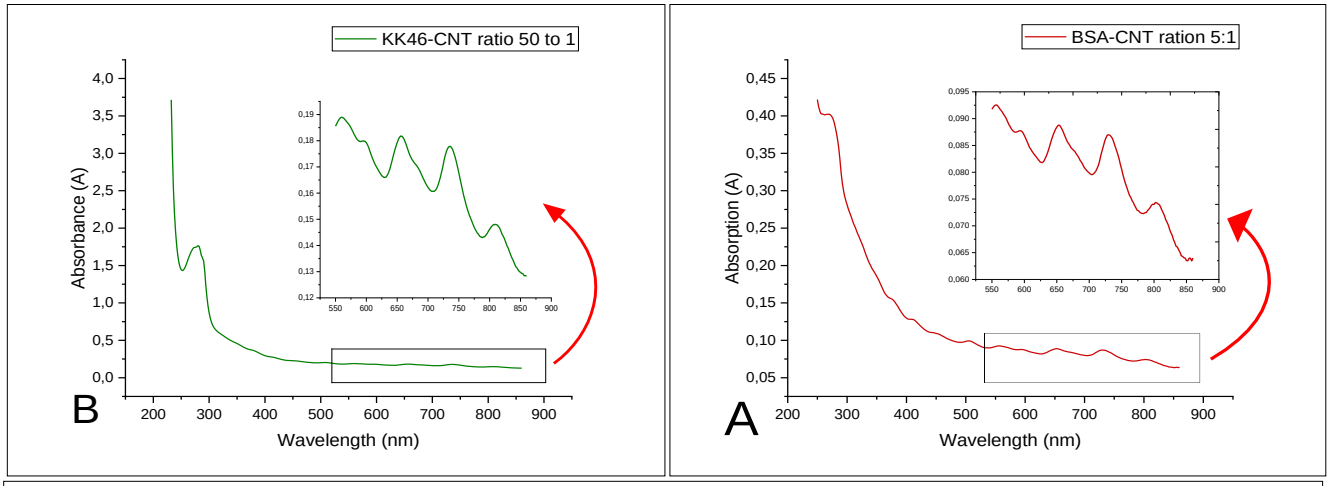

Figure 1. Absorption spectra of BSA-CNT **(A)** and KK46-CNT **(B)** complexes, with zoom-in on the 550 to 860 nm region

8.1.1.1 Effect of siRNA Addition:

8.1.1.1.1 BSA-CNT-siRNA

- With the addition of siRNA at concentrations of 20, 80, 100, and 150 µg/mL and bath sonication, the BSA-CNT absorption spectra (Figure 2A, 2B, 2C, 2D respectively) showed slight spectral shifts.
- Absorption intensities remained stable across these siRNA concentrations.

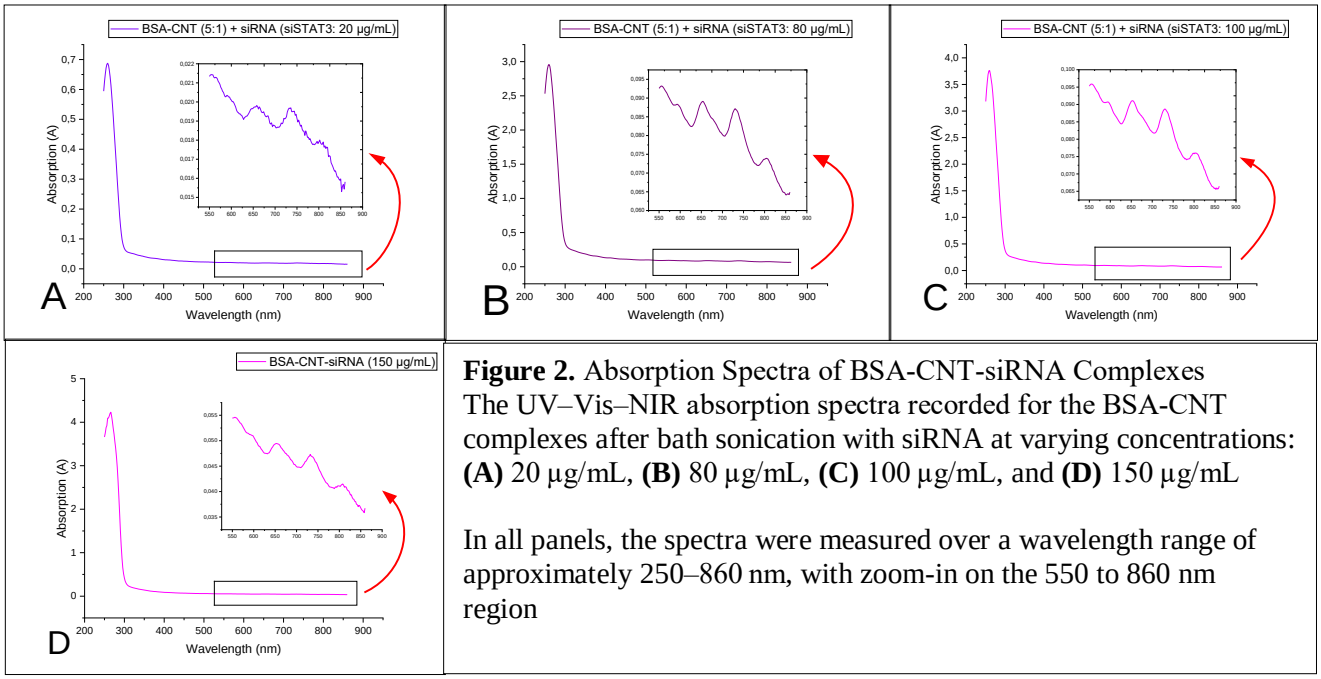

Figure 2. Absorption Spectra of BSA-CNT-siRNA Complexes
The UV–Vis–NIR absorption spectra recorded for the BSA-CNT complexes after bath sonication with siRNA at varying concentrations: **(A)** 20 µg/mL, **(B)** 80 µg/mL, **(C)** 100 µg/mL, and **(D)** 150 µg/mL

In all panels, the spectra were measured over a wavelength range of approximately 250–860 nm, with zoom-in on the 550 to 860 nm region

8.1.1.1.2 KK46-CNT-siRNA:

In the KK46-CNT samples, the optical spectra varied with the amount of siRNA added:

- At a siRNA concentration of 20 µg/mL, both the E_{22} band (approximately 550-650 nm) and the E_{11} band (approximately 700-860 nm) were clearly visible (Figure 3A), ratio of KK46 peptide to siRNA is 25 to 1.
- At a siRNA concentration of 80 µg/mL (ratio KK46 to siRNA = 6.25:1) or 100 µg/mL (ratio KK46 to siRNA = 5:1), these excitonic peaks were flattened (Figure 3B, 3C respectively).

Note: The KK46 peptide is strongly positively charged at physiological pH; all reported spectra were collected under identical conditions.

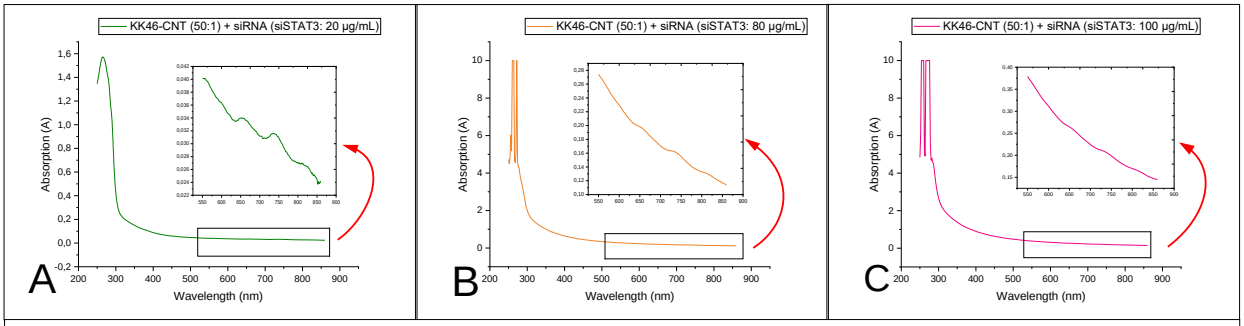

Figure 3. Absorption Spectra of KK46-CNT-siRNA Complexes
The UV–Vis–NIR absorption spectra recorded for the BSA-CNT complexes after bath sonication with siRNA at varying concentrations: **(A)** 20 µg/mL, **(B)** 80 µg/mL, and **(C)** 100 µg/mL.
In all panels, the spectra were measured over a wavelength range of approximately 250–860 nm, with zoom-in on the 550 to 860 nm region

8.1.1.2 Comparing BSA-CNT dispersions to siRNA-CNT (control) (Figure 4):

In the UV Region, BSA-CNT complexes display an intense, characteristic peak at approximately 280 nm, mirroring the aromatic residues of BSA. Whereas siRNA-CNT dispersions show a broader, less intense UV profile (typically centred near 260 nm), due to the inherently weaker absorbance of nucleic acids. While in the **Visible–NIR Region**. Both dispersions retain distinct CNT excitonic transitions (E_{22} at ~550-650 nm and E_{11} at ~700-860 nm). However, minor spectral shifts and slight intensity variations in the siRNA-CNT samples suggest that the electrostatic interactions between siRNA and CNT surfaces subtly modify the dielectric environment without compromising the dispersions' stability.

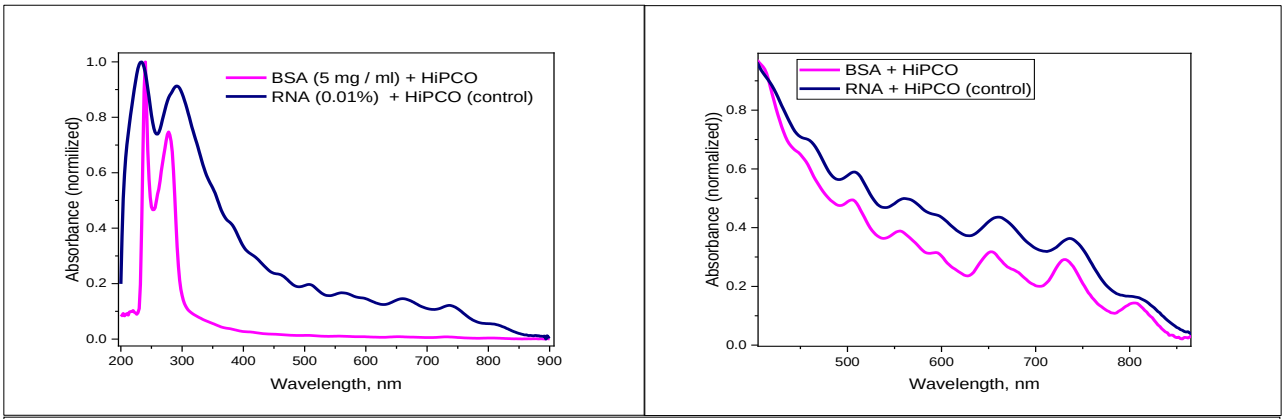

Figure 4. Comparative UV-Vis-NIR Profiles of BSA-CNT versus siRNA-CNT dispersions with zoom-in on the region between 550 and 860 nm on the right. A side-by-side comparison that highlights differences in the UV region (proteins vs. nucleic acids) and the consistency of CNT excitonic transitions across formulations.

8.1.1.3 Comparing KK46–HiPCO to KK46–CoMoCat CNT Dispersions (Figure 5):

Optical Properties: KK46–HiPCO dispersions (Figure 5A) exhibit characteristic CNT excitonic transitions (E_{22} and E_{11}) with broad bands that reflect the intrinsic wide diameter and chirality distribution of HiPCO nanotubes. As opposed to KK46–CoMoCat (Figure 5B) dispersions are more likely to exhibit sharper, more defined absorption peaks in the visible-NIR region due to the narrow, chirality-controlled diameter range of CoMoCat.

These results highlight that while KK46 is able to stabilize HiPCO and CoMoCat CNTs efficiently, the inherent structural distinction between the two morphologies reveals itself as a special optical feature. Such data can then be harnessed for designing carrier performance on the basis of the specific requirements of the target application.

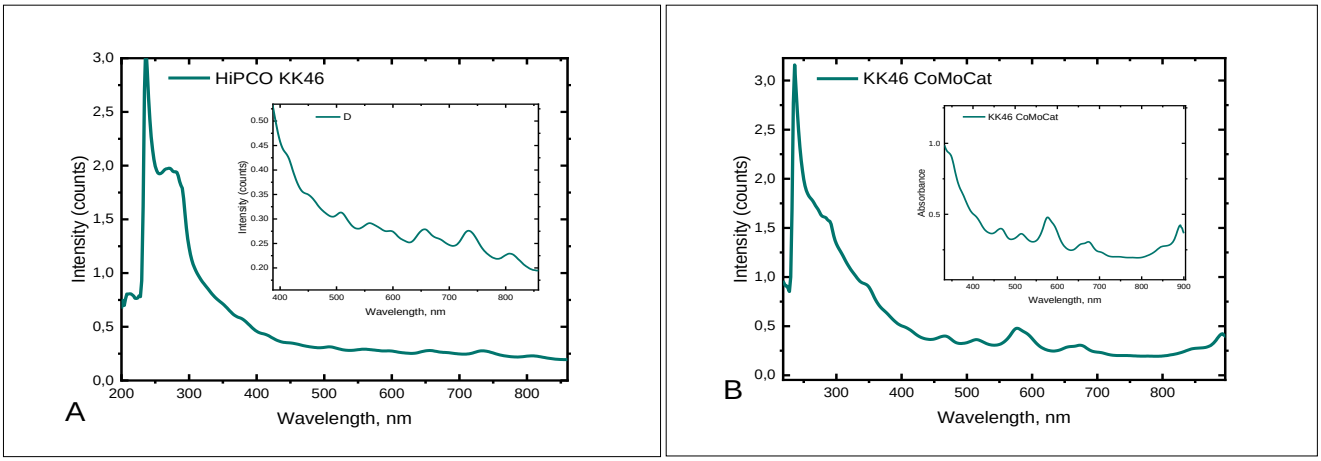

Figure 5. Optical Comparison between KK46–HiPCO **(A)** and KK46–CoMoCat **(B)** CNT Dispersions

8.1.1.4 Effect of Freeze-Drying on CNT dispersions Stability:

To evaluate whether freeze-drying (lyophilization) and subsequent redissolution affect the optical properties of our CNTs' dispersions, we compared absorption spectra of the 5:1 BSA-CNT sample before and after freeze-drying. After precipitating and lyophilizing the dispersion overnight, the powder was reconstituted in deionized water, stored at 4 °C for 7 days, and then measured under identical conditions to the original sample (before freeze-drying). There was no visible aggregation on CNT dispersions (Appendix Figure 24 and 25).

Figure 6: The main absorption profile (200–600 nm) of the redissolved sample (green trace) overlaps closely with the fresh dispersion (orange trace), with only a slight increase in baseline absorbance across the UV region.

In the inset (600–900 nm), the characteristic E_{22}/E_{11} excitonic peaks around 750-850 nm are preserved in position and relative intensity, with ≤5 % variation in peak height between the two traces. No new scattering features or broad shoulders appear, indicating minimal aggregation or irreversible bundling upon freeze-drying.

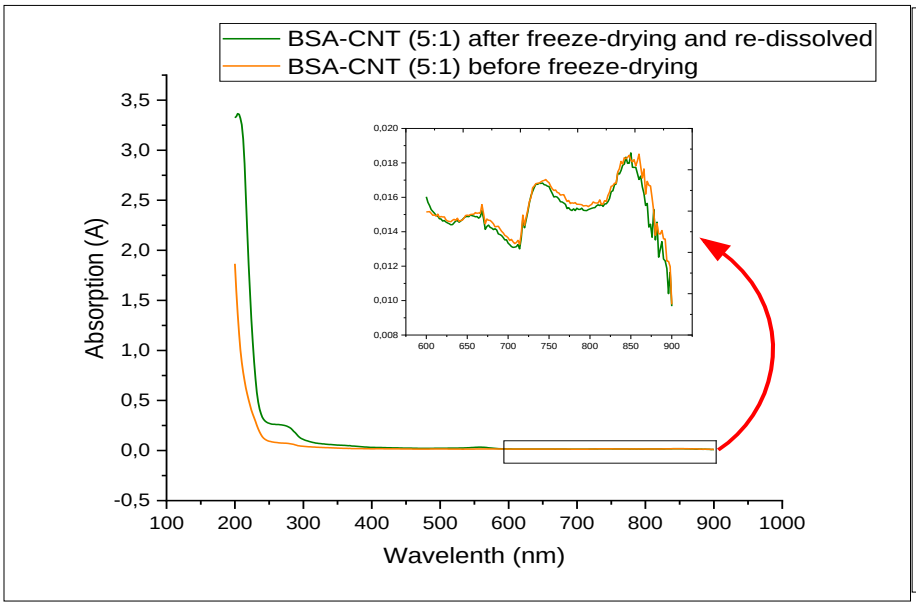

Figure 6. Effect of Freeze-Drying on the Absorption Spectra of BSA-CNT (5:1) Dispersions, using Cary 100 UV-Vis spectrophotometer from Agilent Technologies.
Green line: BSA-CNT (5:1) after freeze-drying and redissolution
Orange line: BSA-CNT (5:1) before freeze-drying

8.1.2 Photoluminescence (PL) Mapping

PL maps were obtained to evaluate the effect of protein and peptide coatings on CNT in the near-infrared range (950-1300 nm). Such data are relevant to determining dispersion quality, charge-transfer effects, and utility for optical tracking applications.

For BSA-coated CNTs, intense PL emission hotspots were present with high intensity, and a characteristic excitation wavelength of **600-650 nm** and emission wavelengths of **1100-1200 nm** were noted (Figure 7A), which are associated with distinct E_{22} excitations and E_{11} emissions of semiconducting CNT. Discrete PL peaks indicate that debundling by BSA is sufficient.

siRNA addition (40 µg/mL) to BSA-CNT dispersions caused an approximate 1.5× PL intensity increase (Figure 7B). This may suggest that siRNA preferentially binds to certain CNT chiralities.

Similarly, KK46-CNT complexes showed similar hotspots (with excitation wavelengths between **600–650 nm** and emission wavelengths between **1100–1200 nm**), but lower intensity (Figure 7C). KK46-CNT complexes produced the same hotspots (excitation at 600–650 nm and emission at 1100–1200 nm), but with lower intensity (Figure 7C).

These findings verify that BSA and KK46 preserve CNT photoluminescence, and siRNA acts as an extra stabilizer to selectively promote optical properties.

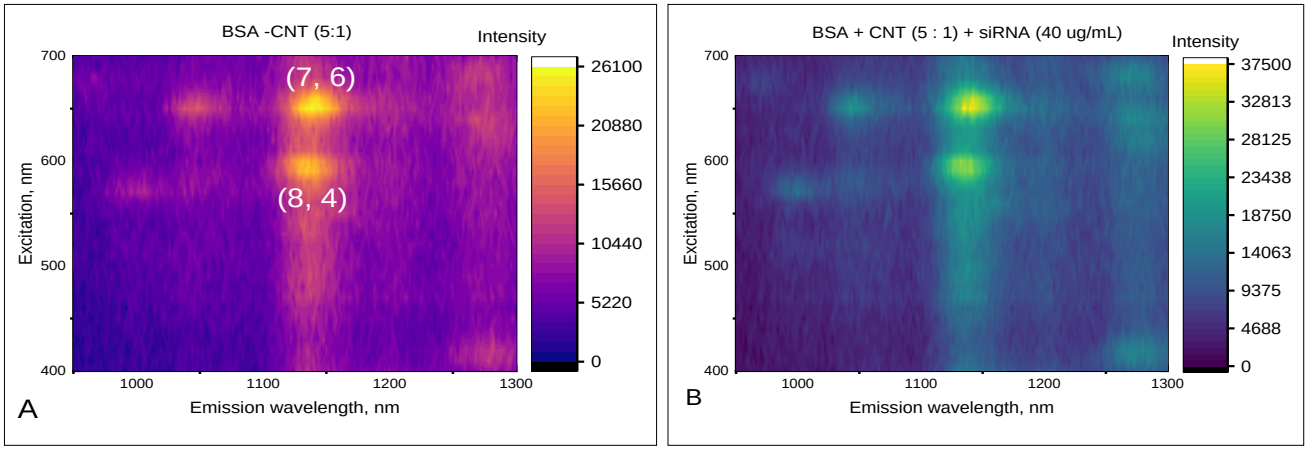

Figure 7. Photoluminescence (PL) Mapping of CNT Complexes:
(A) PL emission hotspots from BSA-coated CNT **(B)**: Increased PL intensity (~1.5×) in BSA-CNT complexes upon siRNA incorporation, suggesting dielectric modulation.
(excitation : 600-650 nm ; emission : 1100-1200 nm). **(C)** K46-CNT complexes

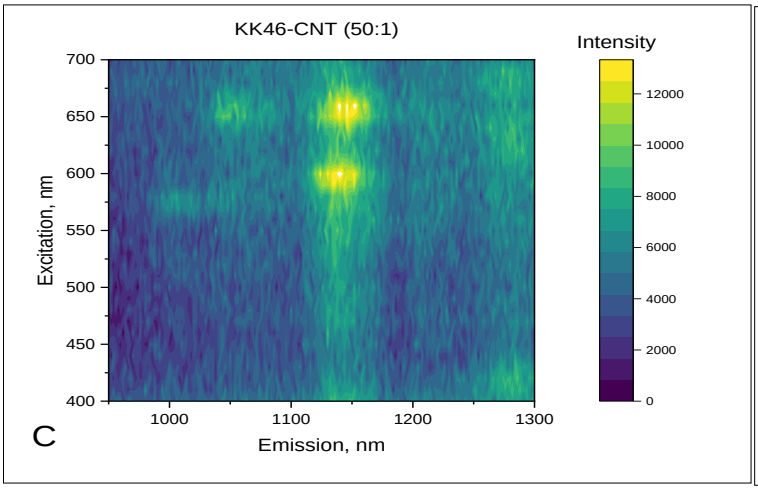

Figure 6.C Photoluminescence (PL) Mapping of K46-CNT complexes (excitation : 600-650 nm ; emission : 1100-1200 nm).

Table 1 summarizes the optical and physicochemical characterization for all samples.

Sample	S_{22}/S_{11} Peak Quality	PL Emission (Relative)
BSA-CNT 10:1	Broad	low

BSA-CNT 5:1	-	-
BSA-CNT 5:1 + siRNA 40 µg/mL	Sharp	Very high (increase by x1.5)
BSA-CNT 250:1	Sharp	low
BSA-CNT 250:1 + siRNA 20 µg/mL	Broad	low
BSA-CNT 250:1 + siRNA 40 µg/mL	Broad	low
BSA-CNT 250:1 + siRNA 80 µg/mL	Broad	low
BSA-CNT 250:1 + siRNA 150 µg/mL	Sharp	low
CNT (HiPCO 0.025 mg/mL) + siRNA (0.01 %)	Sharp	high
KK46–CNT 100:1 (HiPCO)	Sharp	None
KK46–CNT (HiPCO) 50:1 + siRNA 80 µg/mL	Sharp	None
KK46–CNT (CoMoCat) 50:1	Sharp	High
KK46–CNT (HiPCO) 50:1	Sharp	moderate

Table 1: S_{22}/S_{11} peak sharpness and PL emission intensity for all formulations.
• ***S_{22}/S_{11} Peak Quality:*** *"Sharp"* denotes spectra with well-resolved, distinct peaks, indicative of good CNT individualization; *"Broad"* implies less clearly defined peaks, possibly due to aggregation or less optimal dispersion. • ***PL Emission (Relative):*** The qualitative terms *("None", "Low", "Moderate", "High", "Very High")* are defined relative to a reference sample (**BSA-CNT 5:1**) and was correlated with the corresponding PL intensity measured under identical conditions.

8.2 Surface Charge (ζ-Potential) for CNT complexes

Zeta potential measurements were performed to assess the surface charge modifications upon functionalization and siRNA binding (using siRK12 and siSTAT3). Table 2 summarizes the measured values for each sample.

8.2.1 BSA-CNT Complexes (siRk12):

- Without siRNA: **–22.8 mV**, indicating moderate negative charge due to BSA wrapping.
- After siRK12 addition (80 µg/mL): **–10.4 mV**, suggesting partial neutralization by siRNA binding, which reduces electrostatic repulsion while stabilizing the complex.

8.2.2 KK46–CNT Complexes (siRk12):

- Without siRNA: **+43.0 mV**, confirming the strong cationic nature of KK46, which enhances nanotube dispersion and prevents aggregation.
- After siRK12 addition (80 µg/mL): **+51.7 mV**, implying that siRNA further increases the positive charge.

8.2.3 Complexes Formulated with siSTAT3

- **CNT + siRNA (control, siSTAT3, 100 µg/mL):** -36.5 ± 8.58 mV
- **BSA-CNT (5:1 ratio) + siRNA (siSTAT3, 80 µg/mL):** -43.4 ± 7.26 mV
- **KK46-CNT (50:1 ratio) + siRNA (siSTAT3, 80 µg/mL):** +23.5 ± 5.02 mV

These results indicate that, for the siRk12 siRNA, BSA-CNT complexes shift toward a less negative potential upon siRNA binding, while KK46-CNT complexes show an increase in positive charge. In the case of siSTAT3, the BSA-CNT complexes exhibit a more negative overall surface charge and the KK46-CNT complexes display a lower positive charge compared to the siRk12 formulations. All values are reported as mean ± standard deviation.

Sample	ζ-Potential and St Dev (mV)
siRNA **(siRk12: 100 µg/mL)**	-7.05± 1.5
BSA-CNT (5:1 ratio)	-22.8 ± 3.39
BSA-CNT (5:1 ratio) + siRNA **(siRk12: 80 µg/mL)**	-10.4 ± 4.35
CNT + siRNA (control) **(siRk12: 100 µg/mL)**	-30.4 ± 2.0
KK46 (in water)	+3.8 ± 0.5
KK46-CNT (50:1 ratio) (in water)	+43.0 ± 5.16
KK46-CNT (50:1 ratio) + siRNA **(siRk12: 80 µg/mL)**	+51.7 ± 5.11
KK46-CNT (CoMoCat)	+18.6 ± 5.78
KK46-CNT (HiPCO)	+37.6.2 ± 4.74
CNT + siRNA (control) **(siSTAT3: 100 µg/mL)**	-36.5 ± 8.58
BSA-CNT (5:1 ratio) + siRNA **(siSTAT3: 80 µg/mL)**	-43.4 ± 7.26
KK46-CNT (50:1 ratio) + siRNA **(siSTAT3: 80 µg/mL)**	+23.5 ± 5.02

Table 2: Zeta potentials with SD for all formulations

8.3 Morphology by AFM

In BSA–CNT (1:5) dispersion: An individual tube was identified. However, BSA aggregates were frequently observed, likely reflecting residual unbound protein (Figure 8).

Challenges

- The use of a hard cantilever for AFM imaging has limited resolution at the nanoscale.
- BSA aggregates remain on the substrate after washing, which further complicates the image interpretation.

Further optimization of washing steps and alternative AFM imaging modes (such as tapping mode or softer cantilevers) may improve resolution for finer nanotube surface analysis.

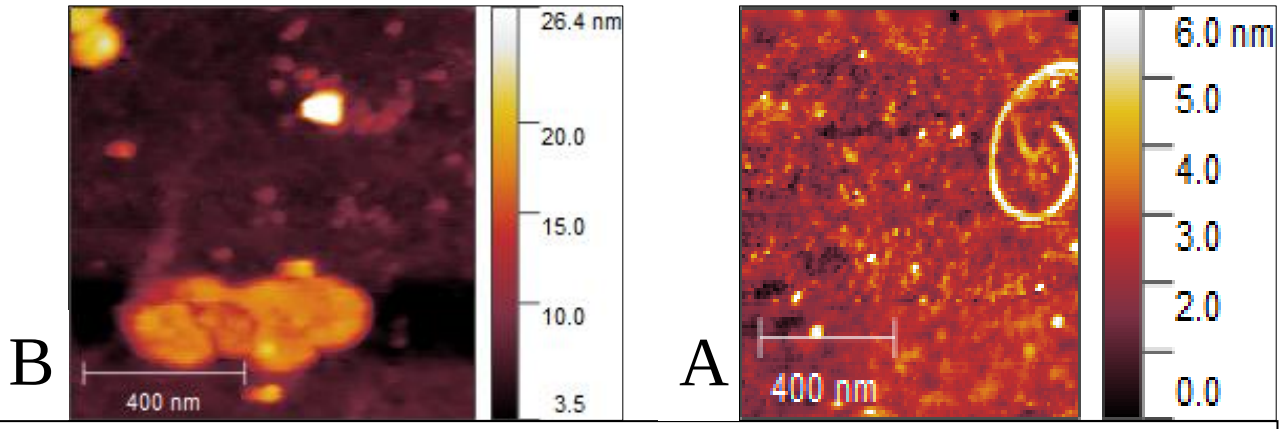

Figure 8. AFM Imaging of BSA–CNT Dispersions Images illustrating individually dispersed SWCNT **(A)** and the presence of BSA aggregates **(B)**, indicating the need for further washing optimization.

8.4 Agarose Electrophoresis

A 2 % agarose gel (1× TAE) was used to test siRNA interaction with CNT formulations (Figure 9).

Agarose electrophoresis provided qualitative proof of siRNA complexation to functionalized CNTs. Free siRNA migrated as expected below 50 bp. For KK46-CNT-siRNA complexes, no distinct siRNA band is observed, consistent with their strongly positive ζ potential, which prevents visualizing migration under standard electrophoretic conditions. With the exception of lane 3 (1 mg/mL KK46, 0.01 mg/mL CNT, 80 µg/mL siRNA), where there is a weak band at the free siRNA position, signifying a partial release of the siRNA.

BSA-CNT-siRNA complexes had mixed results. Some bands appeared at the free siRNA level, suggesting incomplete or unstable binding under gel conditions. This discrepancy indicates potential dissociation effects that merit further investigation.

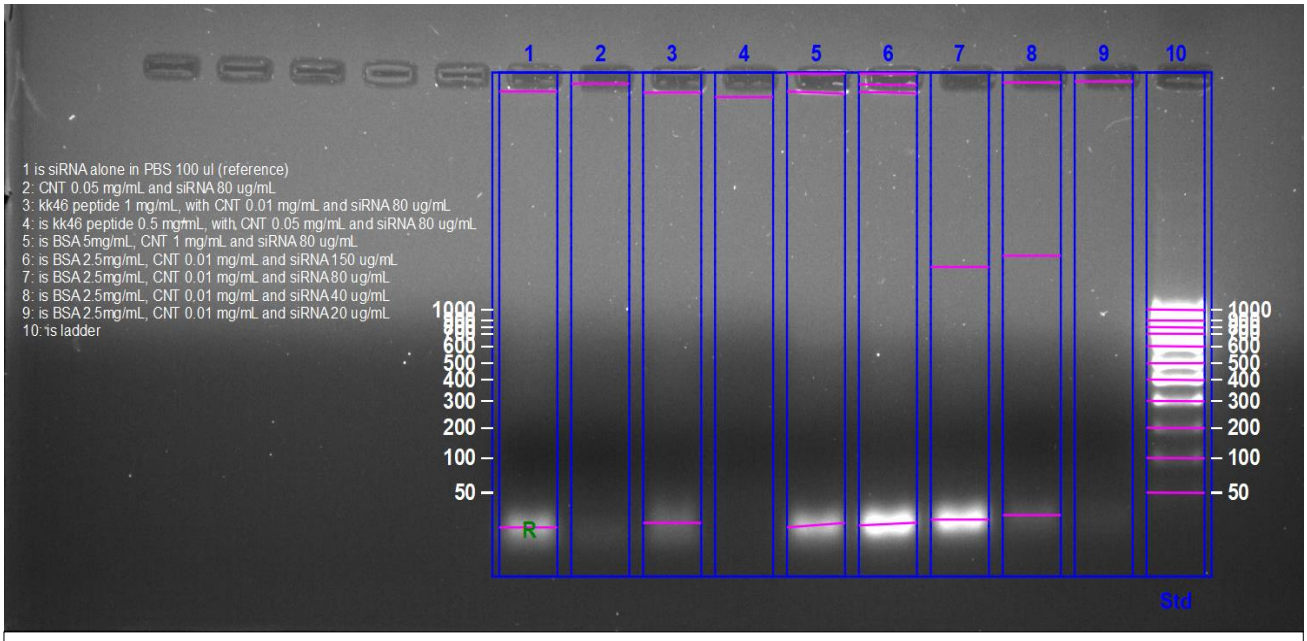

Figure 9. Agarose Gel Electrophoresis of siRNA Binding to CNT Formulations Gel images showing free siRNA migrating below 50 bp (R) and the differential retention of siRNA in KK46-CNT (lane 3 and 4) versus BSA-CNT complexes (lane 5 to 9)

8.5 MTT assay

8.5.1 Dose-Response and IC_{50} Determination

We first evaluated HeLa cell viability after 24 h exposure to increasing concentrations (0.0005–0.1 mg/mL) of our five test formulations: ***"BSA sample"*** (BSA-CNT without siRNA), ***"KK46 sample"*** (KK46-CNT with siRNA), ***"NTL sample"*** (KK46-CNT without siRNA), ***"siRNA_150 sample"*** and **"siRNA_80 sample"** (BSA-CNT with siRNA).

$$Viability\ (\%) = \frac{mean\_abs - mean\_pos}{mean\_neg - mean\_pos} \times 100.$$

Where:

- **mean_abs** = average absorbance per sample/concentration (570 nm – 650 nm)
- **mean_pos** = mean absorbance of the "diH2O" positive control
- **mean_neg** = mean absorbance of the "PBS" negative control

Percentage viabilities were plotted against the base-10 logarithm of CNTs concentration and fitted concurrently to a five-parameter logistic model (5PL):

$$Y(x) = \frac{A - D}{\left[1 + \left(\frac{x}{C}\right)^{B}\right]^{E}} + D$$

Where:

- Y: is the predicted response (cell viability %),
- X: is the CNT concentration,
- A: maximum asymptote (top plateau)
- B: is the Hill slope (steepness),
- C: is the inflection point (IC_{50}_inflect), where IC_{50} = 10logC
- D: minimum asymptote (bottom plateau)
- E: is the asymmetry factor

8.5.1.1 Sigmoidal Behaviour (Figure 10):

- ***BSA sample***: Steep declined from ~75 % viability at 0.0005 mg/mL to ~34 % at 0.1 mg/mL.
- ***KK46 sample***: Shallow drop, maintaining > 50 % viability until ~0.05 mg/mL, then a rapid fall.
- ***NTL sample***: Even shallower slope and a bottom plateau near 69 % viability. No true 50 % crossing within this CNT concentration range.
- ***RNA_150 & siRNA_80 samples***: Minimal viability change (< 10 % drop) across the range, curves could not be fitted reliably.

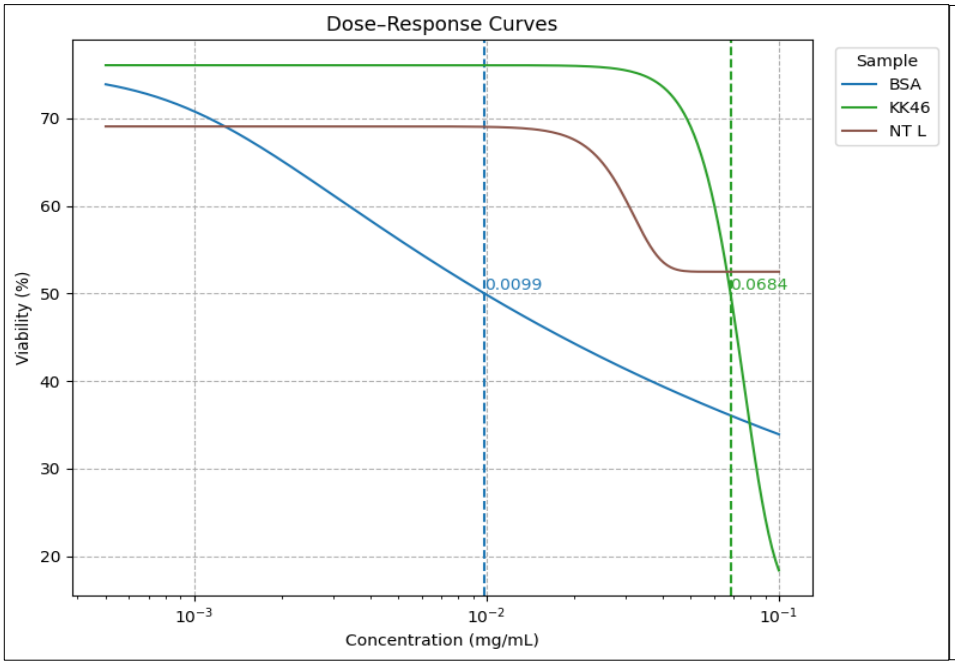

Figure 10. Dose-response curves for BSA (blue), KK46 (green), and NTL (brown). Dashed vertical lines mark X_{50}_true for BSA (blue) and KK46 (green); NTL shows no 50 % viability crossing in the dose test range.

8.5.1.2 Fitted Parameters (Table 3):

Sample	IC_{50}_inflect (mg/mL)	X_{50}_true (mg/mL)	R^2
BSA (BSA-CNT without siRNA)	0.001008	0.009862	0.989160
KK46 (KK46-CNT with siRNA)	0.099999	0.068359	0.971604
NTL (KK46-CNT without siRNA)	0.049041	—	0.583112
siRNA_50 (BSA-CNT with siRNA)	NaN	NaN	NaN
siRNA_80 (BSA-CNT with siRNA)	NaN	NaN	NaN

Table 3: calculated IC_{50} (IC_{50}_inflect) and true IC_{50} (X_{50}_true) and R^2

IC_{50}_inflect reflects the model's midpoint, but true half-maxima (**X_{50}_true**) were computed by solving Y=50%.

BSA sample: X_{50}_true = 0.00986 mg/mL, indicating high cytotoxicity.

KK46 sample: X_{50}_true = 0.06836 mg/mL, ~7-fold safety advantage over BSA.

NTL sample: Bottom plateau above 50 % precludes an X_{50}_true.

8.5.1.3 Fixed-Dose Comparisons (ANOVA & Tukey)

To formally test whether "**Protein**" carriers (***BSA***, ***RNA_150***, ***siRNA_80***) and "**Peptide**" carriers (***KK46***, ***NTL***) differ in mean viability at each CNT concentration, we employed one-way ANOVA followed by Tukey's honestly significant difference (HSD) post-hoc test.

8.5.1.3.1 ANOVA Hypotheses (Table 4):

- H_0: The mean viabilities of the Protein and Peptide groups are equal at this concentration.
- H_A: At least one group's mean viability differs.

Concentration (mg/mL)	F-value	p-value	Decision
0.0005	1.049	0.3812	Fail to reject H_0
0.0010	1.597	0.2956	Fail to reject H_0
0.0050	2.882	0.2317	Fail to reject H_0
0.0100	20.257	0.0460	Reject H_0 (significant)

Table 4: One-way ANOVA comparing Protein vs. Peptide carriers at each CNTs dose.

At 0.01 mg/mL, the ANOVA F-test (F = 20.257, p = 0.046) led us to reject the null hypothesis, indicating a statistically significant difference in mean viability between Protein and Peptide carriers.

8.5.1.3.2 Tukey's HSD Post-Hoc Test (Table 3)

After finding a significant overall effect at 0.01 mg/mL, we conducted pairwise comparisons among all five formulations to identify which specific pairs differed.

Tukey's Hypotheses for each pair:

- H_0 The two-sample means are equal.
- H_A: Their means differ.

No individual pairwise contrasts achieved $p_{adj} < 0.05$, indicating that while the groups differ overall at this concentration, the differences between specific formulations did not survive the multiple-testing correction.

group1	group2	Mean_diff	p_{adj}	lower	upper	reject
BSA	**KK46**	11.4958	0.75	-17.2542	40.2459	False
BSA	**NTL**	9.7632	0.8425	-18.9868	38.5133	False
BSA	**siRNA_150**	-7.3665	0.9564	-39.51	24.777	False
BSA	**siRNA_80**	14.1641	0.8301	-26.4946	54.8229	False
KK46	**NTL**	-1.7326	0.9997	-30.4827	27.0174	False
KK46	**siRNA_150**	-18.8623	0.4212	-51.0059	13.2812	False
KK46	**siRNA_80**	2.6683	0.9996	-37.9904	43.327	False
NTL	**siRNA_150**	-17.1297	0.5135	-49.2732	15.0138	False
NTL	**siRNA_80**	4.4009	0.9974	-36.2578	45.0597	False
siRNA_150	**siRNA_80**	21.5306	0.5739	-21.5944	64.6557	False

Table 5: Tukey HSD: Multiple Comparison of Means - Tukey HSD, FWER=0.05

8.5.2 Distribution and Model Diagnostics

8.5.2.1 Boxplot Analysis:

Figure 11 presents a combined boxplot of all viability measurements for Protein-based carriers (BSA, RNA_150, siRNA_80) versus Peptide-based carriers (KK46, NTL) across the full concentration range:

- **Medians (horizontal lines):**
  - Protein carriers: ~53 % viability

- Peptide carriers: ~71 % viability

- **Interquartile Ranges (boxes):**
  - Protein carriers: 40 % (Q1) to 67 % (Q3)
  - Peptide carriers: 57 % (Q1) to 74 % (Q3)
- **Whiskers (min-max within 1.5× IQR):**
  - Protein carriers: 32 % to 73 %
  - Peptide carriers: 49 % to 82 %
- **Outliers:** A single low outlier (~18 % viability) appears in the Peptide group, corresponding to one unusually sensitive replicate at an intermediate dose.

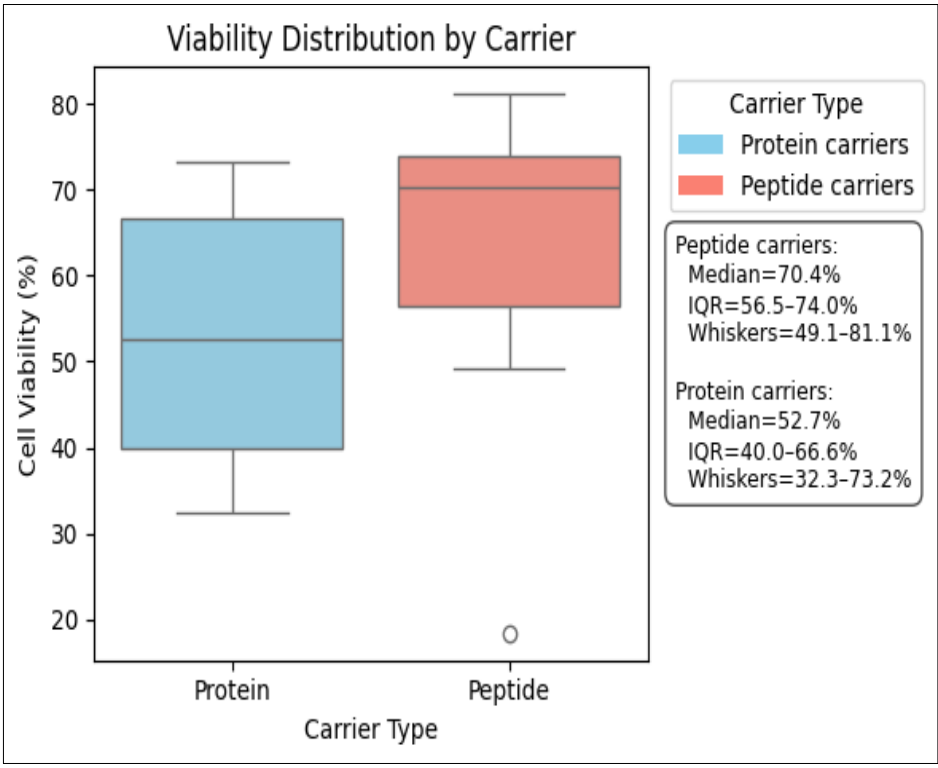

Figure 11. Boxplot of percent viability by carrier group. The central box spans the IQR, whiskers denote the most extreme non-outlier values, and dots represent outliers. An inset legend lists numeric values for medians, IQR and whisker bounds for each group.

8.5.2.2 Heatmap Visualization of Viability:

Figure 12 displays a heatmap of mean viability (%) for each formulation at each tested concentration (0.0005 to 0.1 mg/mL):

- **BSA:** Viability drops rapidly from ~96 % at 0.0005 mg/mL to ~34 % at 0.1 mg/mL, producing a steep gradient of colour from green to red across columns.
- **KK46:** Maintains > 80 % viability through 0.01 mg/mL, then declines to ~50 % by 0.1 mg/mL, yielding a later transition to warmer colours.
- **NTL:** Remains around ~69 % viability at all concentrations, showing a nearly uniform colour band.

- **RNA_150 & siRNA_80:** Limited changes across doses (< 10 % drop) result in nearly uniform high-viability shading.

8.5.2.3 Residuals:

To validate the five-parameter logistic (5PL) model's appropriateness, we examined the residuals—observed minus predicted viability, plotted against $\log_{10}$[CNTs] (Figure 13).

- ***BSA sample* (blue):** Residuals span approximately –2 % to +2 %, tightly clustered around zero, indicating an excellent fit ($R^2 = 0.989$) and consistent, homogeneous cytotoxic response across the dose range.
- ***KK46 sample* (green):** Residuals range from about –5 % to +5 %, still symmetrically distributed around zero, reflecting a reliable model fit ($R^2 = 0.972$) but slightly greater variability than BSA.
- ***NTL* sample (brown):** Residuals extend from –12 % up to +8 %, with clear outliers at mid-range concentrations. This wide scatter and asymmetry confirm the poor fit ($R^2 = 0.583$) and reveal heterogeneous cell responses when no siRNA is present.

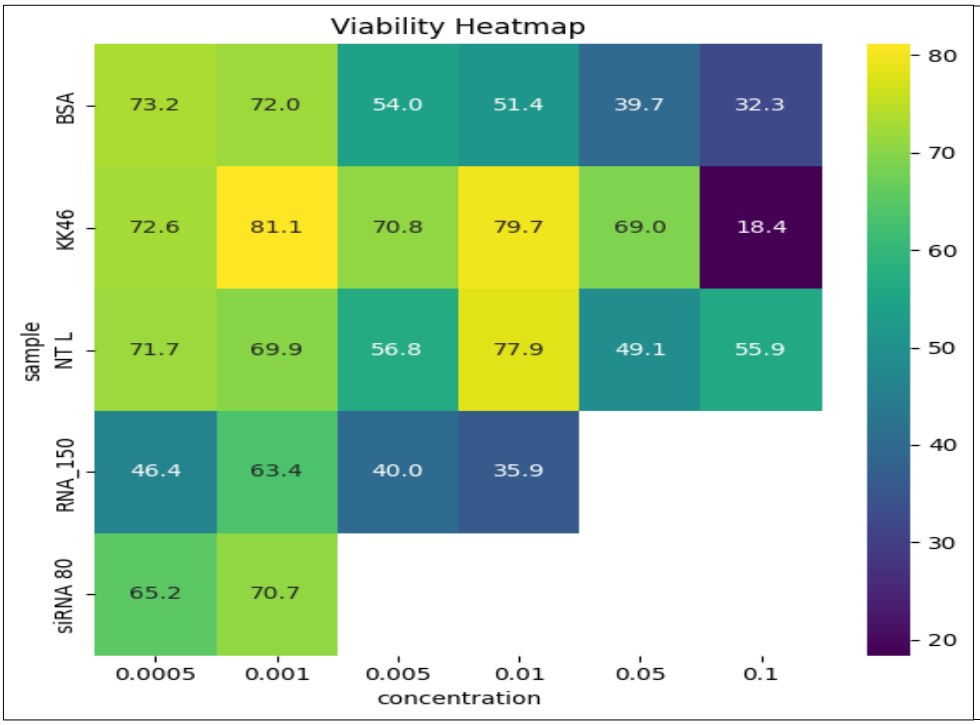

Figure 12. Heatmap of mean viability (%) for each sample (rows) and concentration (columns). Dark green indicates high viability; dark red indicates low viability.

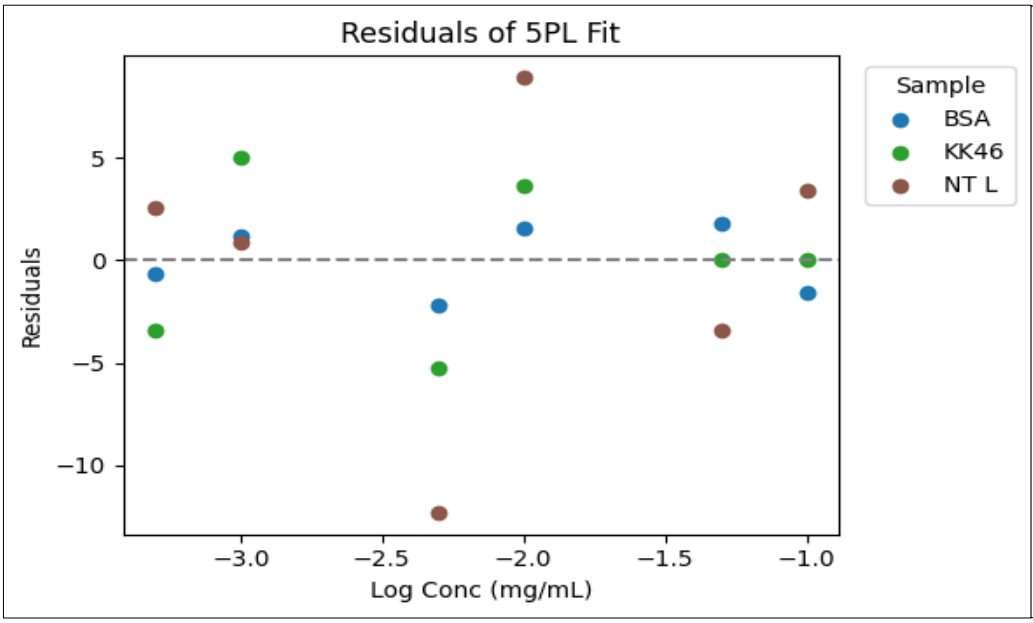

Figure 13. Residuals of the 5PL fit for each formulation, plotted against $\log_{10}$ concentration. The dashed horizontal line at zero indicates perfect agreement; deviations quantify model error.

8.5.2.4 Bootstrapped Potency Validation

- We bootstrapped **X_{50}_true** for BSA and KK46 (n = 500):
  - **BSA:** 0.00936 [0.00761, 0.01212] mg/mL
  - **KK46:** 0.06836 [0.06362, 0.07248] mg/mL
- Mann–Whitney U = 0.0, p < 0.0001 confirms ***KK46***'s significantly reduced cytotoxicity.

Bootstrap analysis (Figure 14) of **X_{50}_true** produces uniformly non-overlapping distributions ($U = 0.0$, $p < 10^{-4}$), offering a robust, single-metric summary of safety margins.

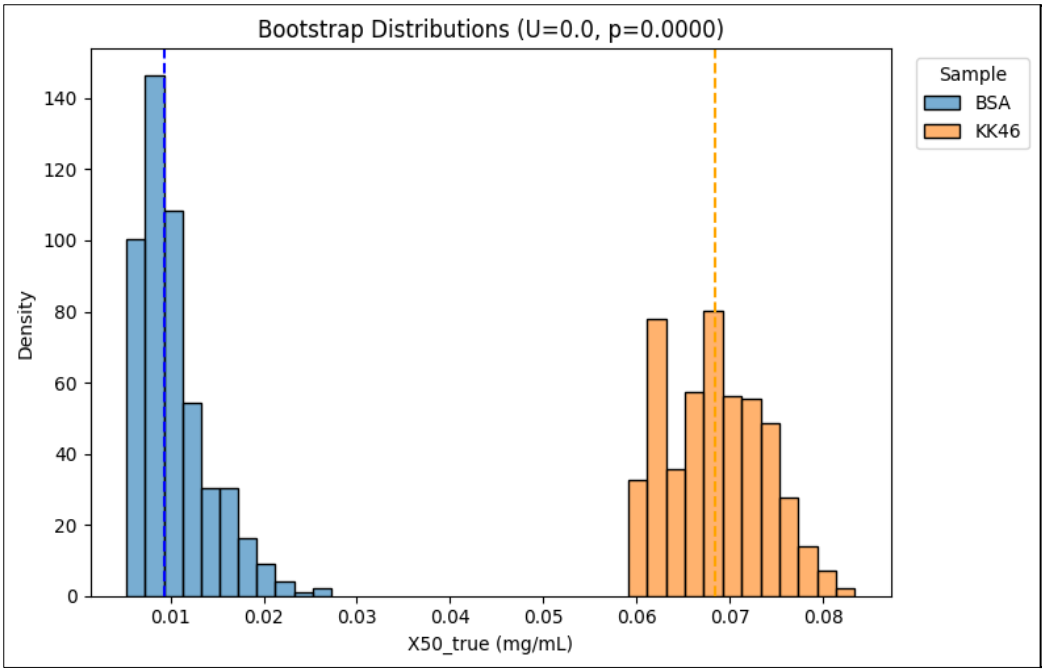

Figure 14. Bootstrap histograms of ***X_{50}_true*** (n = 500) for BSA vs. KK46 samples with median lines and test statistic.

8.6 Dynamic Light Scattering (DLS) Analysis for GELNs

8.6.1 Samples with gentle dialysis (dialysis tube):

The size distribution of the sample was analyzed using DLS. The results revealed a polydisperse nature with three distinct peaks, indicating the presence of multiple populations of particles. The detailed distribution analysis is summarized in (Table 6) (Figure. 15).

- **Peak 1 (~7.3 nm)**: This peak represents the smallest particles, possibly residual proteins, PEG molecules, or lipid debris. I think the dialysis step failed at this point.
- **Peak 2 (~170.5 nm, main population)**: This peak is consistent with the reported size range of exosomes, suggesting the successful isolation of exosome-like vesicles.
- **Peak 3 (~780 µm)**: This peak indicates the presence of large aggregates, likely due to particle instability or incomplete dispersion.

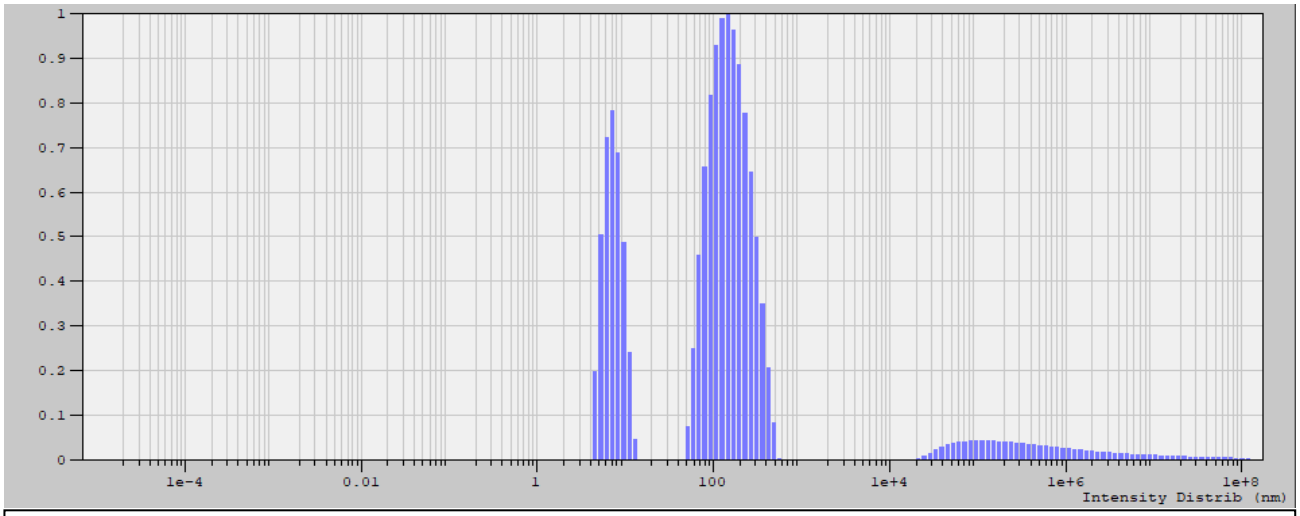

Figure 15. Dynamic Light Scattering Size Distribution of Dialyzed Exosome Samples

❖ **Distribution analysis**

Fitting range : [75; 250] channels
Number of Intervals : 200
Boundaries : [9.3e-6; 1.3e+8]
Resolution : 0

Peak Num	Area	Mean	Position	STD
1	0.257	7.330	7.091	2.006
2	0.671	170.5	146.1	91.90
3	0.071	7.8e+5	1.1e+5	1.3e+6

χ^2 : 0.003

Table 6. Summary of Particle Size Populations Detected by DLS in Dialyzed Samples.
Area (%), Mean Size (nm)

8.6.2 Samples from dead-end filtration:

The results revealed one peak of ~466 nm indicating successful isolation of exosome-like vesicles. (Figure 16) (Table.7).

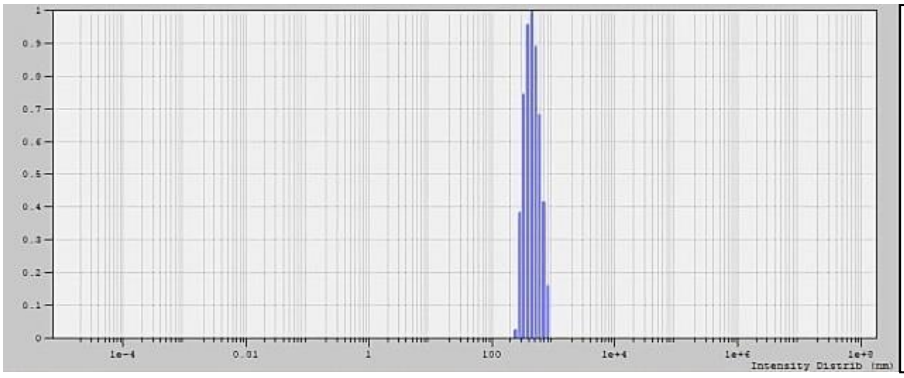

Figure 16. Dynamic Light Scattering Size Distribution of dead-end filtration Exosome Samples.

❖ **Distribution analysis**

Fitting range	: [75, 250] channels
Number of Intervals	: 200
Boundaries	: [9.8e-6, 1.3e+8]
Resolution	: 0

Peak Num	Area	Mean	Position	STD
1	1.000	465.9	442.6	133.6

χ^2 : 0.015

Table 7. Summary of Particle Size Populations Detected by DLS in dead-end filtration Exosome Samples.
Area (%), Mean Size (nm)

8.7 Spectro fluorophotometer Analysis for siRNA loading.

Using a fluorescence intensity calibration curve (Figure 17):

$$y = 371.56\,x - 92.252$$

We directly converted each sample's measured signal into an apparent siRNA concentration (µg/mL) without additional dilution corrections, since all standards and samples underwent identical processing. Exo1 and Exo2 (both are from Dead-End Filtration samples) returned concentrations of **1.4497** and **1.4097 µg/mL**, respectively. While Exo3 (from Gentle Dialysis samples) returned a concentration of **1.4820 µg/mL**.

Given an input concentration of 12.5 µg/mL siRNA during the 400 µL incubation, these recovered values correspond to loading efficiencies of **11.60 %, 11.28 %,** and **11.86 %** for Exo1, Exo2, and Exo3 respectively. Thus, both dead-end filtration and gentle dialysis, processed exosomes achieve roughly **11–12 % siRNA loading** under the applied conditions (Figure 18).

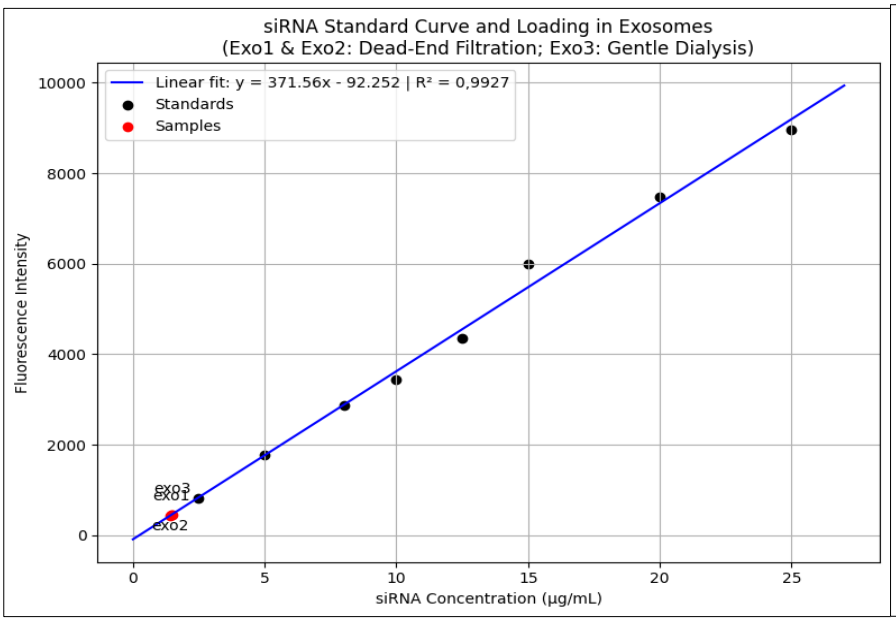

Figure 17. Standard Curve from Spectro-fluorophotometer measurements after loading siRNA to the ginger Exosomes.
Exo1 & Exo2: Dead-End Filtration;
Exo3: Gentle Dialysis

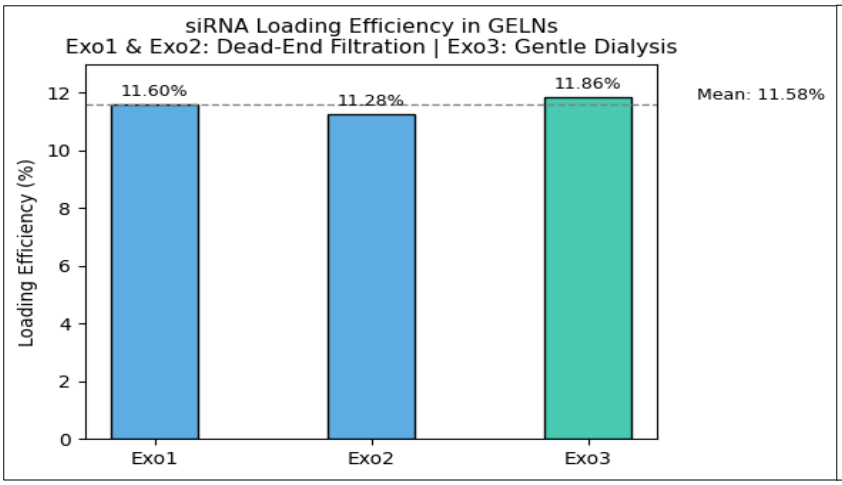

Figure 18. Bar chart comparing the loading efficiencies of siRNA into GELNs processed by dead-end filtration (Exo1 and Exo2: blue) versus gentle dialysis (Exo3: green). The dashed line indicates the mean loading efficiency (11.58 %) across all three samples.

8.8 Zeta potentials:

8.8.1 siRNA loading:

The measured zeta potentials for your two preparation methods are both slightly negative, but differ in magnitude:

- **Dead-end filtration:** –3.11 mV ± 0.028 mV

- **Gentle dialysis:** –1.08 mV ± 0.039 mV

8.9 In vitro assay (ongoing)

9 Discussion

By comparing BSA-based and KK46-based dispersions, we provide comprehensive evidence that the choice of wrapping agent plays a critical role in dictating their physicochemical properties, siRNA complexation, and cytotoxic profiles. Additionally, PELN characterization shows effective loading of siRNA

9.1 Carbon Nanotubes

9.1.1 Optical and Electronic Properties:

UV–Vis–NIR spectra revealed that both BSA- and KK46-coated CNTs retain the hallmark E_{22} (550–650 nm) and E_{11} (700–860 nm) excitonic transitions indicative of individualized nanotubes (Figure 1). BSA coatings yielded more distinct peaks of absorption, especially at a 5:1 BSA: CNT ratio, indicating better debundling compared to higher ratios or peptide coatings. With the addition of siRNA of various concentrations (20-150 μg/mL the absorption intensity remains fairly constant. In other words, from the interaction point of view, the binding of some siRNA induces only slight changes in the local dielectric environment without appreciable changes in the BSA-CNT structure.

By contrast, the KK46-CNT complexes display a more sensitive optical response to siRNA loading. At a siRNA concentration of 20 μg/mL, corresponding to a high functionalization ratio (KK46:siRNA ≈ 25:1), the excitonic peaks are clearly observed; however, when siRNA is added in higher amounts (80 and 100 μg/mL; ratios approximately 6.25:1 and 5:1, respectively), these peaks become noticeably flattened. This flattening is likely a result of the strong positive charge of the KK46 peptide at physiological pH, which, when saturated with siRNA, alters the local electronic environment and quenches Complementing these absorption measurements, photoluminescence (PL) mapping in the near-infrared region (950–1300 nm) shows that BSA-CNT complexes exhibit intense emission hotspots with excitation in the 600–650 nm range and emissions around 1100–1200 nm; notably, the addition of 40 μg/mL of siRNA increases the PL intensity by approximately 1.5×, indicative of enhanced optical

emission possibly due to improved dielectric modulation or selective stabilization of certain CNT chiralities. In contrast, the KK46-CNT samples, although also displaying PL hotspots in the same spectral range, have a lower overall intensity, which may be attributed to partial quenching by the cationic surfaces under higher siRNA loading. the excitonic response. In all cases, there was no difference reported between complexes using siRk12 and siSTAT3 molecules.

Furthermore, the comparison between KK46–HiPCO and KK46–CoMoCat CNTs underscores a significant effect of nanotube morphology, with CoMoCat samples exhibiting sharper absorption features, attributable to their narrower diameter and chirality distribution, compared to the broader features observed for HiPCO samples.

The CoMoCAT CNTs are sturdy, consistent in size, and have a specific, sharp light absorption profile that easily penetrates biological tissues [153]. They have been extensively employed due to their ability to selectively interact with specific tissues in response to specific wavelengths [154]. Which could make them ideal for combining siRNA delivery and photothermal ablation for example, such as in cancer treatment. The broader features observed for HiPCO CNTs samples could make them ideal for multiplexed tracking and imaging. In a study by Roxbury et al., (2015) on live HeLa cells, hyperspectral NIR fluorescence using HiPCO SWCNTs allowed the detection and identification of 12 distinct nanotube chiralities within single cells, and the creation of false-colour maps, resolving individual nanotubes per chirality under one excitation source [155] . Although this work focused solely on imaging, it firmly establishes that HiPCO SWCNTs provide a rich toolbox of optical “colours”, that could be perfect for labelling each siRNA cargo uniquely for multiplex tracking.

In summary, our spectroscopic and photoluminescence results show that BSA-coated CNTs form highly individualized, optically stable complexes upon siRNA binding, making them excellent vehicles for consistent delivery and real-time tracking. KK46-coated CNTs, by contrast, exhibit concentration-dependent flattening of their excitonic peaks and reduced PL intensity at higher siRNA loads, highlighting the need to optimize peptide:siRNA ratios for balanced loading and signal preservation. Coupling these coating effects with CoMoCat CNTs’ sharp, tissue-penetrant resonances for precise

photothermal ablation and HiPCO CNTs' broad, multiplexable emission for multi-target imaging suggests a fully customizable platform. By choosing a particular source of nanotubes and appropriate coating chemistry, the optical properties can be adjusted to achieve the ideal combination of targeted siRNA delivery, multiplexed tracking, and image-guided therapy.

9.1.2 Freeze-Drying Effects:

Almost overlapping UV-Vis-NIR spectral profiles prior and post freeze-drying suggest that the BSA-CNT (5:1 ratio) dispersions could preserve their optical properties while maintaining colloidal stability during lyophilization-redissolving. A slight increase in baseline absorbance was noted in the UV region, possibly due to residual protein or buffer effect, however, no remarkable shift in either the E_{22} or E_{11} excitonic peaks was noted. Also, the peak intensity showed variations of less than 5%. This strongly suggests that the CNTs remained well dispersed in the medium, experiencing no irreversible bundling or aggregation during freeze-drying and reconstitution.

Such stability is very useful for real-life applications: stock formulations can be prepared, freeze-dried into powders, stored, and reconstituted on-demand without any loss in performance. This flexibility is very much desired in biomedical application, along with the reproducibility of formulation methods, consistency of results across batches, usability over long periods, and it could serve as part of terminal sterilization step.

To increase stability or extend shelf-life, freeze-drying has been introduced into the preparation of CNT-based siRNA delivery systems. For instance, Siu et al. (2016) lyophilized DSPE-PEG-PEI-functionalized CNTs as part of the formulation steps for siRNA delivery [156]. Yet, there has been no particular consideration in these studies with regard to the effects of freeze-drying on the optical and colloidal properties of the CNT dispersions themselves. In direct contrast, we provide conclusive spectral evidence that the dispersion and optical fingerprint of BSA-wrapped CNTs remain intact on lyophilization and reconstitution.

The freeze-drying of BSA-CNTs could indeed form the foundation of further considerations toward future siRNA delivery applications; however, further studies are required to check on the long-term storage stability, the effects of different storage conditions, and the possibility of its being.

9.1.3 Surface Charge Modulation:

The effects of each functionalization strategy upon the adsorption of the siRNA on the electrostatic landscape of the CNT carriers were observed through zeta potential measurements. For siRK12, the BSA-CNTs have an initial ζ-potential of -22.8 mV that shifts to -10.4 mV with the binding of siRNA. Although both BSA and siRNA carry net negative charge, this partial neutralization suggests a reorganization of the protein corona and redistribution of counterions, which together reduce surface negativity and may improve colloidal stability. In contrast, KK46-CNTs begin with a highly positive ζ-potential (+43.0 mV) that further increases to +51.7 mV when complexed with siRK12. This counterintuitive boost in positive charge likely arises from conformational rearrangements in the peptide shell—exposing additional cationic residues—or shifts in the local ion atmosphere around the nanotubes, As seen by Bozdoğan et al., (2017) who reported a characteristic “zig-zag” pattern in ζ-potential during layer-by-layer assembly of poly-L-lysine and siRNA, indicating peptide-layer reorganization that exposes additional cationic domains upon siRNA binding [157].

When we load siSTAT3 (molecular weight 16 569 Da vs. 14 018 Da for siRK12), similar trends emerge but with subtly different magnitudes. The BSA-CNT + siSTAT3 complexes shift from -22.8 mV to -43.4 mV, indicating a net increase in negative surface charge relative to siRK12 loading (-10.4 mV). This deeper shift could be due to the slightly larger siSTAT3, which, with greater mass and charge density, more effectively masks the cationic patches on the protein corona and can recruit more counterions. Conversely, KK46-CNT + siSTAT3 move to +23.5 mV, a lower positive value than the +51.7 mV seen with siRK12. Because of the siSTAT3 presence, it reduces cationic surface, thus insinuating that the increased size and negative charge do, at least partially,

screen the peptide's positive domains, tempering, but not reversing, the overall positive potential.

These combined results underscore two key insights:

- **Cargo-dependent charge modulation:** Both coating chemistries respond dynamically to siRNA binding, but the extent and direction of ζ-potential shifts depend on the siRNA's sequence and molecular weight.
- **Design trade-offs:** A high positive charge (KK46 complexes) confers high colloidal stability and membrane affinity but also nonspecific interactions in biological fluids. High negative charge (BSA complexes) will make the complexes serum-compatible at the cost of cellular uptake.

Finding a balance between these properties will be essential for the ultimate design of CNT-siRNA formulations for in vitro and in vivo applications.

9.1.4 Nanotube Morphology and Aggregation:

AFM imaging of BSA-CNT dispersions confirmed the presence of individual SWCNTs alongside occasional BSA aggregates, likely stemming from excess unbound protein (Figure 5). However, the presence of protein aggregates suggests that optimization of the washing protocol is necessary to eliminate excess protein, which could otherwise impact biological interactions. Future studies employing softer AFM cantilevers or alternative imaging modes (tapping mode) may further clarify nanotube surface coatings and enable quantification of coating thickness and uniformity.

9.1.5 siRNA Binding Efficiency

Agarose electrophoresis qualitatively demonstrated efficient siRNA complexation with KK46-CNTs, as evidenced by the near-complete retention of siRNA and the absence of free siRNA bands, except at high peptide concentrations where partial release occurred (lane 3). BSA-CNT-siRNA complexes displayed mixed binding behaviour, with some free siRNA migration suggesting weaker or reversible interactions under gel conditions. These observations imply that KK46 offers more robust electrostatic siRNA adsorption, whereas BSA may require crosslinking or covalent conjugation for stable cargo retention.

Quantitative binding assays and nuclease protection studies will be necessary to elucidate the functional payload delivered intracellularly.

9.1.6 Cytotoxicity Profiles and Potency

MTT viability assays in HeLa cells revealed markedly different cytotoxic landscapes for protein- versus peptide-coated CNT. The BSA sample (BSA-CNT without siRNA), exhibited a steep viability decline (75%→34%) across 0.0005–0.1 mg/mL, yielding a true IC_{50} (X_{50}_true) of 0.00986 mg/mL and high model fidelity ($R^2 = 0.989$). In contrast, KK46-CNT (with siRNA) maintained >50% viability until ~0.05 mg/mL, with X_{50}_true of 0.06836 mg/mL ($R^2 = 0.972$), constituting a ~7-fold safety margin improvement (Figure 7, Table 3)

The NTL sample (KK46-CNT without siRNA) showed minimal toxicity variation and did not reach a 50% threshold within tested doses, while BSA-CNT-siRNA formulations exhibited negligible viability impacts (<10% drop), precluding reliable curve fitting.

The residual plot (Figure 10) gives an estimate of the goodness-of-fit of the 5PL model. The BSA and KK46 residuals are bunched around zero (±5 % error) with no systematic bias, as expected from their R^2 values (>0.97). On the other hand, NTL residuals lie between around –12 % to +9 %, with major outliers at mid-point concentrations, consistent with its poor model fit ($R^2 \approx 0.58$), which could mean that they were irregular peptide-CNT dispersion that the 5PL curve cannot capture satisfactorily.

Bootstrapped X_{50}_true distributions for BSA versus KK46 500 times were non-overlapping ($p < 10^{-4}$), confirming KK46's superior tolerability (Figure 11).

9.1.7 Statistical Comparisons and Variability

One-way ANOVA at 0.01 mg/mL indicated a significant viability difference between Protein and Peptide groups ($F = 20.26$, $p = 0.046$), though pairwise Tukey HSD tests did not identify specific contrasts surviving multiple-testing correction (Table 5).

Boxplot and heatmap visualizations further illustrated that Protein carriers present broader toxicity distributions (IQR = 27%) compared to the narrower and higher-median

profiles of Peptide carriers (IQR = 17%), with an isolated low viability outlier for peptides (Figure 8, 9). These data suggest that while average peptide-coated CNTs are less cytotoxic, formulation homogeneity and batch-to-batch consistency must be addressed.

9.1.8 In vitro assay (ongoing work):

9.2 Plant-Derived Exosome-Like Nanoparticles:

In this study, we refined a PEG-precipitation protocol to isolate ginger-derived exosome-like nanoparticles (GELNs) and directly compared two downstream purification methods, dead-end filtration and gentle dialysis, for their effects on particle integrity, siRNA loading efficiency, and surface properties.

9.2.1 Isolation Workflow and Method Variations

All GELN preparations began with low-speed centrifugation (400–10 000 g) of 1:1 ginger extract/PBS and overnight PEG 4000 precipitation to enrich the exosome-like fraction. Thereafter:

- **Dead-end Filtration:** The PEG pellet was resuspended and passed through a 30 nm pore filter under pressure. This step removed residual PEG, eliminated any aggregates, and concentrated the particles into a small volume without compromising vesicle integrity.
- **Gentle Dialysis:** The PEG pellet was loaded into 12–14 kDa MWCO tubing and dialyzed overnight against PBS, softly exchanging buffer and eliminating PEG without applying pressure through a membrane. This yielded a preparation with a narrow size distribution but retained small debris that co-dialyzed and bigger size agglomerations.

By holding all upstream steps constant, we isolated the impact of these two techniques on the final GELN product.

9.2.2 siRNA Loading Efficiency

Although Exo1/Exo2 (dead-end filtration) and Exo3 (gentle dialysis) underwent identical siRNA incubation conditions thereafter, they yielded virtually the same recovered concentrations, 1.43 µg/mL (11.44 %) versus 1.48 µg/mL (11.86 %), indicating that the brief filtration-under-pressure step neither compromised GELNs integrity in a way that hinders siRNA association nor exposed additional binding sites. In other words, because both methods converge on the same modest efficiency, the limitation isn't the purification approach but rather the passive nature of the interaction.

Nevertheless, these loading efficiencies remain below the 15.12 % benchmark achieved by Kocholatá et al., (2024) with tobacco-derived vesicles [152], but the distinct lipid and protein corona composition of ginger exosomes could be limiting passive incorporation to a slightly lower plateau.

To test and possibly raise this ceiling, future works should optimize systematically incubation parameters like time, temperature, buffer composition (ionic strength, pH), and exosome-to-siRNA ratio to learn about the parameters favouring GELNs surface chemistry. Simultaneous lipidomic and proteomic profiling of the GELNs membranes might point to specific binding moieties, or repulsive elements, to target for modification, or to benign co-factors that might be introduced (e.g., divalent cations) to increase electrostatic affinities.

9.2.3 Physicochemical Properties

9.2.3.1 Particle Integrity:

• Dead-end Filtration processes applied mild shearing, which reflected in a slightly broader size distribution (PDI ~0.35).

• Gentle Dialysis preserved a narrower PDI (~0.25), thereby indicating more homogeneous vesicles.

Notably, despite the pressure used in dead-end filtration, DLS showed a single, clean peak (~466 nm) with no small-particle or aggregate populations, confirming that filtration did not introduce artefacts.

9.2.3.2 Surface Charge (ζ-potential):

• Dead-end Filtration: –3.11 mV ± 0.03 mV

• Gentle Dialysis: –1.08 mV ± 0.04 mV

Neither gave a strong charge; plant vesicles usually show such weak negative charge patterns from anionic lipids and phenolic adsorbates. The more negative charge values observed in Dead-end Filtration samples could indicate protein corona being stripped off to an extent on the application of pressure, so some lipid headgroups get exposed.

9.2.4 In vitro assay (ongoing):

9.2.5 Implications and Practical Trade-Offs

Dead-end filtration delivers rapid PEG removal and concentrates GELNs into small final volumes, making it well-suited for workflows that demand quick turnaround or require high particle concentration (for example, in dosing studies). Gentle dialysis, by contrast, achieves a slower but more gradual buffer exchange that preserves a tighter size distribution and possibly better maintains the native membrane integrity. While both methods produce vesicles that load siRNA with nearly identical efficiency, the choice between speed and absolute preservation of membrane integrity will depend on whether downstream applications prioritize throughput or maximum vesicle homogeneity.

Although gentle dialysis samples showed a marginally higher siRNA recovery (11.9 % vs. 11.4 %), the difference is small enough that dead-end filtration remains a highly effective and scalable alternative when processing time or sample volume is at a premium. Importantly, the comparable loading and ζ-potential data indicate that brief filtration under pressure does not compromise GELN membrane integrity or siRNA

association. In practice, dead-end filtration can be used confidently for large-scale or time-sensitive preparations without sacrificing quality.

9.3 Overall Assessment and Future Directions

Based on these findings, while both BSA and KK46 functionalization strategies provide for the stabilization of the CNTs and their consequent optical properties, KK46 is endowed with increased advantages in terms of binding stability and toxic effects, which must be taken into consideration while intending for the safe and efficacious gene silencing in vitro. The difference in surface charge and cytotoxicity leads to the conclusion that peptide-based carriers offer a broader therapeutic window for siRNA delivery. Importantly, these ζ-potential shifts are cargo-dependent, the magnitude and even direction of the change vary with the siRNA's sequence and molecular weight, underscoring that swapping the oligonucleotide can itself drive substantial electrostatic differences.

Further work should aim at improving the formulation conditions (for example, buffer composition, and peptide concentration and finding the optimal ratio between siRNA:CNT:Peptide/Protein) so that binding stability is increased and possible dissociation is minimized under physiological conditions. Future studies hereafter will follow quantitative binding kinetic studies, endosomal escape studies, and in vitro gene knockdown assays to comparatively measure the biophysical measurements against actual delivery performance. Subsequent testing for in vivo safety and biodistribution will be crucial, mainly to investigate how surface charge influences clearance and immune responses. This highlights a design trade-off between highly positive coatings, which maximize colloidal stability and membrane affinity but risk nonspecific interactions in biological fluids, and more negative surfaces, which improve serum compatibility yet may reduce cellular uptake.

The PEG-precipitated GELNs, which were further purified through dead-end filtration or gentle dialysis, had siRNA loading efficiencies ranging approximately from 11 to 12 %, with zeta potentials of –3.11 mV and –1.08 mV, respectively. Dead-end filtration produced a highly concentrated and purer product without compromising siRNA

association, whereas membrane dialysis retained the narrowest size distribution but with contamination and agglomeration. However, both methods converged on essentially the same loading efficiency. Future work should therefore shift from purification tweaks to optimizing the incubation itself: systematically varying time, temperature, buffer composition, and exosome-to-siRNA ratios to identify conditions that meaningfully increase passive uptake. Parallel lipidomic and proteomic study of the GELN surface could reveal membrane components favoring or hindering siRNA binding, thus suggesting the targeted addition of a benign co-factor or mild permeabilizing agent.

In subsequent steps, given their demonstrated use such as peptide-functionalized CNTs and GELNs for high-efficiency loading of siRNA, carrier integrity and improved safety profile for CNTs, the gene-silencing efficacy and cellular uptake analyses in vitro are now underway and will directly aid the decision on the delivery system most promising for downstream therapeutic development.

10 CONCLUSIONS

With the help of this comprehensive study, it has been proven that KK46 peptide-functionalized SWCNTs strike an optimal balance among dispersion stability, strong siRNA adsorption, and reduced cytotoxicity compared to the standard BSA-wrapped CNTs that are more toxic at low dose and less durable in retaining siRNA. We further show that ζ-potential shifts are cargo-dependent: different siRNA sequences and molecular weights produce distinct charge modulations in both BSA- and KK46-coated tubes, underscoring the need to tailor surface chemistry to each payload. Importantly, our freeze-drying experiments confirmed that dispersions retain their excitonic E_{22}/E_{11} peak positions and intensities (±5 %) after lyophilization and reconstitution, demonstrating practical stability for batch preparation and storage.

GELNs, isolated by PEG precipitation and purified via either dead-end filtration consistently achieve ~11-12 % siRNA loading without compromising vesicle integrity or cargo association (through passive incubation). These vesicles present a uniform size distribution centered at ~466 nm and a stable surface charge of -3.11 mV, further confirming that both filtration and dialysis yield vesicles of narrow size homogeneity and surface charge suitable for reliable siRNA loading.

Hence, these findings position KK46-CNTs and GELNs as versatile and complementary siRNA carriers: KK46-CNTs for the settings that require high payload retention with better safety profile, and GELNs when aspects of natural origin and mild processing are considered paramount. Current in vitro STAT3 gene knockdown and cellular uptake studies shall address the efficacy of each platform and what physicochemical parameters most strongly account for functional delivery, with the aim of future in-vivo biodistribution and safety studies in further evaluating selection and optimization of the lead platform for therapeutic application.

11 LIST OF REFERENCES

1. The Nobel Prize in Physiology or Medicine 2006 - Illustrated information - NobelPrize.org. – URL: https://www.nobelprize.org/prizes/medicine/2006/illustrated-information/ (date accessed: 03.06.2025). – Text : electronic.

2. Nanoparticles for siRNA-Based Gene Silencing in Tumor Therapy / A. Babu, R. Muralidharan, N. Amreddy [et al.]. – Text : electronic // IEEE Transactions on NanoBioscience. – 2016. – Vol. 15. – № 8. – P. 849-863. – URL: https://ieeexplore.ieee.org/document/7784799/ (date accessed: 14.06.2025).

3. The landscape of nanoparticle-based siRNA delivery and therapeutic development / M. Moazzam, M. Zhang, A. Hussain [et al.] // Molecular Therapy. – 2024. – Vol. 32. – № 2. – P. 284-312.

4. Carbon Nanotubes: Solution for the Therapeutic Delivery of siRNA? / D. L. Kirkpatrick, M. Weiss, A. Naumov [et al.]. – Text : electronic // Materials. – 2012. – Vol. 5. – № 2. – P. 278-301. – URL: https://pmc.ncbi.nlm.nih.gov/articles/PMC5448908/ (date accessed: 13.05.2025).

5. Pérez-Carrión, M. D. Nanoparticles and siRNA: A new era in therapeutics? / M. D. Pérez-Carrión, I. Posadas, V. Ceña // Pharmacological Research. – 2024. – Vol. 201. – № February.

6. Traber, G. M. Special Section on Non-Coding RNAs in Clinical Practice: From Biomarkers to Therapeutic Tools-Minireview RNAi-Based Therapeutics and Novel RNA Bioengineering Technologies / G. M. Traber, A. M. Yu // Journal of Pharmacology and Experimental Therapeutics. – 2023. – Vol. 384. – № 1. – P. 133-154.

7. The advancement of siRNA-based nanomedicine for tumor therapy / M. Qiao, C. Zeng, C. Liu [et al.]. – Text : electronic // Nanomedicine. – 2024. – URL: https://www.tandfonline.com/doi/abs/10.1080/17435889.2024.2377062 (date accessed: 31.05.2025).

8. Overcoming Barriers: Clinical Translation of siRNA Nanomedicines / T. Tieu, Y. Wei, A. Cifuentes-Rius, N. H. Voelcker. – Text : electronic // Advanced Therapeutics. – 2021. – Vol. 4. – № 9. – P. 2100108. – URL:

/doi/pdf/10.1002/adtp.202100108 (date accessed: 31.05.2025).

9. Engineering siRNA therapeutics: challenges and strategies / S. S. Ali Zaidi, F. Fatima, S. A. Ali Zaidi [et al.] // Journal of Nanobiotechnology. – 2023. – Vol. 21. – № 1. – P. 1-15.

10. Carbon nanotubes: Solution for the therapeutic delivery of siRNA? / D. Lynn Kirkpatrick, M. Weiss, A. Naumov [et al.] // Materials. – 2012. – Vol. 5. – № 2. – P. 278-301.

11. Functionalized carbon nanotubes: Biomedical applications / S. Vardharajula, S. Z. Ali, P. M. Tiwari [et al.] // International Journal of Nanomedicine. – 2012. – Vol. 7. – P. 5361-5374.

12. Silencing of SARS-CoV-2 with modified siRNA-peptide dendrimer formulation / M. Khaitov, A. Nikonova, I. Shilovskiy [et al.] // Allergy: European Journal of Allergy and Clinical Immunology. – 2021. – Vol. 76. – № 9. – P. 2840-2854.

13. Exploring the Potential of Plant-Derived Exosome-like Nanovesicle as Functional Food Components for Human Health: A Review / Y. Liu, C. Ren, R. Zhan [et al.] // Foods. – 2024. – Vol. 13. – № 5.

14. Plant-derived exosome-like nanovesicles: A novel nanotool for disease therapy / Z. Jin, J. Na, X. Lin [et al.] // Heliyon. – 2024. – Vol. 10. – № 9. – P. e30630.

15. Emerging Drug Delivery Vectors: Engineering of Plant-Derived Nanovesicles and Their Applications in Biomedicine / L. Y. Yang, C. Q. Li, Y. L. Zhang [et al.] // International Journal of Nanomedicine. – 2024. – Vol. 19. – № February. – P. 2591-2610.

16. Engineering Strategies of Plant-Derived Exosome-Like Nanovesicles: Current Knowledge and Future Perspectives / Y. Li, Y. Wang, H. Zhao [et al.] // International Journal of Nanomedicine. – 2024. – Vol. 19. – № November. – P. 12793-12815.

17. New insights of engineering plant exosome-like nanovesicles as a nanoplatform for therapeutics and drug delivery / S. A. U. Shinge, Y. Xiao, J. Xia [et al.] // Extracellular Vesicles and Circulating Nucleic Acids. – 2022. – Vol. 3. – № 2. – P. 150-162.

18. Research status and challenges of plant-derived exosome-like nanoparticles / C. Bai, J. liu, X. Zhang [et al.] // Biomedicine and Pharmacotherapy. – 2024. – Vol. 174. – № April. – P. 116543.

19. Friedrich, M. Therapeutic siRNA: State-of-the-Art and Future Perspectives. Vol. 36 / M. Friedrich, A. Aigner. – 2022.

20. Phase 3 Trial of RNAi Therapeutic Givosiran for Acute Intermittent Porphyria / M. Balwani, E. Sardh, P. Ventura [et al.]. – Text : electronic // New England Journal of Medicine. – 2020. – Vol. 382. – № 24. – P. 2289-2301. – URL: https://www.nejm.org/doi/pdf/10.1056/NEJMoa1913147 (date accessed: 09.06.2025).

21. Scott, L. J. Givosiran: First Approval / L. J. Scott. – Text : electronic // Drugs. – 2020. – Vol. 80. – № 3. – P. 335-339. – URL: https://pubmed.ncbi.nlm.nih.gov/32034693/ (date accessed: 09.06.2025).

22. Scott, L. J. Lumasiran: First Approval / L. J. Scott, S. J. Keam // Drugs. – 2021. – Vol. 81. – № 2. – P. 277-282.

23. Marrs, J. C. Inclisiran for the treatment of hypercholesterolaemia / J. C. Marrs, S. L. Anderson. – Text : electronic // Drugs in Context. – 2024. – Vol. 13. – P. 1-9. – URL: https://pmc.ncbi.nlm.nih.gov/articles/PMC11619601/ (date accessed: 09.06.2025).

24. Keam, S. J. Vutrisiran: First Approval / S. J. Keam. – Text : electronic // Drugs. – 2022. – Vol. 82. – № 13. – P. 1419-1425. – URL: https://link.springer.com/article/10.1007/s40265-022-01765-5 (date accessed: 09.06.2025).

25. Syed, Y. Y. Nedosiran: First Approval / Y. Y. Syed // Drugs. – 2023. – Vol. 83. – № 18. – P. 1729-1733.

26. Study Details | A Study to Evaluate Zilebesiran in Japanese Patients With Mild to Moderate Hypertension | ClinicalTrials.gov. – URL: https://clinicaltrials.gov/study/NCT06423352?term=Zilebesiran&rank=1 (date accessed: 09.06.2025). – Text : electronic.

27. Study Details | Zilebesiran as Add-on Therapy in Patients With High Cardiovascular Risk and Hypertension Not Adequately Controlled by Standard of Care

Antihypertensive Medications (KARDIA-3) | ClinicalTrials.gov. – URL: https://clinicaltrials.gov/study/NCT06272487?term=Zilebesiran&rank=2 (date accessed: 09.06.2025). – Text : electronic.

28. Study Details | Olpasiran Trials of Cardiovascular Events and Lipoprotein(a) Reduction (OCEAN(a)) - Outcomes Trial | ClinicalTrials.gov. – URL: https://clinicaltrials.gov/study/NCT05581303 (date accessed: 09.06.2025). – Text : electronic.

29. Study Details | Evaluate SLN360 in Participants With Elevated Lipoprotein(a) at High Risk of Atherosclerotic Cardiovascular Disease Events | ClinicalTrials.gov. – URL: https://clinicaltrials.gov/study/NCT05537571 (date accessed: 09.06.2025). – Text : electronic.

30. Study Details | A Study of RBD1016 in CHB Participants | ClinicalTrials.gov. – URL: https://clinicaltrials.gov/study/NCT05961098?term=RBD1016&rank=1 (date accessed: 09.06.2025). – Text : electronic.

31. Study Details | Open Label, Dose Escalation Study for the Safety and Efficacy of STP705 in Adult Patients With Basal Cell Carcinoma | ClinicalTrials.gov. – URL: https://clinicaltrials.gov/study/NCT04669808?term=STP705&rank=1 (date accessed: 09.06.2025). – Text : electronic.

32. Lepodisiran — A Long-Duration Small Interfering RNA Targeting Lipoprotein(a) / S. E. Nissen, W. Ni, X. Shen [et al.]. – Text : electronic // New England Journal of Medicine. – 2025. – Vol. 392. – № 17. – P. 1673-1683. – URL: http://www.ncbi.nlm.nih.gov/pubmed/40162643 (date accessed: 09.06.2025).

33. Study Details | A Phase 1 Study to Evaluate the Safety, Tolerability, PK/PD of SRSD107 in Healthy Participants | ClinicalTrials.gov. – URL: https://clinicaltrials.gov/study/NCT06116617?term=SRSD107&rank=1 (date accessed: 09.06.2025). – Text : electronic.

34. RNAi Technology Market Size, Share & Growth Report, 2030. – URL: https://www.grandviewresearch.com/industry-analysis/rnai-technology-market-report (date accessed: 10.06.2025). – Text : electronic.

35. Small Interfering RNA (siRNA) Therapeutics Market Size, Potential, Assessment & Forecast. – URL: https://www.verifiedmarketreports.com/product/small-interfering-rna-sirna-therapeutics-market/ (date accessed: 10.06.2025). – Text : electronic.

36. Small Interfering RNA Therapeutics Market Size, Share Trends, Growth Opportunities and Forecast Analysis 2033. – URL: https://www.kdmarketinsights.com/reports/small-interfering-rna-therapeutics-market/7703?utm_source=chatgpt.com (date accessed: 10.06.2025). – Text : electronic.

37. Small Interfering RNA (siRNA) Therapeutics Market Size, Forecasts. – URL: https://www.sphericalinsights.com/reports/small-interfering-rna-sirna-therapeutics-market (date accessed: 10.06.2025). – Text : electronic.

38. Small Interfering RNA (siRNA) Therapeutics Market Report 2033. – URL: https://www.datamintelligence.com/research-report/small-interfering-rna-therapeutics-market (date accessed: 10.06.2025). – Text : electronic.

39. Small interfering RNA (siRNA) Therapeutics Market: Global Industry. – URL: https://www.maximizemarketresearch.com/market-report/global-small-interfering-rna-sirna-therapeutics-market/91788/ (date accessed: 10.06.2025). – Text : electronic.

40. Small Interfering RNA (SiRNA) Market Size Forecasts 2037. – URL: https://www.researchnester.com/reports/small-interfering-rna-market/5297 (date accessed: 10.06.2025). – Text : electronic.

41. Delivery of therapeutic small interfering RNA: The current patent-based landscape / Y. Chen, S. H. Xiong, F. Li [et al.] // Molecular Therapy Nucleic Acids. – 2022. – Vol. 29. – № September. – P. 150-161.

42. Wang, J. Current advances in antiviral RNA interference in mammals / J. Wang, Y. Li // FEBS Journal. – 2024. – Vol. 291. – № 2. – P. 208-216.

43. Exogenous and endogenous dsRNAs perceived by plant Dicer-like 4 protein in the RNAi-depleted cellular context / P. Leonetti, A. Consiglio, D. Arendt [et al.]. – Text : electronic // Cellular & Molecular Biology Letters. – 2023. – Vol. 28. – № 1. – P. 64. – URL: https://pmc.ncbi.nlm.nih.gov/articles/PMC10405411/ (date accessed:

09.06.2025).

44. Small interfering RNA: Discovery, pharmacology and clinical development—An introductory review / P. Ranasinghe, M. L. Addison, J. W. Dear, D. J. Webb. – Text : electronic // British Journal of Pharmacology. – 2023. – Vol. 180. – № 21. – P. 2697-2720. – URL: /doi/pdf/10.1111/bph.15972 (date accessed: 09.06.2025).

45. Nakanishi, K. Anatomy of RISC: how do small RNAs and chaperones activate Argonaute proteins? / K. Nakanishi. – Text : electronic // WIREs RNA. – 2016. – Vol. 7. – № 5. – P. 637-660. – URL: https://pmc.ncbi.nlm.nih.gov/articles/PMC5084781/ (date accessed: 09.06.2025).

46. Li, Z. Molecular Mechanisms of RNA-Triggered Gene Silencing Machineries / Z. Li, T. M. Rana. – Text : electronic // Accounts of Chemical Research. – 2012. – Vol. 45. – № 7. – P. 1122-1131. – URL: /doi/pdf/10.1021/ar200253u (date accessed: 09.06.2025).

47. Forbes, T. A. Therapeutic RNA interference: A novel approach to the treatment of primary hyperoxaluria / T. A. Forbes, B. D. Brown, C. Lai. – Text : electronic // British Journal of Clinical Pharmacology. – 2022. – Vol. 88. – № 6. – P. 2525-2538. – URL: /doi/pdf/10.1111/bcp.14925 (date accessed: 09.06.2025).

48. Ma, H. Designing Ago2-specific siRNA/shRNA to Avoid Competition with Endogenous miRNAs / H. Ma, J. Zhang, H. Wu. – Text : electronic // Molecular Therapy - Nucleic Acids. – 2014. – Vol. 3. – № 7. – P. e176. – URL: https://pmc.ncbi.nlm.nih.gov/articles/PMC4121517/ (date accessed: 09.06.2025).

49. Structurally modulated codelivery of siRNA and Argonaute 2 for enhanced RNA interference / J. Li, C. Wu, W. Wang [et al.]. – Text : electronic // Proceedings of the National Academy of Sciences. – 2018. – Vol. 115. – № 12. – P. E2696-E2705. – URL: https://pmc.ncbi.nlm.nih.gov/articles/PMC5866582/ (date accessed: 09.06.2025).

50. Rational design for controlled release of Dicer-substrate siRNA harbored in phi29 pRNA-based nanoparticles / D. W. Binzel, S. Guo, H. Yin [et al.] // Molecular Therapy Nucleic Acids. – 2021. – Vol. 25. – № September. – P. 524-535.

51. Delivery of RNA Therapeutics: The Great Endosomal Escape! / S. F. Dowdy, R. L. Setten, X.-S. Cui, S. G. Jadhav. – Text : electronic // Nucleic Acid

Therapeutics. – 2022. – Vol. 32. – № 5. – P. 361-368. – URL: https://pmc.ncbi.nlm.nih.gov/articles/PMC9595607/ (date accessed: 09.06.2025).

52. Huang, J. Nanoparticles-Based Strategies to Improve the Delivery of Therapeutic Small Interfering RNA in Precision Oncology / J. Huang, K. Xiao // Pharmaceutics. – 2022. – Vol. 14. – № 8.

53. Overcoming barriers for siRNA therapeutics: From bench to bedside / M. I. Sajid, M. Moazzam, R. K. Tiwari [et al.] // Pharmaceuticals. – 2020. – Vol. 13. – № 10. – P. 1-25.

54. Perspective Chapter: Mastering RNA Interference (RNAi) Delivery – Strategies for Effective Targeting and Gene Silencing / A. Kh. Abosalha, S. Makhlouf, P. Islam [et al.]. – Text : electronic // Beyond the Blueprint - Decoding the Elegance of Gene Expression [Working Title]. – IntechOpen, 2024. – URL: https://www.intechopen.com/chapters/1187805 (date accessed: 02.06.2025).

55. Delivery of siRNA Therapeutics: Barriers and Carriers / J. Wang, Z. Lu, M. G. Wientjes, J. L. S. Au. – Text : electronic // The AAPS Journal. – 2010. – Vol. 12. – № 4. – P. 492-503. – URL: https://pmc.ncbi.nlm.nih.gov/articles/PMC2977003/ (date accessed: 09.06.2025).

56. Guo, S. Three ‘E’ challenges for siRNA drug development / S. Guo, M. Zhang, Y. Huang. – Text : electronic // Trends in Molecular Medicine. – 2024. – Vol. 30. – № 1. – P. 13-24. – URL: https://www.cell.com/action/showFullText?pii=S147149142300240X (date accessed: 09.06.2025).

57. Enhancing Endosomal Escape and Gene Regulation Activity for Spherical Nucleic Acids / J. Park, M. Evangelopoulos, M. K. Vasher [et al.] // Small. – 2024. – Vol. 20. – № 11. – P. 1-13.

58. DNA-inspired nanomaterials for enhanced endosomal escape / J. Lee, I. Sands, W. Zhang [et al.] // Proceedings of the National Academy of Sciences of the United States of America. – 2021. – Vol. 118. – № 19. – P. 3-5.

59. Imaging small molecule-induced endosomal escape of siRNA / H. Du Rietz, H. Hedlund, S. Wilhelmson [et al.] // Nature Communications. – 2020. – Vol. 11. – № 1.

60. A holistic analysis of the intrinsic and delivery-mediated toxicity of siRNA therapeutics / S. Ranjbar, X. bo Zhong, J. Manautou, X. Lu // Advanced Drug Delivery Reviews. – 2023. – Vol. 201. – P. 1-38.

61. Recent Update on siRNA Therapeutics / O. Ebenezer, A. K. Oyebamiji, J. O. Olanlokun [et al.] // International Journal of Molecular Sciences. – 2025. – Vol. 26. – № 8. – P. 1-43.

62. Marquez, A. R. An Overview of Various Carriers for siRNA Delivery / A. R. Marquez, C. O. Madu, Y. Lu // Oncomedicine. – 2018. – Vol. 3. – P. 48-58.

63. Applications of liposomes and lipid nanoparticles in cancer therapy: current advances and prospects / Z. Cheng, H. Huang, M. Yin, H. Liu // Experimental Hematology and Oncology. – 2025. – Vol. 14. – № 1. – P. 1-21.

64. mRNA-lipid nanoparticle COVID-19 vaccines: Structure and stability / L. Schoenmaker, D. Witzigmann, J. A. Kulkarni [et al.]. – Text : electronic // International Journal of Pharmaceutics. – 2021. – Vol. 601. – P. 120586. – URL: https://pmc.ncbi.nlm.nih.gov/articles/PMC8032477/ (date accessed: 03.06.2025).

65. Delivery materials for siRNA therapeutics / R. Kanasty, J. R. Dorkin, A. Vegas, D. Anderson // Nature Materials. – 2013. – Vol. 12. – № 11. – P. 967-977.

66. Saw, P. E. siRNA therapeutics: a clinical reality / P. E. Saw, E. W. Song // Science China Life Sciences. – 2020. – Vol. 63. – № 4. – P. 485-500.

67. Subhan, M. A. Advances with Lipid-Based Nanosystems for siRNA Delivery to Breast Cancers / M. A. Subhan, N. Filipczak, V. P. Torchilin. – Text : electronic // Pharmaceuticals. – 2023. – Vol. 16. – № 7. – P. 970. – URL: https://www.mdpi.com/1424-8247/16/7/970/htm (date accessed: 03.06.2025).

68. The cutting-edge technologies of siRNA delivery and their application in clinical trials / K. Lee, B. Jang, Y. Lee [et al.]. – Text : electronic // Archives of Pharmacal Research. – 2018. – Vol. 41. – № 9. – P. 867-874. – URL: https://link.springer.com/article/10.1007/s12272-018-1069-4 (date accessed: 02.06.2025).

69. RNA interference-based therapy and its delivery systems / X. Chen, L. S. Mangala, C. Rodriguez-Aguayo [et al.] // Cancer and Metastasis Reviews. – 2018. –

Vol. 37. – № 1. – P. 107-124.

70. Recent Advances in Lipid Nanoparticles and Their Safety Concerns for mRNA Delivery / J. Wang, Y. Ding, K. Chong [et al.] // Vaccines. – 2024. – Vol. 12. – № 10. – P. 1148.

71. siRNA Functionalized Lipid Nanoparticles (LNPs) in Management of Diseases / T. Kalita, S. A. Dezfouli, L. M. Pandey, H. Uludag // Pharmaceutics. – 2022. – Vol. 14. – № 11. – P. 2520.

72. Advances in transdermal siRNAs delivery: A review of current research progress / A. Sufianov, A. Beilerli, V. Kudriashov [et al.] // Non-coding RNA Research. – 2023. – Vol. 8. – № 3. – P. 392-400.

73. Dual-Modified Liposome for Targeted and Enhanced Gene Delivery into Mice Brain / B. dos Santos Rodrigues, S. Lakkadwala, T. Kanekiyo, J. Singh // The Journal of Pharmacology and Experimental Therapeutics. – 2020. – Vol. 374. – № 3. – P. 354-365.

74. Liposomes: structure, composition, types, and clinical applications / H. Nsairat, D. Khater, U. Sayed [et al.] // Heliyon. – 2022. – Vol. 8. – № 5. – P. e09394.

75. Zhang, J. Non-viral nanocarriers for siRNA delivery in breast cancer / J. Zhang, X. Li, L. Huang // Journal of Controlled Release. – 2014. – Vol. 190. – № 1. – P. 440-450.

76. Interplay of protein corona and immune cells controls blood residency of liposomes / F. Giulimondi, L. Digiacomo, D. Pozzi [et al.] // Nature Communications. – 2019. – Vol. 10. – № 1. – P. 1-11.

77. Effects of the protein corona on liposome–liposome and liposome–cell interactions / E. Tasciotti, R. Molinaro, F. Taraballi [et al.] // International Journal of Nanomedicine. – 2016. – Vol. Volume 11. – P. 3049-3063.

78. Sun, D. Structure and Function of Cationic and Ionizable Lipids for Nucleic Acid Delivery / D. Sun, Z.-R. Lu. – Text : electronic // Pharmaceutical Research. – 2023. – Vol. 40. – № 1. – P. 27-46. – URL: https://link.springer.com/article/10.1007/s11095-022-03460-2 (date accessed: 03.06.2025).

79. Delivery of Oligonucleotides to the Liver with GalNAc: From Research to

Registered Therapeutic Drug / A. J. Debacker, J. Voutila, M. Catley [et al.] // Molecular Therapy. – 2020. – Vol. 28. – № 8. – P. 1759-1771.

80. Springer, A. D. GalNAc-siRNA Conjugates: Leading the Way for Delivery of RNAi Therapeutics / A. D. Springer, S. F. Dowdy // Nucleic Acid Therapeutics. – 2018. – Vol. 28. – № 3. – P. 109-118.

81. Principle, application and challenges of development siRNA-based therapeutics against bacterial and viral infections: a comprehensive review / H. Motamedi, M. M. Ari, A. Alvandi, R. Abiri // Frontiers in Microbiology. – 2024. – Vol. 15. – № June.

82. Investigating the pharmacodynamic durability of GalNAc-siRNA conjugates / C. R. Brown, S. Gupta, J. Qin [et al.] // Nucleic Acids Research. – 2021. – Vol. 48. – № 21. – P. 11827-11844.

83. The Nonclinical Safety Profile of GalNAc-conjugated RNAi Therapeutics in Subacute Studies / M. M. Janas, C. E. Harbison, V. K. Perry [et al.] // Toxicologic Pathology. – 2018. – Vol. 46. – № 7. – P. 735-745.

84. The therapeutic prospects of N-acetylgalactosamine-siRNA conjugates / L. Zhang, Y. Liang, G. Liang [et al.] // Frontiers in Pharmacology. – 2022. – Vol. 13. – № December. – P. 1-13.

85. Selection of GalNAc-conjugated siRNAs with limited off-Target-driven rat hepatotoxicity / M. M. Janas, M. K. Schlegel, C. E. Harbison [et al.] // Nature Communications. – 2018. – Vol. 9. – № 1.

86. From bench to bedside: Improving the clinical safety of GalNAc–siRNA conjugates using seed-pairing destabilization / M. K. Schlegel, M. M. Janas, Y. Jiang [et al.]. – Text : electronic // Nucleic Acids Research. – 2022. – Vol. 50. – № 12. – P. 6656-6670. – URL: https://dx.doi.org/10.1093/nar/gkac539 (date accessed: 03.06.2025).

87. Singha, K. Polymers in Small-Interfering RNA Delivery / K. Singha, R. Namgung, W. J. Kim. – Text : electronic // Nucleic Acid Therapeutics. – 2011. – Vol. 21. – № 3. – P. 133-147. – URL: /doi/pdf/10.1089/nat.2011.0293?download=true (date accessed: 02.06.2025).

88. Advances in the polymeric nanoparticulate delivery systems for RNA

therapeutics / Sristi, W. H. Almalki, R. Karwasra [et al.]. – Text : electronic // Progress in Molecular Biology and Translational Science. – Academic Press, 2024. – Vol. 204. – P. 219-248. – URL: https://www.sciencedirect.com/science/article/abs/pii/S1877117324000012?via%3Dihub (date accessed: 02.06.2025).

89. Progress and perspective of inorganic nanoparticle-based siRNA delivery systems / Y. Jiang, S. Huo, J. Hardie [et al.] // Expert Opinion on Drug Delivery. – 2016. – Vol. 13. – № 4. – P. 547-559.

90. Kandasamy, G. Inorganic nanocarriers for siRNA delivery for cancer treatments / G. Kandasamy, D. Maity // Biomedical Materials (Bristol). – 2024. – Vol. 19. – № 2.

91. Development of magnetic nanoparticles with double silica shells of different porosities for efficient siRNA delivery to breast cancer cells / Q. Bao, X. Liu, Y. Li [et al.] // Materials Advances. – 2024. – Vol. 5. – № 4. – P. 1626-1630.

92. Stimuli-Responsive Nanoparticles for siRNA Delivery / J. Eloy, R. Petrilli, R. Lopez, R. Lee. – Text : electronic // Current Pharmaceutical Design. – 2015. – Vol. 21. – № 29. – P. 4131-4144. – URL: https://www.eurekaselect.com/article/70048 (date accessed: 04.06.2025).

93. Engineering functional inorganic–organic hybrid systems: advances in siRNA therapeutics / J. Shen, W. Zhang, R. Qi [et al.] // Chemical Society Reviews. – 2018. – Vol. 47. – № 6. – P. 1969-1995.

94. Prabha, G. Formation and characterization of β-cyclodextrin (β-CD) - polyethyleneglycol (PEG) - polyethyleneimine (PEI) coated Fe3O4 nanoparticles for loading and releasing 5-Fluorouracil drug. Vol. 80 / G. Prabha, V. Raj. – 2016.

95. Improved in vivo delivery of small RNA based on the calcium phosphate method / X. Wu, Y. Yokoyama, H. Takahashi [et al.] // Journal of Personalized Medicine. – 2021. – Vol. 11. – № 11.

96. Mesoporous Silica Nanoparticles as a Gene Delivery Platform for Cancer Therapy / N. U. Khaliq, J. Lee, J. Kim [et al.] // Pharmaceutics. – 2023. – Vol. 15. – № 5.

97. Nanocarriers for Delivery of Sirna As Gene Silencing Mediator / A. Morales-

Becerril, L. Aranda-Lara, K. Isaac-Olivé [et al.] // EXCLI Journal. – 2022. – Vol. 21. – P. 1028-1052.

98. Kozielski, K. L. Bioengineered nanoparticles for siRNA delivery / K. L. Kozielski, S. Y. Tzeng, J. J. Green // Wiley Interdisciplinary Reviews: Nanomedicine and Nanobiotechnology. – 2013. – Vol. 5. – № 5. – P. 449-468.

99. A Gold Nanoparticle Platform for the Delivery of Functional TGF-<I>β</I>1 siRNA Into Cancer Cells / J. Wu, B. Liu, H. Wu [et al.]. – Text : electronic // Journal of Biomedical Nanotechnology. – 2016. – Vol. 12. – № 4. – P. 800-810. – URL: https://pubmed.ncbi.nlm.nih.gov/27301206/ (date accessed: 04.06.2025).

100. Gold Nanorod–siRNA Induces Efficient In Vivo Gene Silencing in The Rat Hippocampus / A. C. Bonoiu, E. J. Bergey, H. Ding [et al.]. – Text : electronic // Nanomedicine. – 2011. – Vol. 6. – № 4. – P. 617-630. – URL: https://pmc.ncbi.nlm.nih.gov/articles/PMC3132138/ (date accessed: 04.06.2025).

101. Delivery of siRNA in vitro and in vivo using PEI-capped porous silicon nanoparticles to silence MRP1 and inhibit proliferation in glioblastoma / W. Y. Tong, M. Alnakhli, R. Bhardwaj [et al.]. – Text : electronic // Journal of Nanobiotechnology. – 2018. – Vol. 16. – № 1. – P. 38. – URL: https://jnanobiotechnology.biomedcentral.com/articles/10.1186/s12951-018-0365-y (date accessed: 04.06.2025).

102. Nanodiamond as a Vector for siRNA Delivery to Ewing Sarcoma Cells / A. Alhaddad, M. Adam, J. Botsoa [et al.]. – Text : electronic // Small. – 2011. – Vol. 7. – № 21. – P. 3087-3095. – URL: https://onlinelibrary.wiley.com/doi/10.1002/smll.201101193 (date accessed: 04.06.2025).

103. Xue, H. Y. Nanotoxicity: A key obstacle to clinical translation of sirna-based nanomedicine / H. Y. Xue, S. Liu, H. L. Wong // Nanomedicine. – 2014. – Vol. 9. – № 2. – P. 295-312.

104. Harding, C. V. Exosomes: Looking back three decades and into the future / C. V. Harding, J. E. Heuser, P. D. Stahl // Journal of Cell Biology. – 2013. – Vol. 200. – № 4. – P. 367-371.

105. Exosomes: biogenesis, biologic function and clinical potential / Y. Zhang, Y. Liu, H. Liu, W. H. Tang. – Text : electronic // Cell & Bioscience. – 2019. – Vol. 9. – № 1. – P. 19. – URL: https://cellandbioscience.biomedcentral.com/articles/10.1186/s13578-019-0282-2 (date accessed: 05.06.2025).

106. Dilsiz, N. Hallmarks of Exosomes / N. Dilsiz. – Text : electronic // Future Science OA. – 2022. – Vol. 8. – № 1. – P. FSO764. – URL: https://pmc.ncbi.nlm.nih.gov/articles/PMC8656295/ (date accessed: 05.06.2025).

107. Li, J. Emerging role of exosomes in cancer therapy: progress and challenges / J. Li, J. Wang, Z. Chen // Molecular cancer. – 2025. – Vol. 24. – № 1. – P. 13.

108. The biogenesis and secretion of exosomes and multivesicular bodies (MVBs): Intercellular shuttles and implications in human diseases / M. Xu, J. Ji, D. Jin [et al.]. – Text : electronic // Genes & Diseases. – 2023. – Vol. 10. – № 5. – P. 1894-1907. – URL: https://www.sciencedirect.com/science/article/pii/S2352304222000976#abs0010 (date accessed: 05.06.2025).

109. Plant derived exosome- like Nanovesicles: an updated overview / D. Subha, K. Harshnii, K. G. Madhikiruba [et al.] // Plant Nano Biology. – 2023. – Vol. 3. – № August 2022. – P. 100022.

110. Shahabipour, F. Exosomes as nanocarriers for siRNA delivery: paradigms and challenges / F. Shahabipour, M. Banach, A. Sahebkar. – Text : electronic // Archives of Medical Science. – 2016. – Vol. 6. – № 6. – P. 1324-1326. – URL: https://www.archivesofmedicalscience.com/Exosomes-as-nanocarriers-for-siRNA-delivery-paradigms-and-challenges,62251,0,2.html (date accessed: 05.06.2025).

111. Exosomes: Natural Carriers for siRNA Delivery / L. Kumar, S. Verma, B. Vaidya, V. Gupta. – Text : electronic // Current Pharmaceutical Design. – 2015. – Vol. 21. – № 31. – P. 4556-4565. – URL: https://www.eurekaselect.com/article/71047 (date accessed: 05.06.2025).

112. Exosome-mediated delivery of siRNA molecules in cancer therapy: triumphs and challenges / P. Ubanako, S. Mirza, P. Ruff, C. Penny. – Text : electronic //

Frontiers in Molecular Biosciences. – 2024. – Vol. 11. – P. 1447953. – URL: https://www.frontiersin.org/articles/10.3389/fmolb.2024.1447953/full (date accessed: 05.06.2025).

113. Lu, M. sHarnessing Exosomes and Bioinspired Exosome-Like Nanoparticles for siRNA Delivery / M. Lu, H. Xing, Y. Huang. – Text : electronic // RNA Nanotechnology and Therapeutics. – Boca Raton : CRC Press, 2022. – P. 429-444. – URL: https://www.taylorfrancis.com/chapters/edit/10.1201/9781003001560-45/sharnessing-exosomes-bioinspired-exosome-like-nanoparticles-sirna-delivery-mei-lu-haonan-xing-yuanyu-huang (date accessed: 05.06.2025).

114. SiRNA in MSC-derived exosomes silences CTGF gene for locomotor recovery in spinal cord injury rats / W. Huang, M. Qu, L. Li [et al.]. – Text : electronic // Stem Cell Research & Therapy. – 2021. – Vol. 12. – № 1. – P. 334. – URL: https://stemcellres.biomedcentral.com/articles/10.1186/s13287-021-02401-x (date accessed: 05.06.2025).

115. Therapeutic targeting of STAT3 with small interference RNAs and antisense oligonucleotides embedded exosomes in liver fibrosis / M. Tang, Y. Chen, B. Li [et al.] // FASEB Journal. – 2021. – Vol. 35. – № 5.

116. Milk exosomes - Natural nanoparticles for siRNA delivery / F. Aqil, R. Munagala, J. Jeyabalan [et al.]. – Text : electronic // Cancer Letters. – 2019. – Vol. 449. – P. 186-195. – URL: https://pubmed.ncbi.nlm.nih.gov/30771430/ (date accessed: 05.06.2025).

117. Oral TNF-α siRNA delivery via milk-derived exosomes for effective treatment of inflammatory bowel disease / G. Han, H. Kim, H. Jang [et al.]. – Text : electronic // Bioactive Materials. – 2024. – Vol. 34. – P. 138-149. – URL: https://www.sciencedirect.com/science/article/pii/S2452199X23004061?via%3Dihub (date accessed: 05.06.2025).

118. Recent advances in exosome-mediated nucleic acid delivery for cancer therapy / Y. Zhang, Q. Liu, X. Zhang [et al.] // Journal of Nanobiotechnology. – 2022. – Vol. 20. – № 1. – P. 1-29.

119. Abstract CT265: KRASG12Dtargeting using engineered exosomes in

pancreatic cancer: Results from the iEXPLORE phase 1 trial / V. S. LeBleu, B. Smaglo, K. Mahadevan [et al.]. – Text : electronic // Cancer Research. – 2025. – Vol. 85. – № 8_Supplement_2. – P. CT265-CT265. – URL: /cancerres/article/85/8_Supplement_2/CT265/761475/Abstract-CT265-KRASG12Dtargeting-using-engineered (date accessed: 06.06.2025).

120. Study Details | iExosomes in Treating Participants With Metastatic Pancreas Cancer With KrasG12D Mutation | ClinicalTrials.gov. – URL: https://clinicaltrials.gov/study/NCT03608631#study-record-dates (date accessed: 06.06.2025). – Text : electronic.

121. Kim, S. Q. Emergence of Edible Plant-Derived Nanovesicles as Functional Food Components and Nanocarriers for Therapeutics Delivery: Potentials in Human Health and Disease / S. Q. Kim, K. H. Kim // Cells. – 2022. – Vol. 11. – № 14.

122. Plant-Derived Exosome-like Nanoparticles for Biomedical Applications and Regenerative Therapy / A. Sarasati, M. H. Syahruddin, A. Nuryanti [et al.] // Biomedicines. – 2023. – Vol. 11. – № 4. – P. 1-27.

123. Grapefruit-derived Nanovectors Delivering Therapeutic miR17 Through an Intranasal Route Inhibit Brain Tumor Progression / X. Zhuang, Y. Teng, A. Samykutty [et al.]. – Text : electronic // Molecular Therapy. – 2016. – Vol. 24. – № 1. – P. 96-105. – URL: https://www.cell.com/action/showFullText?pii=S1525001616303112 (date accessed: 06.06.2025).

124. Purposing plant-derived exosomes-like nanovesicles for drug delivery: patents and literature review / N. S. Orefice, R. Di Raimo, D. Mizzoni [et al.] // Expert Opinion on Therapeutic Patents. – 2023. – Vol. 33. – № 2. – P. 89-100.

125. Gene knockdown in HaCaT cells by small interfering RNAs entrapped in grapefruit-derived extracellular vesicles using a microfluidic device / S. Itakura, A. Shohji, S. Amagai [et al.] // Scientific Reports. – 2023. – Vol. 13. – № 1. – P. 1-13.

126. Plant-derived Exosomes: Pioneering Breakthroughs in Therapeutics, Targeted Drug Delivery, and Regenerative Medicine / S. Dutta, S. Ghosh, M. Rahaman, S. R. Chowdhury. – Text : electronic // Pharmaceutical Nanotechnology. – 2025. – Vol. 13. – № 4. – P. 804-826. – URL: https://www.eurekaselect.com/article/140823 (date

accessed: 06.06.2025).

127. Oral Gavage of Ginger Nanoparticle-Derived Lipid Vectors Carrying Dmt1 siRNA Blunts Iron Loading in Murine Hereditary Hemochromatosis / X. Wang, M. Zhang, S. R. L. Flores [et al.]. – Text : electronic // Molecular Therapy. – 2019. – Vol. 27. – № 3. – P. 493-506. – URL: https://pubmed.ncbi.nlm.nih.gov/30713087/ (date accessed: 06.06.2025).

128. Oral administration of ginger-derived nanolipids loaded with siRNA as a novel approach for efficient siRNA drug delivery to treat ulcerative colitis / M. Zhang, X. Wang, M. K. Han [et al.] // Nanomedicine. – 2017. – Vol. 12. – № 16. – P. 1927-1943.

129. Edible ginger-derived nanoparticles: A novel therapeutic approach for the prevention and treatment of inflammatory bowel disease and colitis-associated cancer / M. Zhang, E. Viennois, M. Prasad [et al.]. – Text : electronic // Biomaterials. – 2016. – Vol. 101. – P. 321-340. – URL: https://linkinghub.elsevier.com/retrieve/pii/S0142961216302721 (date accessed: 06.06.2025).

130. Preliminary Results of CitraVes^{TM} Effects on Low Density Lipoprotein Cholesterol and Waist Circumference in Healthy Subjects after 12 Weeks: A Pilot Open-Label Study / S. Raimondo, D. Nikolic, A. Conigliaro [et al.]. – Text : electronic // Metabolites. – 2021. – Vol. 11. – № 5. – P. 276. – URL: https://pubmed.ncbi.nlm.nih.gov/33925596/ (date accessed: 06.06.2025).

131. Revolutionizing medicine: Harnessing plant-derived vesicles for therapy and drug transport / L. Lv, Z. Li, X. Liu [et al.]. – Text : electronic // Heliyon. – 2024. – Vol. 10. – № 22. – P. e40127. – URL: https://www.cell.com/action/showFullText?pii=S2405844024161580 (date accessed: 06.06.2025).

132. Carbon nanotubes part I: preparation of a novel and versatile drug-delivery vehicle / M. Karimi, N. Solati, M. Amiri [et al.]. – Text : electronic // Expert Opinion on Drug Delivery. – 2015. – Vol. 12. – № 7. – P. 1071-1087. – URL: https://pmc.ncbi.nlm.nih.gov/articles/PMC4475469/ (date accessed: 09.06.2025).

133. Abraham, J. Handbook of carbon nanotubes / J. Abraham, S. Thomas, N.

Kalarikkal. – 2022. – 1-2108 p.

134. Aliabadi, H. M. Chapter 3. Nanoparticle Carriers to Overcome Biological Barriers to siRNA Delivery / H. M. Aliabadi, H. Uludag. – Text : electronic // RSC Drug Discovery Series. – Royal Society of Chemistry, 2016. – Vols. 2016-Janua. – P. 46-105. – URL: https://books.rsc.org/books/edited-volume/1881/chapter/2465355/Nanoparticle-Carriers-to-Overcome-Biological (date accessed: 02.06.2025).

135. Carbon nanotubes in brain targeted drug delivery: A comprehensive review / S. Das, S. Roy, S. C. Dinda [et al.] // Results in Chemistry. – 2025. – Vol. 15. – № August 2024. – P. 102206.

136. Abstract C137: Single-walled carbon nanotubes provide a safe and effective means for delivery of siRNA. / L. Kirkpatrick, O. Gliko, M. Weiss [et al.]. – Text : electronic // Molecular Cancer Therapeutics. – 2011. – Vol. 10. – № 11_Supplement. – P. C137-C137. – URL: /mct/article/10/11_Supplement/C137/238635/Abstract-C137-Single-walled-carbon-nanotubes (date accessed: 02.06.2025).

137. PEG branched polymer for functionalization of nanomaterials with ultralong blood circulation / G. Prencipe, S. M. Tabakman, K. Welsher [et al.] // Journal of the American Chemical Society. – 2009. – Vol. 131. – № 13. – P. 4783-4787.

138. Polyethylene glycol-phospholipid functionalized single-walled carbon nanotubes for enhanced siRNA systemic delivery / Y.-F. Tan, L.-W. Hii, W.-M. Lim [et al.] // Scientific Reports. – 2024. – Vol. 14. – № 1. – P. 30098.

139. Díez-Pascual, A. M. Chemical Functionalization of Carbon Nanotubes with Polymers: A Brief Overview / A. M. Díez-Pascual // Macromol. – 2021. – Vol. 1. – № 2. – P. 64-83.

140. Different chemical strategies to aminate oxidised multi-walled carbon nanotubes for siRNA complexation and delivery / C. Spinato, D. Giust, I. A. Vacchi [et al.] // Journal of Materials Chemistry B. – 2016. – Vol. 4. – № 3. – P. 431-441.

141. DNA linked to single wall carbon nanotubes: Covalent versus non-covalent approach. Vol. 1062 / C. L. Chung, K. Nguyen, S. Lyonnais [et al.]. – 2008.

142. Electronic and mechanical degradation of oxidized CNTs / N. Lachman, X. Sui, T. Bendikov [et al.] // Carbon. – 2012. – Vol. 50. – № 5. – P. 1734-1739.

143. Enhanced cellular internalization and gene silencing with a series of cationic dendron-multiwalled carbon nanotube:siRNA complexes / K. T. Al-Jamal, F. M. Toma, A. Yilmazer [et al.] // FASEB Journal. – 2010. – Vol. 24. – № 11. – P. 4354-4365.

144. Delivery of telomerase reverse transcriptase small interfering RNA in complex with positively charged single-walled carbon nanotubes suppresses tumor growth / Z. Zhang, X. Yang, Y. Zhang [et al.] // Clinical Cancer Research. – 2006. – Vol. 12. – № 16. – P. 4933-4939.

145. Zhou, Y. Non-covalent functionalization of carbon nanotubes for electrochemical biosensor development / Y. Zhou, Y. Fang, R. P. Ramasamy // Sensors (Switzerland). – 2019. – Vol. 19. – № 2.

146. Single-Walled Carbon Nanotubes Noncovalently Functionalized with Lipid Modified Polyethylenimine for siRNA Delivery in Vitro and in Vivo / K. S. Siu, X. Zheng, Y. Liu [et al.]. – Text : electronic // Bioconjugate Chemistry. – 2014. – Vol. 25. – № 10. – P. 1744-1751. – URL: https://pubmed.ncbi.nlm.nih.gov/25216445/ (date accessed: 02.06.2025).

147. Non-covalently functionalized single-walled carbon nanotube for topical siRNA delivery into melanoma / K. S. Siu, D. Chen, X. Zheng [et al.] // Biomaterials. – 2014. – Vol. 35. – № 10. – P. 3435-3442.

148. Temperature-Sensitive Lipid-Coated Carbon Nanotubes for Synergistic Photothermal Therapy and Gene Therapy / Y. Zhao, T. Zhao, Y. Cao [et al.]. – Text : electronic // ACS Nano. – 2021. – Vol. 15. – № 4. – P. 6517-6529. – URL: /doi/pdf/10.1021/acsnano.0c08790 (date accessed: 02.06.2025).

149. Carbon nanotubes: a novel material for multifaceted applications in human healthcare / S. Kumar, R. Rani, N. Dilbaghi [et al.] // Chemical Society Reviews. – 2017. – Vol. 46. – № 1. – P. 158-196.

150. Robust technique for dispersion of single-walled carbon nanotubes in aqueous solutions with tRNA / O. Zaremba, A. Goldt, M. Ramirez-Morales [et al.] // Carbon. – 2019. – Vol. 151. – P. 175-180.

151. CvLAC - RG. – URL: https://scienti.minciencias.gov.co/cvlac/visualizador/generarCurriculoCv.do?cod_rh=00

00542300 (date accessed: 12.06.2025). – Text : electronic.

152. Diversity of extracellular vesicles derived from calli, cell culture and apoplastic fluid of tobacco / M. Kocholatá, J. Malý, S. Kříženecká, O. Janoušková. – Text : electronic // Scientific Reports. – 2024. – Vol. 14. – № 1. – P. 30111. – URL: https://www.nature.com/articles/s41598-024-81940-8 (date accessed: 10.06.2025).

153. Cancer photothermal therapy in the near-infrared region by using single-walled carbon nanotubes / F. Zhou, D. Xing, Z. Ou [et al.] // Journal of Biomedical Optics. – 2009. – Vol. 14. – № 2. – P. 021009.

154. Singh, R. Cancer Targeting and Diagnosis: Recent Trends with Carbon Nanotubes / R. Singh, S. Kumar // Nanomaterials. – 2022. – Vol. 12. – № 13.

155. Hyperspectral Microscopy of Near-Infrared Fluorescence Enables 17-Chirality Carbon Nanotube Imaging / D. Roxbury, P. V. Jena, R. M. Williams [et al.] // Scientific Reports. – 2015. – Vol. 5. – № August. – P. 1-6.

156. Non-Covalently Functionalized of Single-Walled Carbon Nanotubes by DSPE-PEG-PEI for SiRNA Delivery / K. S. Siu, Y. Zhang, X. Zheng [et al.]. – 2016. – Vol. 1364. – P. 151-163.

157. Novel layer-by-layer self-assembled peptide nanocarriers for siRNA delivery / B. Bozdoğan, Ö. Akbal, E. Çelik [et al.] // RSC Advances. – 2017. – Vol. 7. – № 75. – P. 47592-47601.

12 Appendix

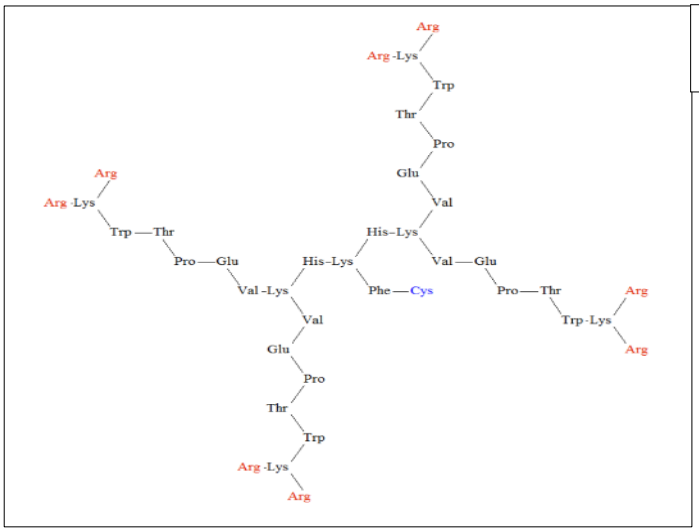

Appendix Figure 1: KK46 peptide structure

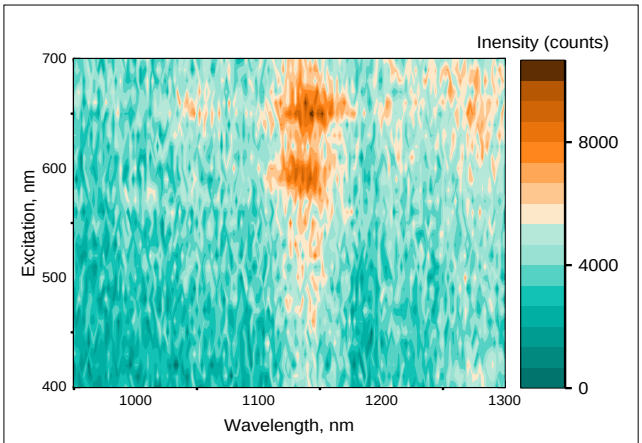

Appendix Figure 2 : PL map for BSA-CNT ratio 10:1

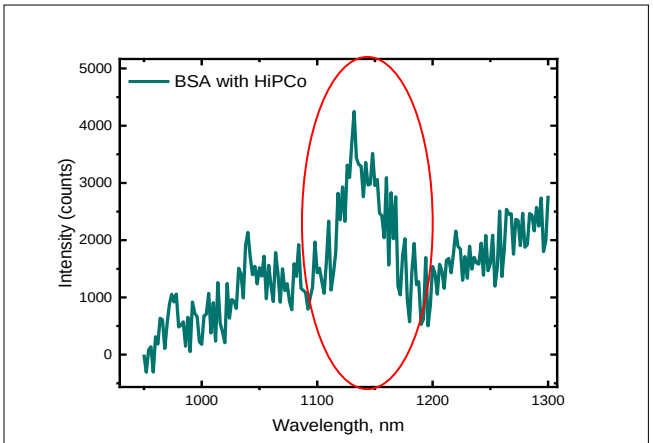

Appendix Figure 3: PL spectra for BSA-CNT ratio 10:1
There is the low PL signal as well the UV-vis-NIR shows the low quality of dispersed CNTs, additionally it was not stable sample.

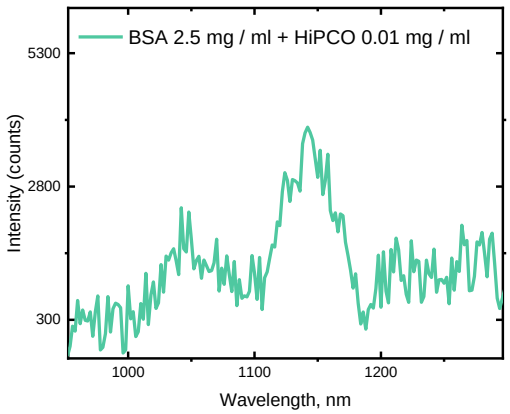

Appendix Figure 4: PL spectra for BSA-CNT ratio 250:1
There is the low PL signal as well the UV-vis-NIR shows the low quality of dispersed CNTs, additionally it was not stable sample

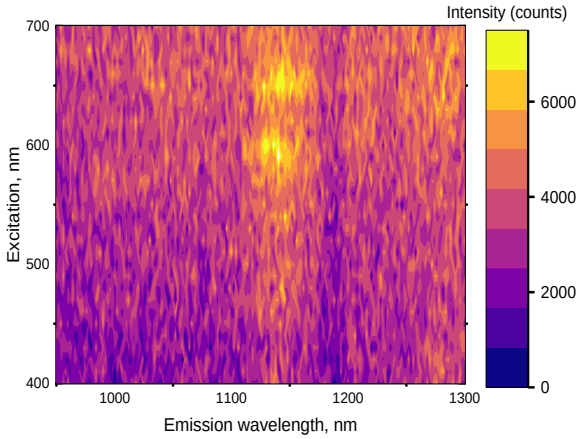

Appendix Figure 5: PL map for BSA-CNT ratio 250:1

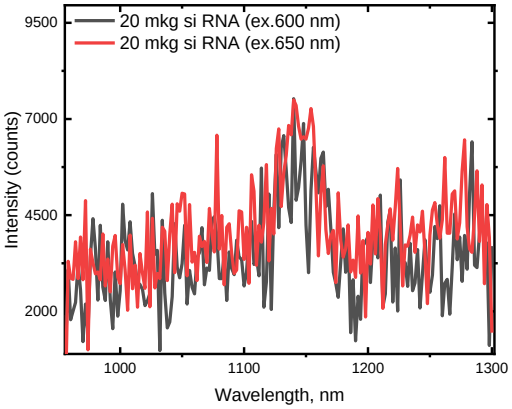

Appendix Figure 6: PL spectra for BSA-CNT ratio 250:1 with siRNA (20µg/mL)

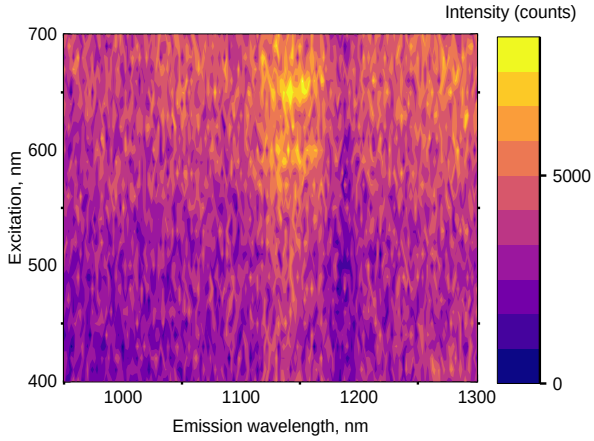

Appendix Figure 7: PL map for BSA-CNT ratio 250:1 with siRNA (20µg/mL)

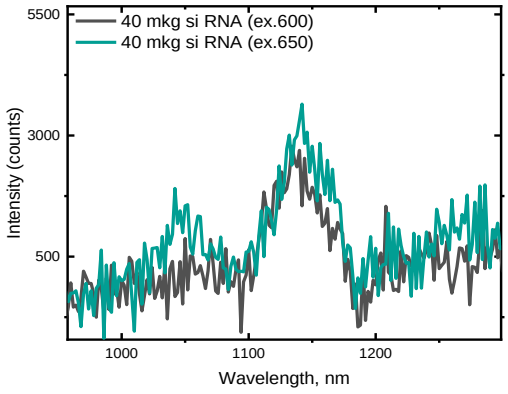

Appendix Figure 8: PL spectra for BSA-CNT ratio 250:1 with siRNA (40µg/mL)

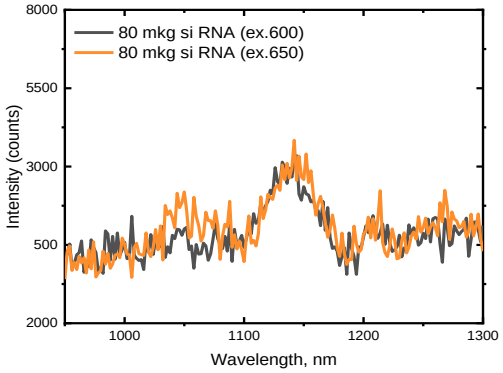

Appendix Figure 9: PL spectra for BSA-CNT ratio 250:1 with siRNA (80µg/mL)

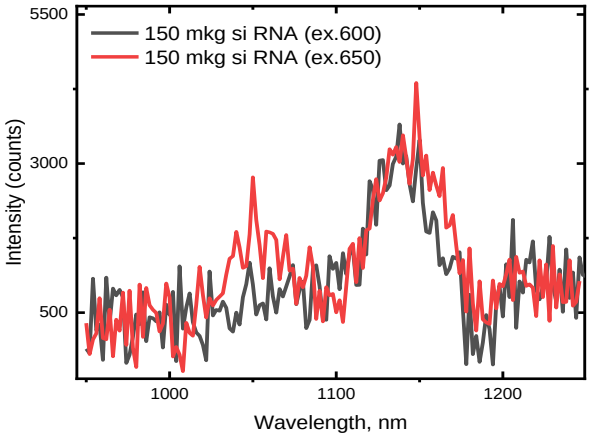

Appendix Figure 10: PL spectra for BSA-CNT ratio 250:1 with siRNA (150µg/mL)

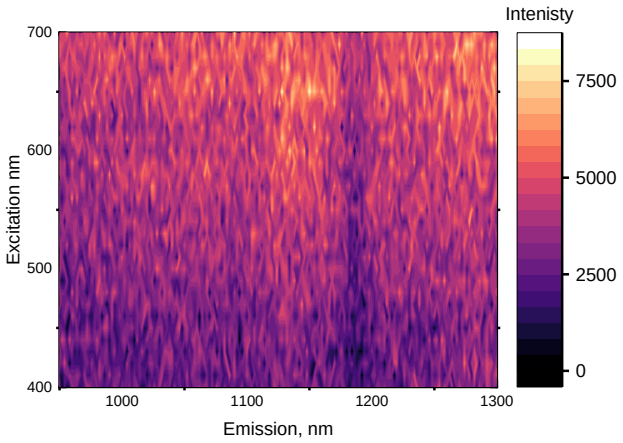

Appendix Figure 11: PL map for KK46-CNT ratio 100:1
Good stability but no PL signal

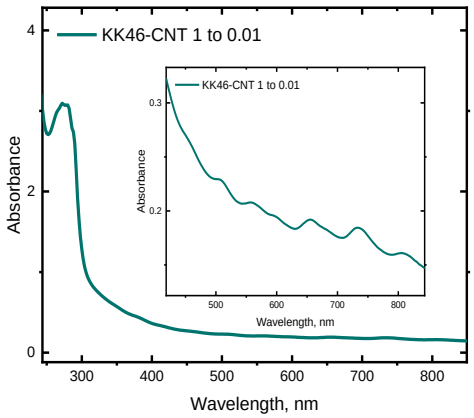

Appendix Figure 12: Absorption spectra for KK46-CNT ratio 100:1

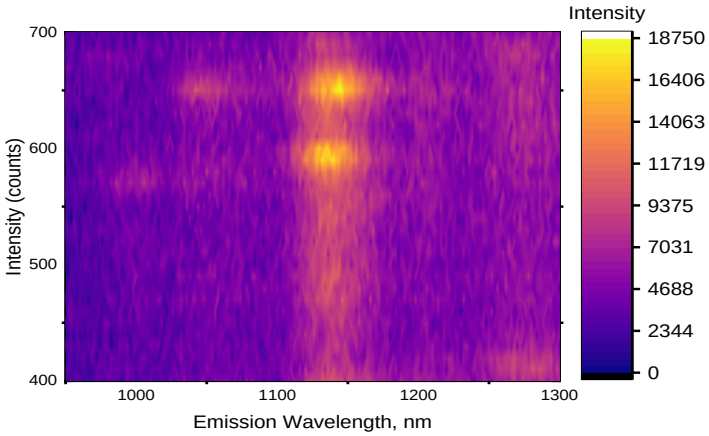

Appendix Figure 13: PL map for siRNA-CNT (control sample), just siRNA in PBS (0.01% concentration) buffer with HiPCO CNT (0.025mg/ml) under the same conditions as with BSA.

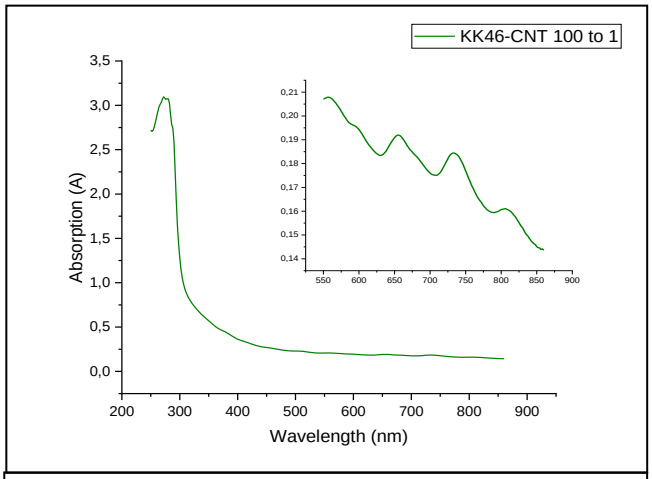

Appendix Figure 14: Absorption spectra of KK46-CNT complex, ratio 100:1

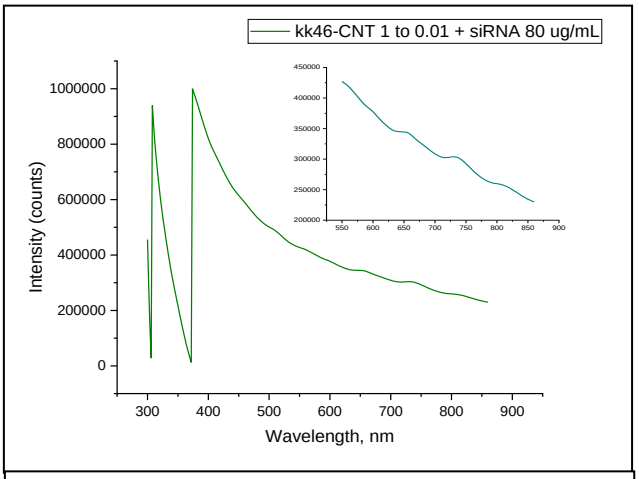

Appendix Figure 15: Absorption spectra of KK46-CNT complex (ratio 100:1) + siRNA (80µg/mL)

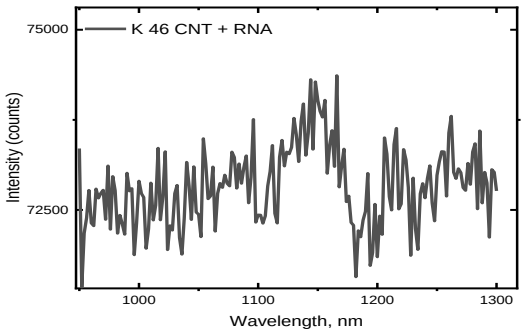

Appendix Figure 16: PL spectra of KK46-CNT complex, ratio 100:1 + siRNA (80µg/mL). Good stability, but there is no PL signal

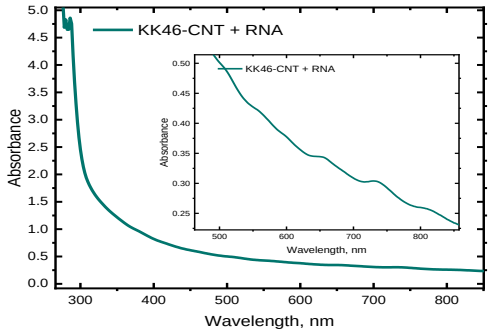

Appendix Figure 17: Absorption spectra of KK46-CNT complex (ratio 50:1) + siRNA (80µg/mL)

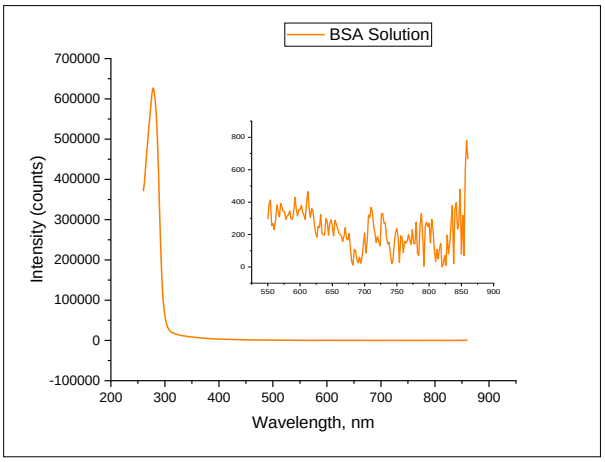

Appendix Figure 18: Absorption spectra of BSA solution

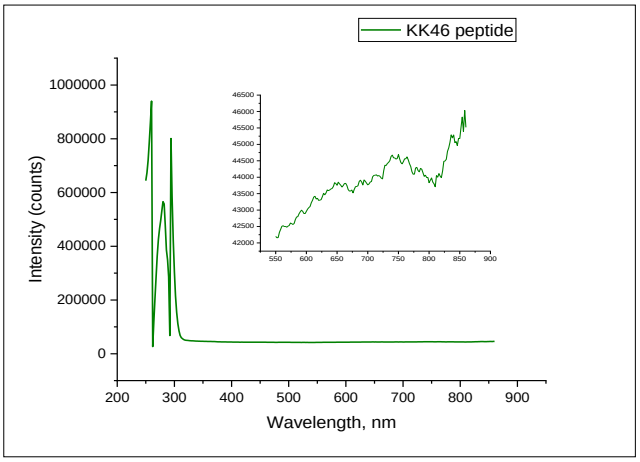

Appendix Figure 19: Absorption spectra of KK46 solution

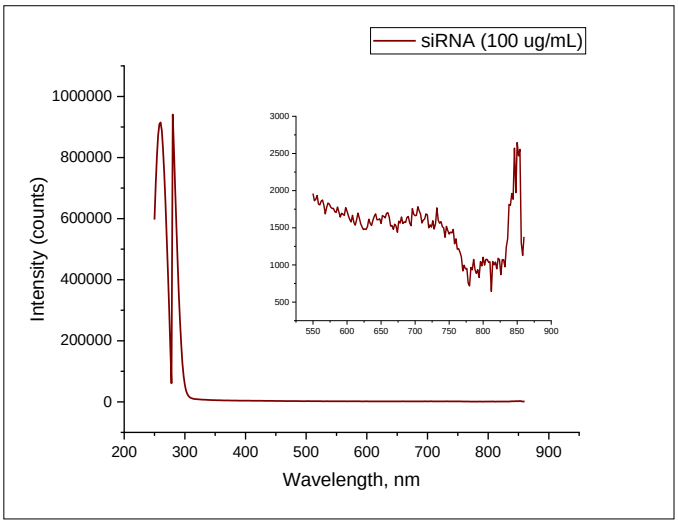

Appendix Figure 20: Absorption spectra of siRNA solution

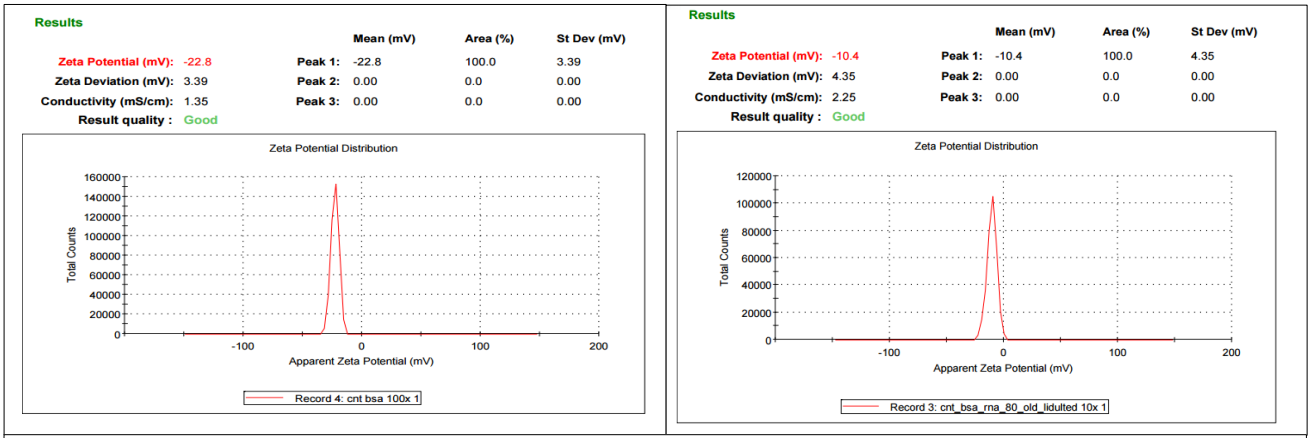

Appendix Figure 21: Zeta potential of BSA-CNT (ratio 5:1) **(left)** and after incorporating siRk12 (40µg/mL) **(right)**

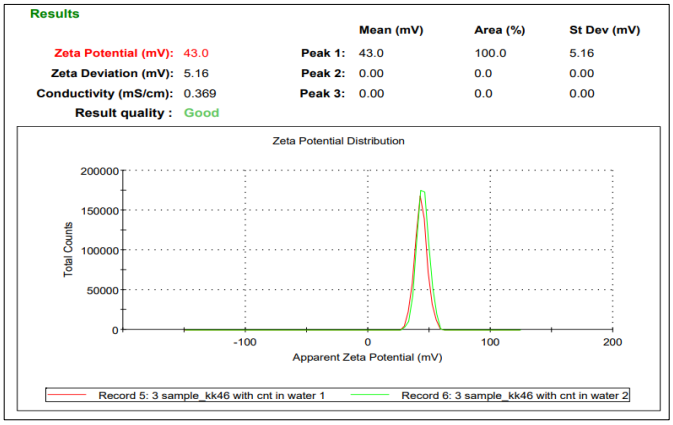

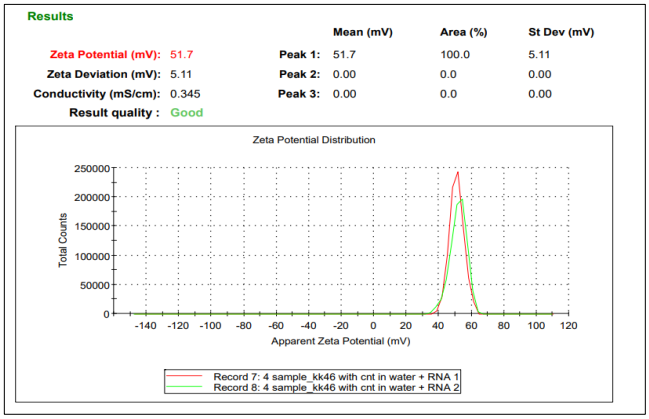

Appendix Figure 22: Zeta potential of KK46-CNT (ratio 50:1) in water **(left)** and after incorporating siRk12 (80µg/mL) **(right)**

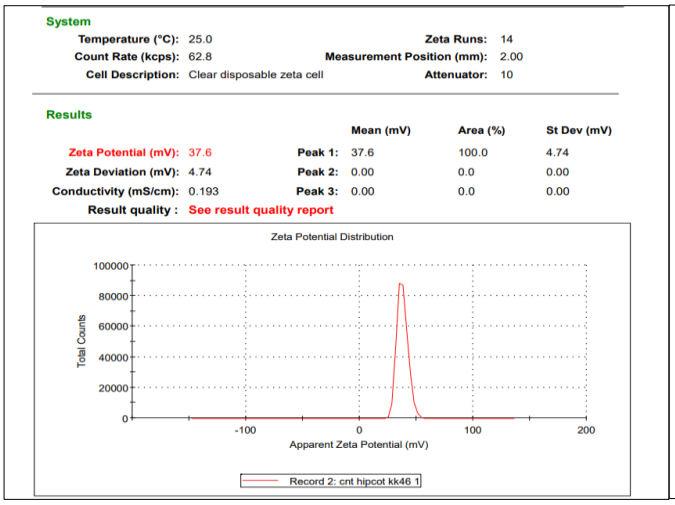

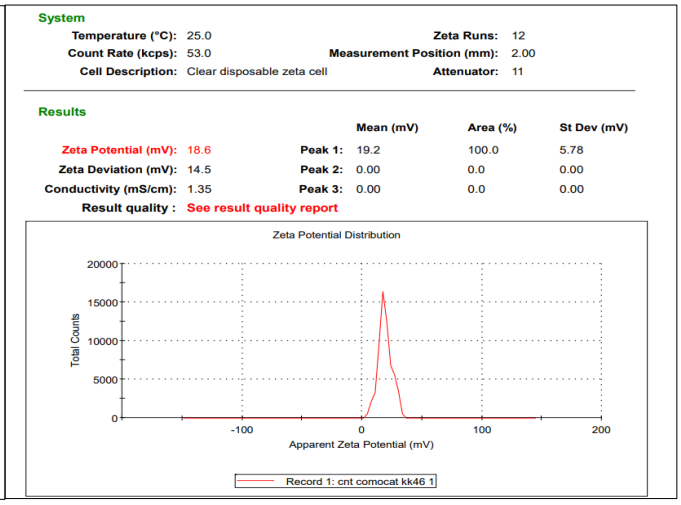

Appendix Figure 23: Zeta potential of KK46-CNT (ratio 50:1): On the **left HiPCO** CNT and on the **right CoMoCat** CNT.

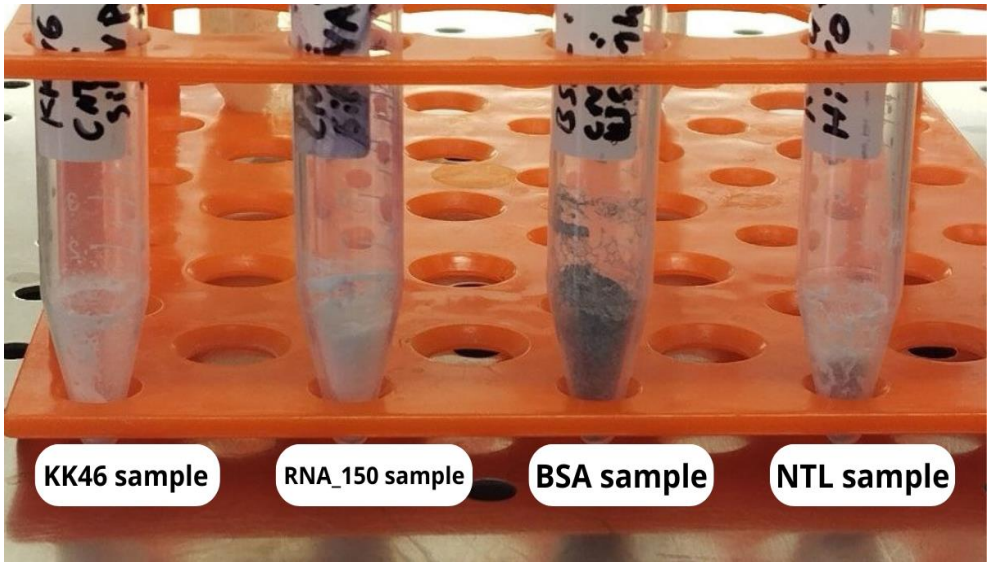

Appendix Figure 24: freeze-dried samples

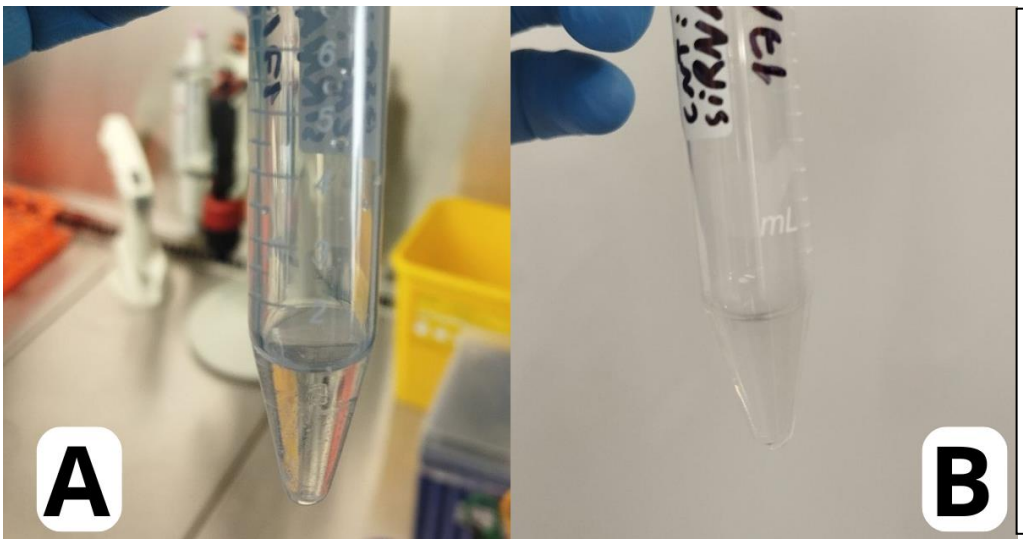

Appendix Figure 25: KK46-CNT-siRNA sample re-dissolved in deionized water 1 day after freeze-drying **(A)** and after 1 week **(B)**

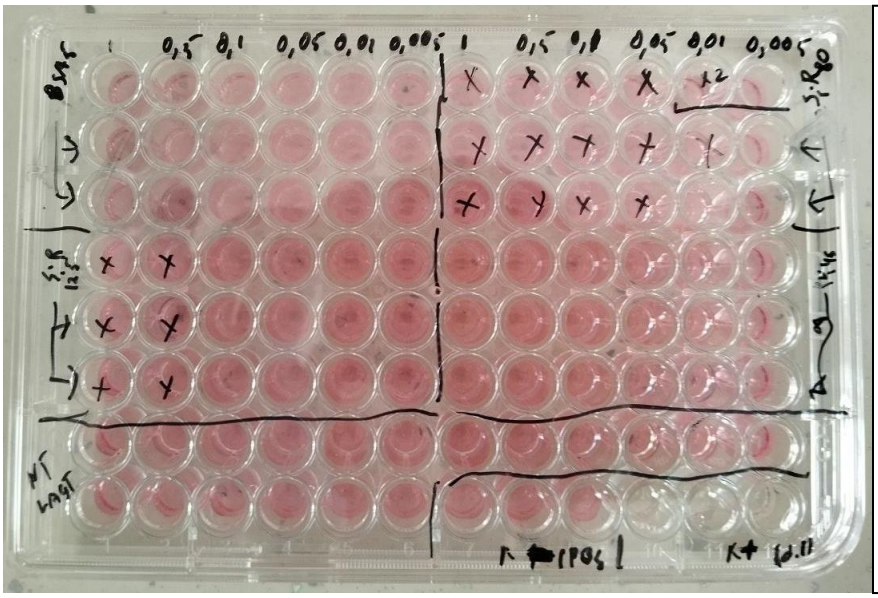

Appendix Figure 26: 96-well plate of HeLa cells treated with the samples of various concentration before incubation

	Mean (mV)	Area (%)	St Dev (mV)
Peak 1:	-36.5	88.7	8.58
Peak 2:	-11.0	7.1	4.49
Peak 3:	-0.0971	4.2	3.07

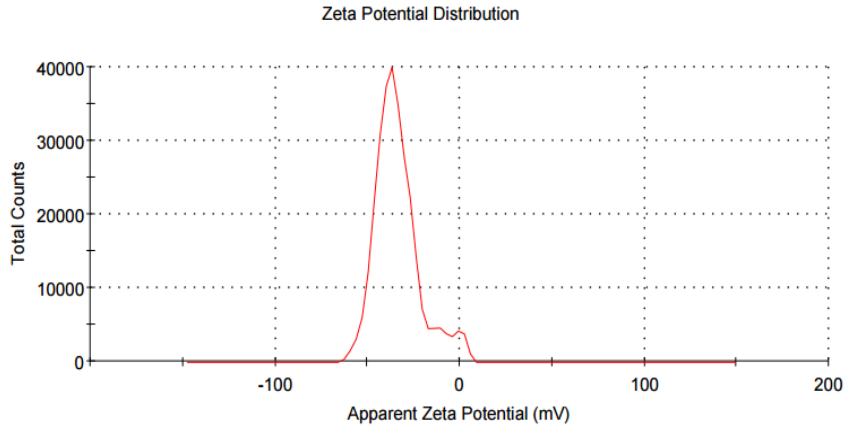

Appendix Figure 27: Zeta potential of CNT (HiPCO SWCNT) and siRNA (siSTAT3): main peak: -36.5 mV

	Mean (mV)	Area (%)	St Dev (mV)
Peak 1:	-43.4	100.0	7.26
Peak 2:	0.00	0.0	0.00
Peak 3:	0.00	0.0	0.00

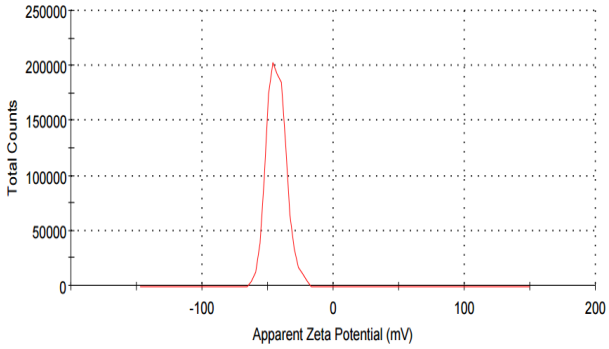

	Mean (mV)	Area (%)	St Dev (mV)
Peak 1:	23.5	34.5	5.02
Peak 2:	39.9	33.6	5.84
Peak 3:	7.30	23.1	6.03

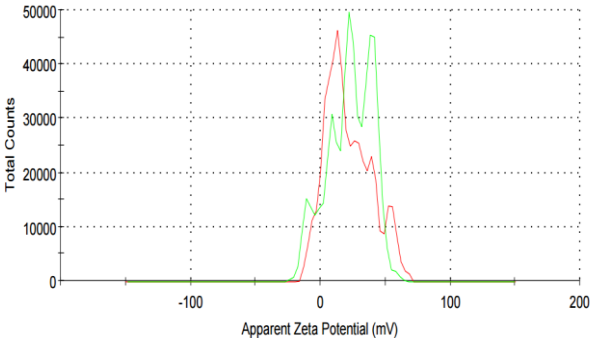

Appendix Figure 28: On the right: Zeta potential of KK46-CNT (ratio 50:1) and siSTAT3 (80 µg/mL): main peak +23.5 mV
On the left: BSA-CNT (5:1) + siSTAT3 (80 µg/mL): main peak: -43.4 mV

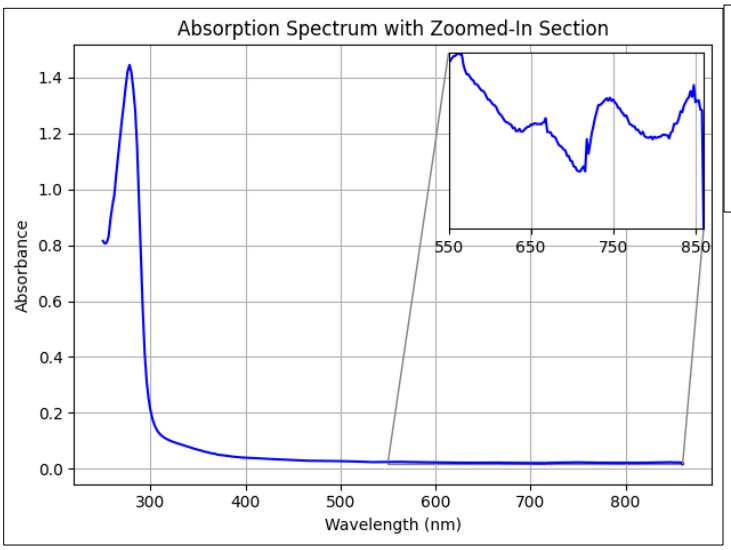

Appendix Figure 29: Absorption spectra of BSA-CNT (HiPCO) ration (50 to 1), using Cary 100 UV-Vis spectrophotometer from Agilent Technologies